MOLECULAR MECHANISMS OF COPPER TRANSFER FROM THE METALLOCHAPERONE ATOX1 TO THE WILSON DISEASE PROTEIN

by

Joel M. Walker

A THESIS DISSERTATION

Presented to the Department of Biochemistry and Molecular Biology

and the Oregon Health and Science University

School of Medicine

in partial fulfillment of

the requirements for the degree of

Doctor of Philosophy

February 3, 2005

School of Medicine
Oregon Health & Science University

CERTIFICATE OF APPROVAL

This is certify that the Ph.D. thesis of

Joel M. Walker

has been approved

[redacted]
Thesis Mentor – Dr. Svetlana Lutsenko

[redacted]
Thesis Committee Chair – Dr. David Farrens

[redacted]
Committee Member – Dr. Caroline Enns

[redacted]
Committee Member – Dr. Jack Kaplan

[redacted]
Committee Member – Dr. Maria Schumacher

TABLE OF CONTENTS

LIST OF FIGURES

LIST OF TABLES

LIST OF ABBREVIATIONS

Å	Angstrom
AEBSF	4-(2-aminoethyl)benzenesulfonyl fluoride
ATP	adenosine triphosphate
BCA	bicinchoninic acid
BCS	bathocuproine disulfonate
C-	carboxy-
CAPS	3-(cyclohexylamino)propanesulfonic acid
CBD	chitin binding domain
Ci	Curie
COS-7	green monkey kidney cell line
CPM	7-diethyl-amino-3-(4′-maleimidylphenyl)-4-methylcoumarin
CCS	copper chaperone for Cu/Zn-superoxide dismutase
Da	Dalton
DNA	deoxyribonucleic acid
DTT	dithiothreitol
E (chemical context)	total energy
EC_{50}	effective concentration for 50% activity
EDTA	ethylenediaminetetraacetic acid
E. coli	*Escherichia coli*
EPR	electron paramagnetic resonance spectroscopy
EXAFS	extended X-ray absorption fine structure

eV	electron volt
FT	Fourier transform
F_w	goodness-of-fit parameter
γ	gamma
g	gravity
G (chemical context)	guanine
GST	glutathione-S-transferase
H (protein context)	histidine
H (chemical context)	hydrogen
HAH1	human Atx1 homologue 1
HEPES	1-piperazineethane sulfonic acid, 4-(2-hydroxyethyl)-monosodium salt
HepG2	human hepatoma cell line
HT	His_6-tag
ICC	Indian childhood cirrhosis
K_a	binding affinity
kb	kilobase
kcal	kilocalories
kDa	kilodalton
MBP	maltose binding protein
mMBS	mutated metal-binding site
MBS	metal-binding site
MNKP	Menkes disease protein

mRNA	messenger ribonucleic acid
MS	multiple scattering
MWCO	molecular weight cut-off
N-	amino-
N-MNKP	amino terminal domain of MNKP
NMR	nuclear magnetic resonance spectrocopy
NTA	nitrilotriacetic acid
N-WNDP	amino terminal domain of WNDP
PCR	polymerase chain reaction
PDB	protein data bank
PVDF	polyvinylidene difluoride
Q	glutamine
R	bond length distance
RNA	ribonucleic acid
RT-PCR	real-time PCR
SDS-PAGE	sodium dodecyl sulfate-poly-acrylamide gel electrophoresis
Sf9	*Spodoptera frugiperda* cells
σ^2	Debye-Waller factor
SOD1	Cu/Zn-superoxide dismutase
T (chemical context)	thymine
TCA	trichloroacetic acid
TCEP	tris-(2-carboxyethyl)phosphine hydrochloride

TM	transmembrane
TPCK	L-1-tosylamido-2-phenylethyl chloromethyl ketone
Tricine	*N*-[2-hydroxy-1,1-bis(hydroxymethyl)ethyl]glycine
Tris	tris(hydroxymethyl)aminomethane
UV	ultraviolet
XAS	X-ray absorption spectroscorpy
w/w	weight/weight
WNDP	Wilson disease protein
WT	wild type
x (protein context)	any amino acid

ACKNOWLEDGEMENTS

I would like to sincerely thank my advisor and mentor Dr. Svetlana Lutsenko, whom I have been incredibly fortunate to have as a scientific role model. Her genuine interest in my success as a student, as a research scientist and as a friend has given me the strength to achieve my goals. She has provided me with an excellent environment to pursue my research and with her unending patience and advice she has helped me develop confidence in my abilities as a scientist. I am proud to be her first graduate student.

I wish to thank the current and past members of the Lutsenko laboratory. I want to specifically thank Dr. Ruslan Tsivkovskii, Dr. Natalie Barnes, Mee Min, Matthew Cooper and Brian MacArthur for their encouragement, their friendship, and stimulating discussions. Furthermore, I would like to thank all of my friends at OHSU who have made my time here a wonderful experience. I would like to especially thank my classmate Dr. Jay Janz for his friendship, advice, and encouragement through the phrase "strength and honor".

I would also like to thank the members of my research advisory committee – Dr. Jack Kaplan, Dr. David Farrens, Dr. Caroline Enns and Dr. Maria Schumacher. They have all provided me with useful suggestions and advice.

Finally, I thank my parents John and Mary Ann who have given me the tools to succeed in whatever endeavor I undertake. Their constant support, encouragement, advice, and friendship have given me the strength to become a scientist.

I dedicate this dissertation in loving memory of Loretta Kottman.

ABSTRACT

Copper is an essential nutrient required for function of several biologically active enzymes located in various cell compartments. However, copper accumulation has toxic effects within the cell as evidenced by pathologies observed in patients with Wilson disease. To manage the vital role copper in human physiology, a novel class of proteins, called metallochaperones has evolved. These proteins function to temporarily sequester copper and to distribute the metal to specific target proteins throughout the cell. Several structural aspects of the copper distribution pathway have been studied in detail. The focus of this dissertation involves understanding the molecular mechanisms of copper transfer from the metallochaperone Atox1 to the copper-transporting P-type ATPase, the Wilson disease protein (WNDP).

The Wilson disease protein transports copper into the secretory pathway for incorporation into the ferroxidase ceruloplasmin and also functions to excrete copper from the cell when copper is elevated. Several disease mutations of WNDP were shown to disrupt protein-protein interactions with the metallochaperone Atox1 suggesting that these interactions are important for WNDP function in the cell. To better understand functional interactions between Atox1 and WNDP, we generated the recombinant Atox1 in the apo and copper-bound form, determined the stoichiometry of copper binding, and developed biochemical protocols to study transfer of copper. Using these techniques we demonstrate that recombinant Atox1 transfers up to 6 copper atoms to the amino-terminal domain of the Wilson disease protein (N-WNDP). This copper transfer stimulates the catalytic activity of full-length WNDP providing strong evidence for the direct effect of Atox1 on the transporter.

The data described in this dissertation suggest that the role of Atox1 is to regulate the copper occupancy of WNDP. The copper-Atox1 transfers the metal to N-WNDP, while the incubation of apo-Atox1 with copper-bound N-WNDP results in the removal of copper from the latter and down-regulation of the WNDP catalytic activity. Interestingly, even a large excess of apo-Atox1 is insufficient to remove all the copper from N-WNDP and completely inactivate the enzyme. This partial reversibility favoring forward copper transfer reaction could be essential for the function of Atox1 in a cell where copper delivery to WNDP should be achieved when both apo- and copper-bound Atox1 forms are present.

The experiments described in this dissertation also explored the molecular mechanism of Atox1-mediated copper transfer to N-WNDP. There has been no information in the literature on how copper is transferred to the multiple copper-binding sites in copper transporters and how specificity towards different sites, if any, is achieved. Our results show that chaperone Atox1 preferentially delivers copper to metal-binding site 2 (MBS2) of N-WNDP and that this step is essential for further migration of copper to the intramembrane copper-binding sites of WNDP. This preference for MBS2 is likely due to specific protein-protein interactions between MBS2 and Atox1 as the incubation of N-WNDP with free copper results in non-selective loading of multiple metal-binding sites. Furthermore, copper binding to MBS2 results in specific conformational changes in N-WNDP enabling Atox1 to load the other MBS with copper. We propose a model for Atox1-mediated copper delivery to N-WNDP where MBS2 and MBS3 function as the switch facilitating copper binding to MBS5,6 and eventual transfer to the intramembrane portion of WNDP.

In summary, the research presented in this dissertation provides the first biochemical evidence of direct copper transfer from the metallochaperone Atox1 to Wilson disease protein and details the molecular mechanisms involved in the first step of Atox1-mediated copper delivery to the intramembrane portion of WNDP. These findings represent an important contribution to the understanding of copper metabolism in the cell.

Chapter 1

Introduction

1. 1: Physiological role of copper in the human body

1. 1.1: Copper is an essential element

The micronutrient copper is an essential element needed for the proper function of a cell and for the organism as a whole. It is a transition metal that can exist in two distinct redox states, Cu^{1+} and Cu^{2+}. These two redox states are useful in biological systems by enabling copper to donate or to accept an electron during enzymatic reactions.

The biologically significant property of copper lies in its role as a cofactor to several enzymes critical for cell survival. These copper-dependent enzymes function in a diverse array of cellular and biochemical pathways (1). For example, the mitochondrial cytochrome C oxidase functions in the electron transport chain, while the cytosolic Cu/Zn-superoxide dismutase converts oxygen radicals to oxygen and hydrogen peroxide. In the secretory pathway, copper binds to several proteins including the multicopper ferroxidase ceruloplasmin as well as tyrosinase, an enzyme essential for the production of the pigment melanin.

The role of copper in cell metabolism goes beyond utilization of copper as a cofactor for protein function. The unbound form of copper can presumably generate oxygen radicals in solution through Fenton chemistry. The generation of reactive oxygen species can have deleterious consequences for the cell including protein modification, lipid peroxidation, and DNA damage (2-4). This negative function results in the tight regulation of copper in the cell and in the body.

1. 1.2: Copper homeostasis in the human body

A delicate balance of copper is required to maintain normal cell homeostasis. Copper deficiency leads to the loss of copper-dependent protein functions and multisystem disorders. Similarly, copper overload is associated with significant organ damage (5). Therefore, the copper uptake and excretion processes must be regulated to keep a proper physiological concentration of copper and maintain the mineral balance (Figure 1. 1).

The primary source of copper for the human body is the diet. The major sources of this micronutrient include vegetables, animal milk products, shellfish and grains (6, 7). It has been estimated that the body needs about 0.75 mg/day copper and most diets contain about 0.6-1.6 mg/day (6, 8). This suggests that the average person ingests enough copper to sustain a healthy metabolism.

The major point of copper entry in gastrointestinal tract are the enterocytes lining the intestinal mucosa. These cells facilitate copper transport from the diet to the blood where copper binds to histidine, serum albumin or transcuprein (9, 10). These serum proteins then deliver copper to tissues throughout the body, including the liver, brain and kidney, where it can be incorporated into newly synthesized copper-dependent proteins. The excess copper is excreted from the blood by the liver. The liver exports copper into the bile allowing it to be removed from the body in the stool. It has been estimated in mammals that about 50% of the ingested copper rapidly reappears in the bile, while the rest of copper is absorbed (7). The other minor site of copper excretion is the urine where the average person excretes 0.02-0.05 mg/day (8).

1. 2: Diseases of copper metabolism

1. 2.1: Acquired and genetic causes of copper deficiency

Copper deficiency in humans can be either dietarily acquired or caused by genetic disorders. Acquired deficiency arises from a diet low in copper, whereby the body cannot absorb enough copper from the ingested nutrients to meet the daily requirement. This situation, for example, is present in malnourished infants who consume a diet based on copper-deficient cow's milk or infant formula lacking supplemented copper (11, 12). Copper deficiency in these infants results in low ceruloplasmin levels, neutropenia, anemia, and bone abnormalities leading to bone lesions and fractures (13, 14). Fortunately, these clinical symptoms can be quickly reversed through the supplementation of copper in the diet.

The systemic copper deficiency in infants also results from a disruption of the copper transport across the epithelial layer of the gastrointestinal tract. Two X-linked genetic diseases, Occipital Horn Syndrome and Menkes disease, have been identified as leading to copper deficiency in the body (15).

Occipital Horn Syndrome, also known as Type IX Ehlers-Danlos disease, is a milder form of copper deficiency (16). This disease is caused by mutations in the gene ATP7A which affect splice site junctions during mRNA processing (17, 18). The disease phenotype is characterized by lax skin and vascular abnormalities(19), but patients only have mild neurological disease and are able to live into adulthood (15).

The classical genetic disease of severe copper deficiency is Menkes disease. The characterization of Menkes disease is an excellent example of the serendipitous nature of scientific research connections. In 1962, John Menkes identified a neurological

syndrome affecting boys in early childhood (20). These boys all had peculiar, bristled, or "kinky" hair. They also had reduced pigmentation due to a loss of tyrosinase activity and died between the ages of 7 months and 3.5 years. Subsequently, Gillespie and colleagues discovered that copper-deficient sheep in Australia displayed steely wool (21). This led David Danks and coworkers to connect the "kinky" hair phenotype observed in Australian sheep with the low serum copper levels due to copper deficiency in Menkes disease patients (22).

Classical Menkes disease is caused by mutations or deletions in the gene ATP7A (23-25). The deletions are predominantly the result of translocation breakpoints of the X chromosome. The frequency of Menkes disease is about 1 per 100,000 male births with most patients dying by three years of age (15).

Patients with Menkes disease show a systemic copper deficiency due to impaired absorption in the intestine and the entrapment of copper in the epithelial cells at the blood-brain barrier (Figure 1. 1) (15). The lack of copper in the body leads to a loss of function of several copper requiring enzymes including tyrosinase, cytochrome C oxidase and lysyl oxidase (15). This results in the clinical pathologies characteristic of Menkes disease patients. These symptoms include the coarse "kinky" hair, demyelination of neurons in the brain, skin and joint laxity, reduced pigmentation, and neurological abnormalities such as seizures and impaired visual tracking (19).

1. 2.2: Copper toxicosis and Wilson disease

Similarly to acquired dietary copper deficiency, some people exhibit acquired copper toxicosis due to an elevated intake of copper from the diet. If the body does not

excrete excess copper, the liver becomes saturated and this may result in hepatic damage. For example, patients with Indian childhood cirrohsis (ICC) have hepatic copper levels 10-100 times that of normal children (26). In these patients, the excess copper is primarily present in the nuclear fraction leading to increased DNA damage through fragmentation (27). When left untreated, ICC has a 90% mortality rate six months after diagnosis (28). Although it has not been determined whether a genetic component is involved, ICC has been largely eradicated through changes in infant-feeding practices and with the use of the copper chelating drug D-penicillamine (28).

Wilson disease is the classic example of a genetic disease characterized by copper toxicosis. Samuel Wilson initially described it in 1912 when four patients were diagnosed with a progressive lenticular degeneration associated with liver cirrhosis (29). About 35 years later, Cunnings showed that patients with Wilson disease had elevated copper levels (30). Shortly thereafter, Scheinberg and Gitlin found a deficiency in serum ceruloplasmin levels in Wilson disease patients (31). These initial observations laid the foundation for the recent genetic and biochemical characterization of Wilson disease.

Wilson disease is an autosomal recessive disorder caused by mutations in the gene ATP7B (32-34). Over 200 different disease mutations have been identified from patients with more than half of them resulting from missense mutations of ATP7B (35). The disease frequency is about 1 per 30,000 births with a heterozygous carrier frequency of about 1 per 100 (36). The disease symptoms usually appear during childhood but rarely before the age of three (37). However, the diagnosis of Wilson disease in adulthood usually occurs after other diseases of the liver (viral hepatitis, alcohol-induced cirrhosis) have been ruled out (38).

The symptoms of Wilson disease include elevated copper levels in several organs including the liver, brain and kidney (37). Copper accumulation in the liver, due to a loss of copper export into the bile, leads to hepatic failure or liver cirrhosis as shown in Figure 1. 1 (39). Wilson disease patients also show an increased incidence of neurological abnormalities (tremors, speech impediments, dystonia in the face and neck) along with the occasional presentation of Kayser-Fleischer rings in the cornea of the eye (38). Finally, Wilson disease patients have an increased copper concentration in their urine with a drastic decrease in the serum ceruloplasmin concentration (8).

The only United States Food and Drug Administration approved treatment involves the ingestion of the drug D-penicililamine (40). D-penicililamine, a copper chelator, works by increasing the excretion of copper in the urine. Unfortunately, D-penicililamine is toxic to the body and leads to severe side effects.

These clinical observations emphasize the central role of the copper-transporting ATPases in human copper homeostasis. The function of these transporters is critically dependent on the copper chaperone Atox1. Characterization of Atox1 and understanding the mechanism of the Atox1-mediated copper transport are central issues discussed in this dissertation.

1. 3: The copper chaperones

1. 3.1: The cellular copper distribution network

The mammalian cell utilizes a specific molecular machinery to temporarily sequester and transport copper from the cellular uptake system to the essential cupro-enzymes located in the various cell compartments. This unusual method of the

intracellular ion distribution is mediated by small specialized proteins, termed metallochaperones or copper chaperones (41). Three copper chaperones, Cox17p, Atox1, and CCS, have been identified which deliver the metal ion to the mitochondria, to the secretory pathway, and to the abundant cytosolic protein superoxide dismutase, respectively (Figure 1. 2). This distribution network is needed as the amount of free copper in the cytosol was estimated to be less than one copper atom per cell (42).

Copper enters the cell through the high-affinity copper transporter Ctr1 (43, 44). What happens subsequently remains to be determined. One possible mechanism of copper release from Ctr1 involves the direct retrieval of copper from Ctr1 by the chaperones, and preliminary evidence shows copper exchange between yeast Ctr1 and Atx1 (45). However, until direct transfer to the other chaperones is demonstrated, it cannot be excluded that copper is released from Ctr1 directly into cytosol and an unidentified molecule (possibly glutathione) temporarily sequesters copper before binding to the chaperones. Excess copper entering the cell can also be stored by binding to cytosolic metallothioneins, but this cellular process has not been well characterized (46).

The three pathways involving the copper-binding chaperones are shown in Figure 1. 2. In the first pathway, the chaperone Cox17p is thought to bring copper to the mitochondria and deliver it to either the Sco1p or Cox11p proteins, which then insert the copper into cytochrome C oxidase (47). Interestingly, recent studies demonstrated that when Cox17p is tethered to the inner membrane of the mitochondria, copper is still delivered to Sco1p or Cox11p, suggesting that Cox17p may not be the main copper chaperone for the mitochondria (48). A second pathway involves CCS, which inserts

copper into cytosolic Cu/Zn-superoxide dismutase (SOD1) (49). The third pathway involves the delivery of copper by Atox1 to WNDP and MNKP for transport into the secretory pathway. Copper transported into the secretory pathway by WNDP binds to ceruloplasmin while proteins such as tyrosinase and lysyl oxidase receive copper from MNKP (50, 51). The delivery of copper by the metallochaperone Atox1 to the WNDP forms the essential subject matter of this dissertation as discussed in Chapters 2 and 3.

1. 3.2: Mechanism of SOD1 activation by CCS

The metallochaperone dependent maturation process of the highly abundant cytosolic protein Cu/Zn-superoxide dismutase is best characterized. The mature form of SOD1 requires the insertion of a zinc ion and a copper ion, the formation of an intramolecular disulfide bond, and homodimerization (52-54).

The first step in the maturation of SOD1 is the insertion of zinc into the nascent protein. Zinc binds to four distinct residues in SOD1 (52, 53). The mechanism of zinc delivery and binding to SOD1 remains unknown. However, Fabio Arnesano and colleagues have shown that zinc binding to SOD1 is a critical step in the eventual homodimerization of SOD1 (55).

The formation of the intramolecular disulfide bond in SOD1 and the loading of copper involve interaction with the copper chaperone CCS. The structural features of these two proteins lay the foundation for understanding the process of copper transfer and SOD1 maturation. The structure of SOD1 was initially determined to be a β-barrel with a Greek key fold (56). In comparison, the chaperone CCS contains three separate domains: an Atx1-like copper-binding Domain I, Domain II, which has an SOD1-like structure and

is involved in heterodimerization with SOD1, and Domain III that is required for copper insertion and is involved in the disulfide bond formation (57, 58).

The crystal structure of heterodimeric CCS and SOD1 complex showed a disulfide bond between Cys229 of CCS and Cys57 of SOD1 (58). Recent studies by Thomas O'Halloran and colleagues have shown that the formation of this intermolecular disulfide bond is important for the proper maturation of SOD1 (54). After the formation of the CCS-SOD1 disulfide bond and the proper insertion of copper into SOD1, a rearrangement occurs enabling the formation of the essential intramolecular disulfide bond in SOD1 between Cys57 and Cys146. This then facilitates the homodimerization of SOD1 leading to a functional protein (55).

While the structural basis of the chaperone-target recognition has been determined, the mechanism of copper insertion from CCS to SOD1 has not yet clarified. In fact copper binding to CCS alone is not really understood. The model proposed by Eisses *et.al.* suggests that human CCS forms a bridged copper cluster between the two cysteines in the Atx1-like CxxC motif in Domain I and the CxC motif in Domain III (59). At the same time, in the crystal structure of yeast CCS alone or in complex with SOD1, these two domains are located on opposite sides of the protein (57, 58), suggesting marked conformational rearrangement upon copper binding. Although the structural and copper-binding information was obtained using proteins isolated from different species, the sequence similarity of human and yeast SOD1 and functional data suggest that these two proteins work in a similar fashion (42, 57, 60-62).

In spite of all the structural and biochemical characterization of CCS and SOD1, the main question of how CCS inserts the copper atom into SOD1 remains unresolved.

The similar lack of mechanistic understanding of copper delivery is also characteristic of the other two copper transfer pathways, where the amount of structural information markedly exceeds the functional data. Therefore, the major focus of this thesis was to obtain such mechanistic information and gain insight into the biochemical basis of Atox1-mediated copper delivery to the copper transporters in the secretory pathway.

1. 3.3: The yeast copper chaperone Atx1

The biology of the metallochaperone-mediated copper delivery to the secretory pathway has been extensively characterized in yeast. In fact, the first metallochaperone discovered was the small cytosolic yeast protein Atx1 (63, 64). Atx1 is 73 residues in length and contains a MTCxxC copper binding motif where Cu(I) binds to the cysteines in the CxxC motif with a linear two-coordinate geometry (41, 63, 64).

The initial genetic experiments by Lin and colleagues showed that Atx1 was involved in copper delivery to the secretory compartment and that this process was required for normal iron metabolism. An *atx1*Δ strain failed to grow on iron-deficient media but growth occurred with the addition of copper to the media (64). Furthermore, Huffman and O'Halloran demonstrated that Atx1 functioned in the delivery of copper specifically to the copper-transporting ATPase Ccc2p (65). These findings provided an interesting link to the earlier studies in which Andrew Dancis and colleagues showed that iron uptake in yeast is tightly controlled by the availability of copper (66). High-affinity iron uptake is mediated by the Ftr1p transporter, which functions in a complex with the copper-dependent ferroxidase Fet3p (67). The ferroxidase Fet3p obtains its copper in the secretory pathway from Ccc2 completing the link between copper uptake and subsequent

iron uptake (68, 69). Disruption of copper delivery to the secretory pathway by inactivation of either Ccc2p or Atx1 results in the generation of copper deficient and non-functional Fet3p and in an iron-starved yeast phenotype. This observation has been utilized as the basis of the convenient complementation assay used for measuring copper transport into the secretory vesicles.

Many aspects of the Atx1-mediated copper delivery to the secretory pathways have been recapitulated in the mammalian system. At the same time, there are several important differences, which include a more complex organization of mammalian target proteins and the additional levels of regulation in higher eucaryotes.The work described in Chapters 2 and 3 focuses on the aspects of the copper transfer mechanism that are unique to mammalian cells. The sections below summarize our current knowledge of mammalian Atox1 and also compare and contrast human Atox1 with yeast Atx1.

1. 3.4: The mammalian copper chaperone Atox1

Atox1 is a conserved and widely expressed protein. The human copper chaperone Atox1 (also known as the Human Atx1 Homologue 1, HAH1) was initially identified by screening a liver cDNA library for homologues of Atx1 (70). The identification of other mammalian homologues of Atox1 in sheep (71), rats (72, 73), mice (74), and dogs (75), has lead to extensive characterization of its expression pattern. Human Atox1 mRNA expression was found in many tissues including the brain, the spleen, the intestine, as well as a variety of other cell lines (70). Atox1 mRNA is detected throughout the brain (72); with higher levels of expression observed in the pyramidal neurons of the cerebral

cortex, the hippocampus, and the locus coeruleus, i.e. the regions of the brain that have high levels of metals (72).

Moore and co-workers used immunostaining of kidney tissue to show Atox1 localization in the glomeruli, the loops of Henle of the medullla, and in the juxtamedullary and cortical portion of the nephrons (76). The localization of Atox1 correlates with the reported pattern for copper-transporting ATPases, although more definitive co-localization studies remain to be performed. In the liver, Atox1 localizes to the hepatocytes lining the hepatic sinusoids, which delivers nutrients and secreted proteins from the liver to the rest of the body (76). Atox1 localization in cells surrounding the hepatic vein is consistent with its role in copper delivery to the biosynthetic pathway, perhaps for copper incorporation into ceruloplasmin. Localization in other organs has yet to be characterized.

Genetics studies of Atox1. Genetic characterization of the human copper chaperone Atox1 has also been done. The gene for the human Atox1 contains 4 exons and 3 introns spanning a 16 kb region of the genome, with the start codon located at the 3′ end of exon 1 and the termination codon in exon 3 (77). *Atox1* was determined to reside in the chromosome region 5q32-33 (70) immediately adjacent to the SPARC gene (78). The gene for Atox1 encodes for a small cytosolic protein of 68 amino acids and shares 47% identity and 58% homology to yeast Atx1 (Figure 1. 3) (70). Similarly to Atx1, Atox1 contains a conserved MTCxxC sequence motif. Cu(I) binds to the two cysteines of this motif with a linear coordination geometry (79, 80) and a calculated binding affinity of $K_a = 2.45 \times 10^5\ M^{-1}$ (81).

The role of the human copper chaperone Atox1 in the delivery of copper into the secretory pathway of the cell has been investigated using a genetic approach. A complementation assay utilizing the *atx1*Δ yeast strain demonstrated that Atox1 delivered copper to the secretory pathway and restored copper insertion into Fet3p (70). Furthermore, mutation of the copper binding cysteines in the MTCxxC motif of Atox1 abrogated Fet3p activity in the *atx1*Δ yeast strain (79), suggesting that the two cysteines were important for Atox1-mediated copper transfer to the secretory pathway.

The generation of the Atox1 knockout mouse provided further support to the role of Atox1 in copper delivery to the secretory pathway. The disruption of the mouse *Atox1* gene locus eliminated the production of Atox1 protein. As the result, the Atox1$^{-/-}$ animals show a Menkes disease-like phenotype. They are hypo-pigmented, display skin laxity, and stunted growth (82), indicative of a systemic copper deficiency. Despite this copper deficiency, however, more than half of the knockout mice reached adulthood and were able to reproduce. This result suggests that although Atox1 is important, there may be other less efficient pathways facilitating copper delivery to the secretory pathway, which enable the Atox1$^{-/-}$ mice to survive.

Functional characterization of Atox1. Prior to the initiation of the work described in this dissertation, the only mechanistic information on Atox1 was the demonstration of direct protein-protein interactions between Atox1 and the copper-transporting ATPases, WNDP and MNKP. Hamza and co-workers used GST pull-down assays of endogenously expressed WNDP in HepG2 cells or transiently transfected WNDP and MNKP in COS-7 cells to demonstrate interaction between Atox1 and WNDP or MNKP (83). The interaction between Atox1 and WNDP was enhanced when the cells were

grown in elevated copper. Yeast 2-hybrid assays supported these results showing a copper dependent interaction between Atox1 and N-WNDP and N-MNKP (84). Interestingly, several patient disease mutations in the N-WNDP disrupted interaction with Atox1 suggesting that the WNDP function requires Atox1-mediated copper delivery to the N-WNDP (83).

1. 3.5: The chaperones Atx1 and Atox1 have similar structural features

Structural characterization of Atx1 and Atox1 was the first step towards understanding the copper transfer mechanism mediated by these proteins (85). The overall structural organization of Atx1 and Atox1 is very similar. Using X-ray crystallography Amy Rosenzweig and co-workers. demonstrated that the structure of copper-bound Atox1 is composed of a β_1-α_1-β_2-β_3-α_2-β_4 fold, which is very similar to the crystal structure of Hg(II) bound Atx1 (85). The MTCxxC copper-binding motif is located in an exposed loop at the N-terminal end of the first α-helix, allowing for easy access of the copper-binding cysteines to the solvent or to interacting proteins during copper binding and transfer (Figure 1. 3). Interestingly, the electrostatic surface potential for Atox1 and Atx1 is very positive due to several conserved lysine residues on the surface of the protein adjacent to the CxxC motif. It has been proposed that these lysine residues play an important role in interactions between the chaperone and its target. Mutagenesis analysis of Atx1 support this hypothesis (86), however mutations of the equivalent Lys in human Atox1 do not disrupt interactions between Atox1 and its targets (79). The Atx1-Ccc2a docking experiments described in Section 1.5 and information in

Chapter 3 address whether these lysines are important for the function of Atox1 and what this role could be.

The current model for Atx1/Atox1-mediated copper transfer suggests that the chaperone binds copper as a monomer with the 1:1 stoichiometry, docks to the target protein via specific protein-protein contacts, transfers copper to the acceptor site and then dissociates. It seems plausible that the binding and release of copper from Atox1 will be accompanied by structural changes and that such changes could be important for overall copper transfer process. Changes in the structure of Atox1 and Atx1 upon copper binding were indeed observed by NMR spectroscopy and were found to be similar for these two chaperones (87, 88).

Arnesano and colleagues showed that copper binding to Atx1 caused the MTCxxC loop to become more rigid inducing an extra turn in the first α-helix (87). This resulted in a change in the solvent accessibility of the two cysteines whereby the first cysteine flips from a solvent accessible position in the apo-Atx1 form into a more buried orientation in the copper-bound form. The second cysteine goes from about 45% solvent accessibility in the apo-form to 3% accessibility in the copper-bound form (87). These changes, when taken together, suggest that the flexible loop with the exposed cysteines in the absence of copper is designed to easily capture the ion either from the solution or another protein. However, once copper is bound it becomes buried in a position within the protein making it less accessible from the solvent. This observation raises an interesting question as to how this buried copper becomes available for transfer and what is the driving force for copper transfer. Presumably, docking of copper-Atox1 to the target protein induces further changes in the structure of the copper-Atox1 complex that

are favorable for copper release. The details of this process remains to be established. The studies described in Chapter 3 address the issue of directional copper transfer and shed some light as to why copper is transferred from Atox1 to the MBS2 of WNDP.

1. 4: The copper-transporting ATPases

To regulate the intracellular copper concentration, cells have developed a sophisticated network of copper-trafficking proteins that includes the copper-transporting ATPases and metallochaperones, such as Atox1. In humans, Wilson disease protein (WNDP) and the Menkes disease protein (MNKP) are copper-transporting ATPases that interact with Atox1. The studies described in Chapter 2 revealed that Atox1 controls copper occupancy of WNDP (and presumably MNKP) and regulates the catalytic activity of this transporter.

The copper-transporting ATPases belong to a large family of ion transporting P-type ATPases. After the initial discovery of the Na^+,K^+-ATPase by Jens Skou in 1957, over 100 different P-type ATPases have been identified in the evolutionarily diverse kingdoms of archaea, bacteria, and eukaryotes (89, 90). These transporters utilize the energy from the hydrolysis of ATP to transport metal cations across the membrane and against the concentration gradient. The cations transported include the transition metals copper, cadnium, and zinc (91-93) and other metals including sodium, potassium, magnesium, and calcium (94).

1. 4.1: Evolutionary conservation of copper-transporting ATPases

The copper-transporting ATPases are found in organisms of all phylogenetic kingdoms. These transporters are highly conserved; the biggest difference among these proteins is the number of copper-binding sites at the N-terminal domain of the ATPase. The prokaryotic bacteria *Enterococcus hirae* contain two copper-transporting ATPases, CopA and CopB, which have only one metal-binding site in the N-terminal copper binding domain (93). In the simple eukaryote *Saccharomyces cerevisiae*, the copper-transporting ATPase Ccc2p contains two metal-binding sites in its N-terminal copper binding domain (95). The human copper-transporting ATPases, the Wilson disease protein (WNDP) and the Menkes disease protein (MNKP), each contain six metal binding sites in their N-terminus (24, 32). The presence of multiple metal-binding sites in the human proteins suggests that the copper-transfer mechanism in humans is more complex than in prokaryotes and that functional interactions between the metal-binding sites of the copper-transporting ATPases are likely. Our studies described in Chapter 3 tested this prediction and provided experimental evidence for regulatory interactions between the multiple metal-binding sites in WNDP.

1. 4.2: Sequence characteristics of the Menkes and Wilson disease proteins

The important sequence characteristics and key functional properties of WNDP and MNKP have been described. It has been shown that WNDP and MNKP encode for copper-transporting ATPases sharing 54% sequence identity and 65% sequence homology (34). The predicted organization of the two copper-transporting ATPases is shown in Figure 1. 4.

Both proteins have eight putative transmembrane segments, a large cytsolic ATP binding domain and a cytosolic N-terminal copper-binding domain with six metal binding repeats. Within the sixth transmembrane segment resides the conserved CPC sequence motif (94). Mutation of the two cysteines in this motif to serines results in a complete loss of the copper transport across the membrane (96). It is assumed that the CPC motif has a similar function in MNKP, since mutation of the first Cys in this motif is associated with the loss of MNKP function and Menkes disease (97).

The WNDP and MNKP also share a similar cytosolic ATP-binding domain. The cytosolic ATP-binding domain contains the residues required for ATP coordination and the site of catalytic phosphorylation (Figure 1. 4). The aspartic acid residue in the conserved DKTG motif is a target of catalytic phosphorylation; mutation of this residue leads to a loss of catalytic activity and copper transport function (98-101). Another important sequence is the GDGxND motif, which is thought to orient the $\beta\gamma$-phosphates of ATP during hydrolysis (102). In addition, WNDP and MNKP also have a conserved SEHPL sequence where the histidine residue in WNDP has been shown to be essential for the proper orientation of ATP during catalysis (103).

The third large region of sequence similarity resides in the N-terminal copper-binding domain of WNDP and MNKP (N-WNDP and N-MNKP, respectively). The N-WNDP and N-MNKP comprise about 650 amino acids with each domain containing six independently folded metal-binding sites (MBS) of about 70 amino acids and flexible loop regions (Figure 1. 4) (34). In N-MNKP there is a large loop of about 70 amino acids between MBS1 and MBS2. In contrast, N-WNDP has a large loop of about 70 amino acids between MBS4 and MBS5 and a smaller loop between MBS3 and MBS4. It is

currently unclear whether or not this difference in loop structure has any consequences for spatial organization of the metal-binding sites and for the copper transfer mechanism. However, as described in Chapter 3, the transfer of copper from Atox1 to N-WNDP alters the loop structure, suggesting that the regions connecting the metal-binding sites are important for the function of the protein.

The alignment of all six of the metal-binding sites from N-WNDP and N-MNKP shows a significant region of sequence conservation (Figure 1. 5) (104). Five of the six MBS from both N-WNDP and N-MNKP contain the GMTCxxCxxxIE sequence motif where there is a threonine prior to the first cysteine. In contrast, the third MBS of both N-WNDP and N-MNKP has the GMHCxxCxxxIE sequence with a conserved histidine present prior to the first cysteine. Additional information about the sequence alignment of the six MBS in the Wilson disease protein is presented in Chapter 3.

1. 4.3: Copper binding characteristics of N-WNDP and N-MNKP

The copper-binding properties of the N-WNDP and N-MNKP are similar. Svetlana Lutsenko and co-workers expressed recombinant N-WNDP and N-MNKP as fusion proteins and copper loaded both proteins in *E. coli* (105). Upon purification of N-WNDP and N-MNKP, the measured copper-binding stoichiometry was 5-6, suggesting that each metal-binding site bound one copper. Using equilibrium dialysis experiments, it was later demonstrated that N-MNKP binds copper with an apparent affinity of $K_a = 19$ μM^{-1} and that copper binding is cooperative (106). In contrast, Wernimont *et.al* used isothermal calorimetry to monitor copper binding to N-WNDP and showed that N-WNDP binds copper with similar apparent affinity of $K_a = 20$ μM^{-1} but does not show

any cooperative binding of copper (81). This difference may be a result of the different structural organization in the N-terminal domains.

The copper-binding environment of N-WNDP and N-MNKP was further studied using X-ray absorption spectroscopy (XAS) and extended X-ray absorption fine structure analysis (EXAFS). These studies showed that copper binds to both proteins as Cu(I) (107, 108), in a distorted linear 2-coordinate geometry where the third coordinate may come from an exogenous ligand, such as DTT, or from an adjacent copper atom (109, 110). Although these studies focused on the entire N-WNDP and N-MNKP domains, the copper binding environment of an individual MBS was not studied in detail. To better understand the mechanism of copper transfer, the studies in Chapter 3 investigated the copper binding characteristics of the second metal-binding site of N-WNDP, an acceptor of copper during the transfer process, and compare them with the copper-binding environment of Atxo1, a metal donor.

1. 4.4: Functional properties of the Wilson disease protein

The Wilson disease protein has two functional roles in the cell: biosynthetic and homeostatic. For the biosynthetic function, WNDP localizes to the *trans*-Golgi network under normal cellular conditions. At the *trans*-Golgi network, WNDP transports copper into the secretory pathway for insertion into ceruloplasmin (111-113). Upon exposure of the cell to elevated copper, the WNDP traffics to an unidentified vesicular compartment (111, 114, 115) and potentially to the plasma membrane (116), where it functions to export copper from the cell.

The biochemical properties of WNDP were characterized by Tsivkovskii and colleagues (100). Copper binding to WNDP facilitates the hydrolysis of ATP and transient phosphorylation of the invariant aspartate residue in the ATP-binding domain. Using radioactive [γ^{32}P]-ATP to follow catalytic phosphorylation of WNDP, Tsivkovskii and colleagues demonstrated a copper dependent increase in activity of WNDP. The addition of the copper specific chelator bathocuproine disulfonate resulted in an inhibition of catalytic activity but the subsequent addition of free copper in solution resulted in a reactivation of the WNDP with $EC_{50} = 1.5 \pm 0.6$ μM. These experiments provided convincing evidence that the catalytic activity of WNDP was copper-dependent. However, the concentration of free copper in a cell is negligible (42) and is insufficient for stimulation of WNDP activity. Therefore, it seemed likely that copper-Atox1 complex might substitute for free copper and that the Atox1-mediated transfer of copper would be directly linked to stimulation of WNDP activity. The studies described in Chapter 2 of this dissertation tested this hypothesis.

The role of the N-terminal domain of WNDP in its copper transport function has been studied in detail. Several laboratories demonstrated that the N-WNDP is essential for the function of WNDP in the cell. Deletion of the entire N-WNDP or mutation of all six MBS CxxC motifs caused a complete loss of the *in vivo* copper transport (96, 101). However, if MBS6 was left intact, the transport function and catalytic activity of WNDP were detected, suggesting that MBS6 was sufficient for copper transport (96, 101, 117). Unfortunately, these results alone could not explain the function of other five N-terminal MBS of N-WNDP.

To address this important issue, both deletion and mutagenesis studies were performed. It was shown that the deletion of MBS6 alone with an intact MBS1-5 resulted in a loss of copper transport function while mutation of the cysteines of MBS6 led to a functional protein (101, 117). Huster and Lutsenko demonstrated that MBS5 and MBS6 could each regulate the affinity of the intramembrane copper-binding sites which suggested that MBS5 and MBS6 played a role in the delivery of copper to the intramembrane sites of WNDP (117). Interestingly, the replacement of MBS1-2, MBS1-3 or MBS1-4 at the position of MBS5-6 resulted in a complete loss of copper transport function (96). This result suggested that MBS1-4 have a separate function compared to MBS5-6 or that MBS1-4 are structurally different from MBS5-6.

1. 4.5: Structural characteristics of the copper-transporting ATPase metal-binding sites

The sequence alignments of the individual metal-binding sites of N-WNDP, N-MNKP and yeast Ccc2p suggest that they all have a similar overall fold, which is largely identical to the fold of Atox1 (Figure 1. 5). This raises the question of how Atox1 recognizes its target proteins. To date, no high-resolution structural information is available for N-WNDP. However, the solution structures for MBS2 and MBS4 of N-MNKP (N-MNKP2 and N-MNKP4, respectively) and the first MBS of Ccc2p (Ccc2a) were determined by several investigators (118-121). The NMR solution structures all revealed the β_1-α_1-β_2-β_3-α_2-β_4 ferrodoxin-like fold. Similarly to the location of metal-binding site in the copper chaperones Atx1 and Atox1, the copper-binding sequence GMT/HCxxC in each MBS is located in the exposed loop prior to the first α-helix,

suggesting that copper has easy access to the metal-binding cysteines (118). A conserved phenylalanine is a structural feature of the MBS that is absent in the chaperone and is located in close proximity to the CxxC motif. This Phe residue has been suggested to stabilize copper binding (120) and might also function in the formation of a hydrophobic core with the methionine in the MTCxxC motif and a leucine in loop 3 (121). Importantly, the electrostatic surface potential of several metal-binding sites showed a large negative patch near the CxxC motif on the side of interaction with the chaperone protein. This observation led to the suggestion that the docking of the copper chaperone to the MBS is driven by the complementary electrostatic interaction between the positively charged surface of Atx1/Atox1 and a negative surface of MBS. This hypothesis is plausible and therefore attractive. However, our experiments as described in Chapter 3 and modeling experiments indicate that the surface complementarity is not the major force that determines selective docking of Atox1 to the metal binding sites in N-WNDP and that the consideration of the spatial arrangements of MBS is essential for understanding of the selectivity of copper transfer.

Copper binding to the MBS does not change the overall fold of the proteins (119, 121). However, differences have been noted in the consequences of copper binding to the CxxC motif of human N-MNKP2 and MBS1 of Ccc2p (Ccc2a). As shown in Figure 1. 5, copper binding to N-MNKP2 resulted in an extra one turn of α_1-helix and the ordering of the first cysteine of the CxxC motif into a conformation facilitating copper binding (121). In contrast, the Ccc2a structure underwent very little reordering upon copper binding except that the CxxC motif became less flexible (119). The reduced flexibility results in a decrease in solvent accessibility for the first cysteine from 45% to

25% (119). The reorganization of the copper binding motif might have important implications for copper transfer and copper-binding environment at this specific metal-binding site. Moreover, the changes in the helical structure of N-MNKP2 upon copper binding could also affect other regions of the N-terminal copper binding domain through changes in the tertiary structure of the domain. The results from Chapter 3 suggest that copper binding to MBS2 of N-WNDP impacts several other regions in N-WNDP.

1. 5: Structural characterization of copper transfer from Atx1 to Ccc2p

The copper transfer from a copper chaperone to an isolated MBS has been studied mainly in yeast using Atx1 and an isolated metal-binding domain of the copper-transporting ATPase Ccc2, Ccc2a. The biochemical characterization of copper transfer from Atx1 to Ccc2a showed that each protein has similar affinities for copper (65). Furthermore, the incubation of both proteins together led to equilibrium, where each protein bound about 50% of the copper. This result suggested that a directional transfer from Atx1 to Ccc2a, if it occurs, would require the presence of the other Ccc2 domains.

The mechanism of copper transfer from Atx1 to Ccc2a was also studied using NMR spectroscopy and computer simulated docking experiments. These studies yielded several interesting results. The complex formation is apparently triggered by electrostatic interactions between the positively charged patch on Atx1 and the negatively charged region of Ccc2a, as discussed in earlier sections. Structural analysis of the lysine residues K24 and K28 of the α_1-helix of Atx1 shows the formation of salt bridges through electrostatic interactions with glutamate residues in Ccc2a (122). Furthermore, mutation

of these lysines resulted in reduced copper delivery to the secretory pathway and slower cell growth on iron deficient media using *in vivo* assays (86).

After the Atx1-Ccc2a complex is formed there is very little change in the overall structure of Ccc2a when comparing the apo-Ccc2a, Cu-Ccc2a, and the adduct Atx1-Ccc2a structures (122). In contrast, major changes were observed in Atx1 upon complex formation. The Atx1-Ccc2a complex resulted in an Atx1 structure which was intermediate between the apo-Atx1 and Cu-Atx1 forms (122). Specifically, adduct formation resulted in a reorganization of the copper-binding loop of Atx1 where the second Cys became more solvent accessible, facilitating a relaxed copper-binding state. In fact, in several docking experiments between Cu-Atx1 and apo-Ccc2a, this rotation by the second Cys of Atx1 might help to expel the copper atom from Atx1, allowing the cysteines of Ccc2a to capture the copper upon transfer (123).

The other main area of movement in Atox1 upon complex formation is in the loop spatially adjacent to the metal-binding site, containing the conserved KTGK motif. The lysine residues moved away upon adduct formation to an orientation similar to the apo-Atx1. Arnesano and colleagues postulated that the role of this conserved lysine may be in the stabilization of the Cu(I) bisthiolate center upon copper transfer from Atx1 to Ccc2a (87).

While copper transfer from Atx1 to Ccc2a is somewhat characterized, very little is known about the transfer mechanism between their human equivalents, Atox1 and the metal-binding sites in N-WNDP or N-MNKP. The X-ray crystallographic structure of Atox1 was originally solved as a copper-bound dimer (124). The dimeric structure of Atox1 is thought to be an artifact of crystallization as the copper atom is completely

shielded from the solvent and unavailable for transfer. (In addition, the monomeric nature of Atox1 in a cell is directly demonstrated by our gel-filtration experiments, see Appendix.) Consequently, it was proposed that the dimer represents a model of the copper-transfer intermediate between the chaperone (donor protein) and the MBS (acceptor protein) (124). In contrast to Atx1, the dimeric Cu-Atox1 crystal structure showed the conserved lysine in the KTGK motif, Lys60, formed a bridged hydrogen-bond network through one water molecule to the backbone oxygen of the second Cys of the opposite monomer (124). Whether Lys60 of Atox1 (similarly to the homologous lysine in Atx1), is involved in stabilizing the copper-binding region upon transfer, or is instead important for electrostatic interactions with a MBS has yet to be determined.

1. 6: Questions addressed in this dissertation

My published research (125, 126) as reported in Chapters 2 and 3 of this dissertation addresses important questions regarding the role of the metallochaperone Atox1 in the delivery of copper to the copper-transporting ATPase ATP7B, the Wilson disease protein. Can Atox1 directly transfer copper to all six of the MBS of the full-length N-WNDP, and does the transfer affect the catalytic activity of WNDP? Can Atox1 perform this copper transfer function alone? Does Atox1 randomly transfer copper to the metal-binding sites on N-WNDP or does it transfer to a preferential site? If one site is the preferential site, what structural characteristics make it the special site? Is copper transfer reversible? The answers of these questions contribute to an understanding of the mechanisms of copper transfer from the metallochaperone Atox1 to the Wilson disease protein.

Figure 1. 1.

Copper distribution in the human body. Copper enters the body from dietary sources. Upon digestion copper crosses the intestinal epithelial layer where it enters the portal vein for transport to the liver. The liver distributes copper to the body including the brain or the liver excretes copper into the bile duct where it is then eliminated from the body in the stool. Menkes disease results in a block of copper uptake from the intestine and copper transport across the blood-brain barrier. In contrast, Wilson disease blocks copper excretion from the liver into the bile.

Figure 1. 1.

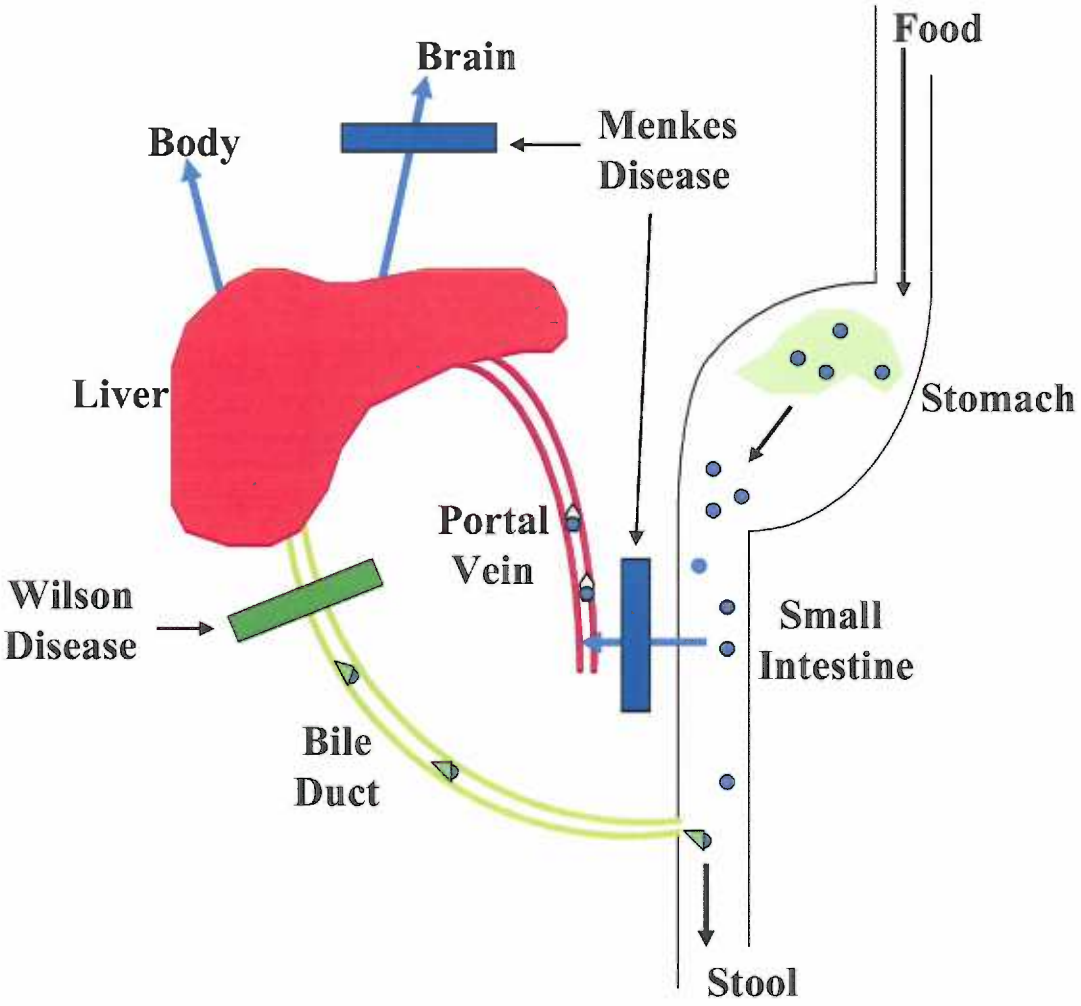
Food
Brain
Body
Menkes
Disease
Liver
Stomach
Portal
Vein
Wilson
Disease
Small
Intestine
Bile
Duct
Stool

Figure 1. 2.

Copper metabolism in a human cell. Schematic representation showing the distribution of copper in a human cell. Copper enters the cell through the copper transporter Ctr1 and is bound to the three metallochaperones or to metallothioneines. Cox17 delivers copper to the mitochondria. The copper chaperone for superoxide dismutase (CCS) delivers copper to Cu/Zn-SOD1 (SOD1). Atox1 delivers copper to the *trans*-Golgi network where the Wilson disease protein (WNDP) and the Menkes disease protein (MNKP) transport copper across the membrane for incorporation into copper dependent enzyme ceruloplasmin. Under elevated copper conditions WNDP and MNKP traffic to vesicular compartments and the plasma membrane to export copper from the cell.

Figure 1. 2.

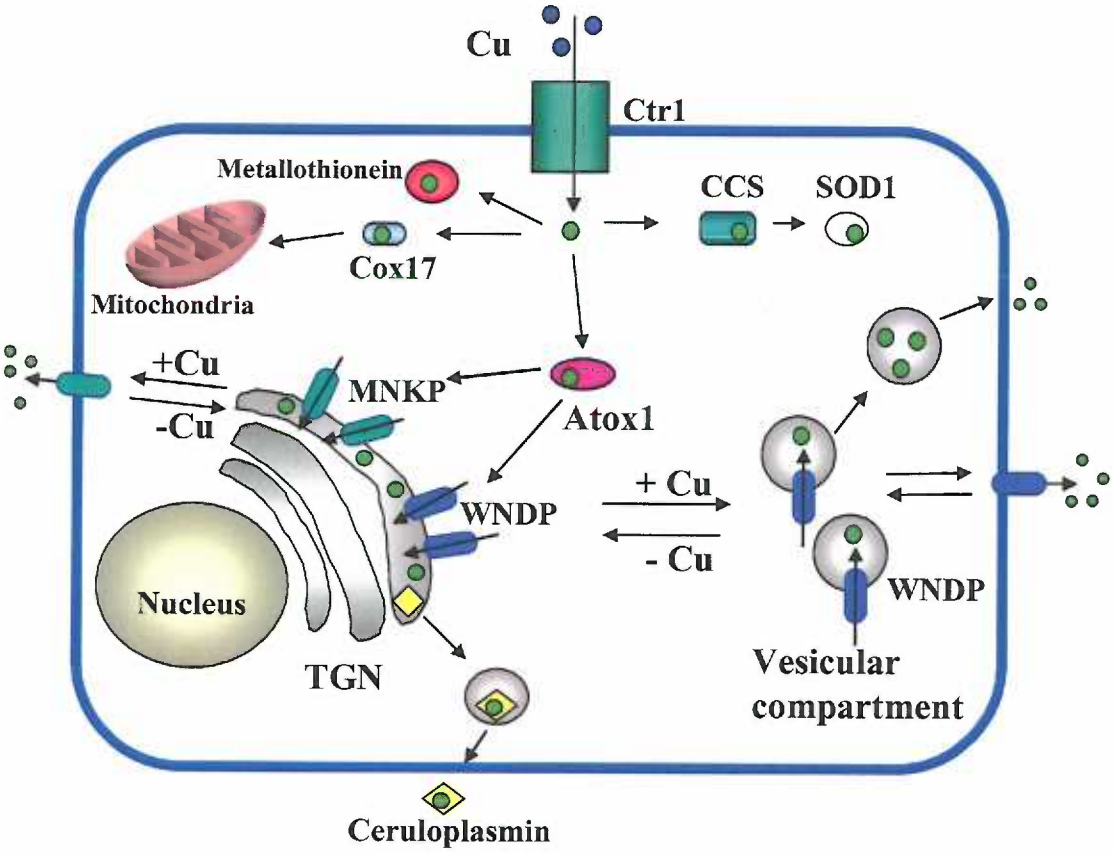
Cu
Ctr1
Metallothionein
CCS
SOD1
Cox17
Mitochondria
+Cu
-Cu
MNKP
Atox1
WNDP
+ Cu
- Cu
Nucleus
TGN
WNDP
Vesicular
compartment
Ceruloplasmin

Figure 1. 3.

The copper chaperones Atx1 and Atox1 have many similarities. *A,* sequence alignment of the yeast chaperone Atx1 and the human chaperone Atox1. The MTCxGC motif is shown in blue with the copper-binding cysteines shown in red. The conserved lysine in the KTGK motif is shown in orange. *B,* ribbon model showing the NMR solution structures of apo- and Cu-bound Atox1 (1TL4 and 1TL5, respectively). The two structures are orientated such that the α_1-helix is in the same position for each model. The α-helices are in blue and the β-sheets are in green. The two cysteine residues (red) in the CxxC motif are coordinating the copper atom (light blue). The conserved lysine is shown in orange.

Figure 1. 3.

A)

```
Atox1    MPKHEFSVDMTCGGCAEAVSRVLNKLG-GVK-YDIDLPNKKVCIESEHSMDTLLATLKKTG TVSYLGLE
Atx1  MAEIKHYQFNVVMTCSGCSGAVNKVLTKLEPDVSKIDISLEKQLVDVYTTLPYDFILEKIKKTG EVRS-GKQL
```

B)

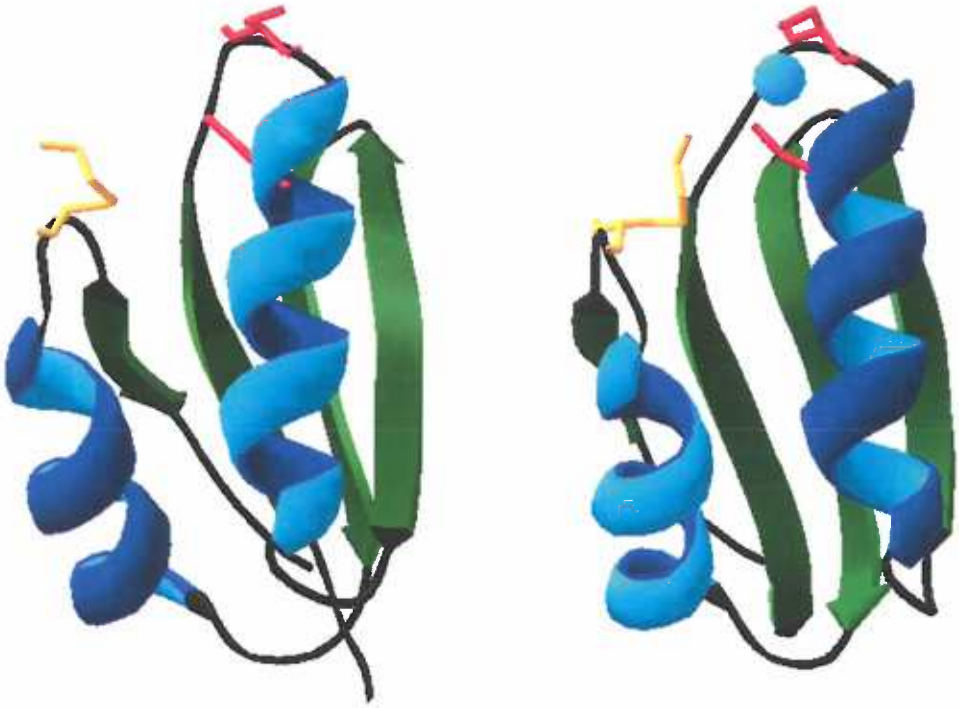

Apo-Atox1 **Cu-Atox1**

Figure 1. 4.

Two-dimensional model of the Wilson disease protein. The schematic shows the sequence motifs important for essential function of a human copper-transporting P-type ATPase. The blue ovals with the CxxC motif in white represent the six metal-binding sites in the N-WNDP copper-binding domain with the number of each MBS shown in purple. The CPC motif present in transmembrane domain 6 is shown in yellow and the invariant aspartate critical for catalytic phosphorylation is highlighted in red.

Figure 1. 4.

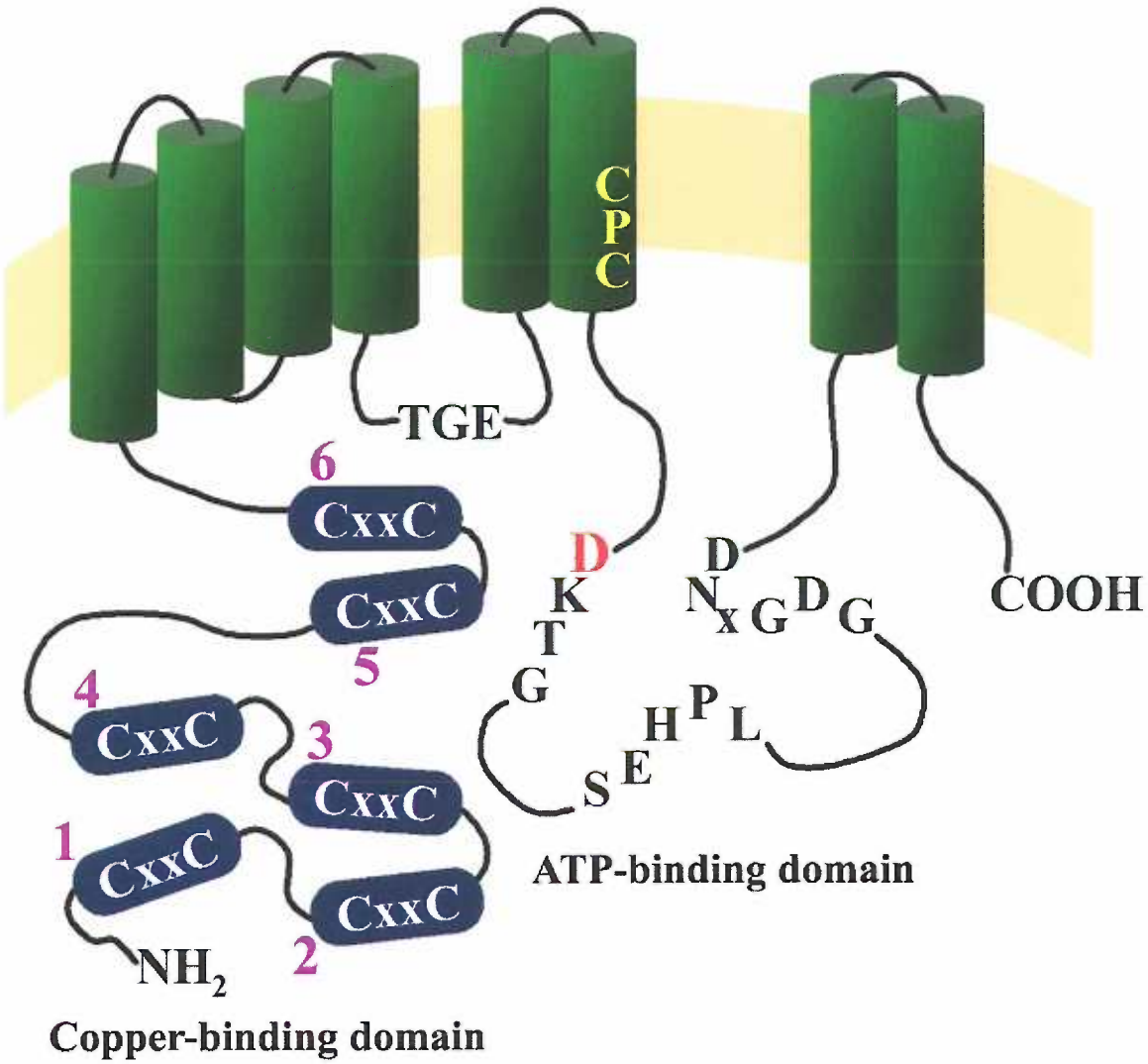
C
P
C
TGE
6
CxxC
CxxC
5
4
CxxC
3
CxxC
1
CxxC
CxxC
2
NH2
Copper-binding domain
D
K
T
G
S
E
H
P
L
ATP-binding domain
D
Nx
G
D
G
COOH

Figure 1. 5.

Structural characteristics of the N-WNDP, N-MNKP, and Ccc2p metal-binding sites. *A,* sequence alignment of the six MBS of N-WNDP and N-MNKP and the two MBS of Ccc2p. Each MBS sequence contains 69 amino acid residues. The blue stretch of residues highlights the GMT/HCxxCxxxIE copper-binding motif where the copper coordinating cysteines are shown in purple. The conserved phenylalanine is shown in green. The unique sequence characteristics of MBS3 of N-WNDP and N-MNKP are also identified with the histidine in the copper-binding motif in red and the proline motif highlighted in cyan. *B,* Ribbon model showing the NMR solution structures of apo- and Cu-bound N-MNKP2 (1S6O and 1S6U, respectively). The two structures are orientated such that the α_1-helix is in the same position for each model. The α-helices are in blue and the β-sheets are in dark green. The two cysteine residues (purple) in the CxxC motif are coordinating the copper atom (light blue). The conserved phenylalanine is shown in light green.

Figure 1. 5.

A)

```
WNDP MBS1   ATSTVRILGM TCQSCVKSIE DRISNLKGII SMKVSLEQGS ATVKYVPSVV CLQQVCHQIG DMGFEASIA
WNDP MBS2   AVVKLRVEGM TCQSCVSSIE GKVRKLQGVV RVKVSLSNQE AVITYQPYLI QPEDLRDHVN DMGFEAAIK
WNDP MBS3   VTLQLRIDGM HCKSCVLNIE ENIGQLLGVQ SIQVSLENKT AQVKYDPSCT SPVALQRAIE ALP-FGNFK
WNDP MBS4   STTLIAIAGM TCASCVHSIE GMISQLEGVQ QISVSLAEGT ATVLQNPSVI SPEELRAAIE DMGFEASVV
WNDP MBS5   QKCFLQIKGM TCASCVSNIE RNLQKEAGVL SVLVALMAGK AEIKYDPEVI QPLEIAQFIQ DLQFEAAVM
WNDP MBS6   GNIELTITGM TCASCVHNIE SKLTRTNGIT YASVALATSK ALVKFDPEII GPRDIIKIIE EIGFHASLA

MNKP MBS1   NSVTISVEGM TCNSCVWTIE QQIGKVNGVH HIKVSLEEKN ATIIYDPKLQ TPKTLQEAID DMGFDAVIH
MNKP MBS2   VVLKMKVEGM TCHSCTSTIE GKIGKLQGVQ RIKVSLDNQE ATIVYQPHLI SVEEMKKQIE AMGFPAFVK
MNKP MBS3   STATFIIDGM HCKSCVSNIE STLSALQYVS SIVVSLENRS AIVKYNASSV TPESLRKAIE AVSFGLYRV
MNKP MBS4   QETVINIDGM TCNSCVQSIE GVISKKPGVK SIRVSLANSN GTVEYDPLLT SPETLRGAIE DMGFDATLS
MNKP MBS5   SKCYIQVTGM TCASCVANIE RNLRREEGIY SILVALMAGK AEVRYNPAVI QPPMIAEFIR ELGFGATVI
MNKP MBS6   GVLELVVRGM TCASCVHKIE SSLTKHRGIL YCSVALATNK AHIKYDPEII GPRDIIHTIE SLGFEASLV

Ccc2 MBS1   REVILAVHGM TCSACTNTIN TQLRALKGVT KCDISLVTNE CQVTYDNEVT ADSIKEIIED -CGFDCEIL
Ccc2 MBS2   KEGLLSVQGM TCGSCVSTVT KQVEGIEGVE SVVVSLVTEE CHVIYEPSKT TLETAREMIE DCGFDSNII
```

B)

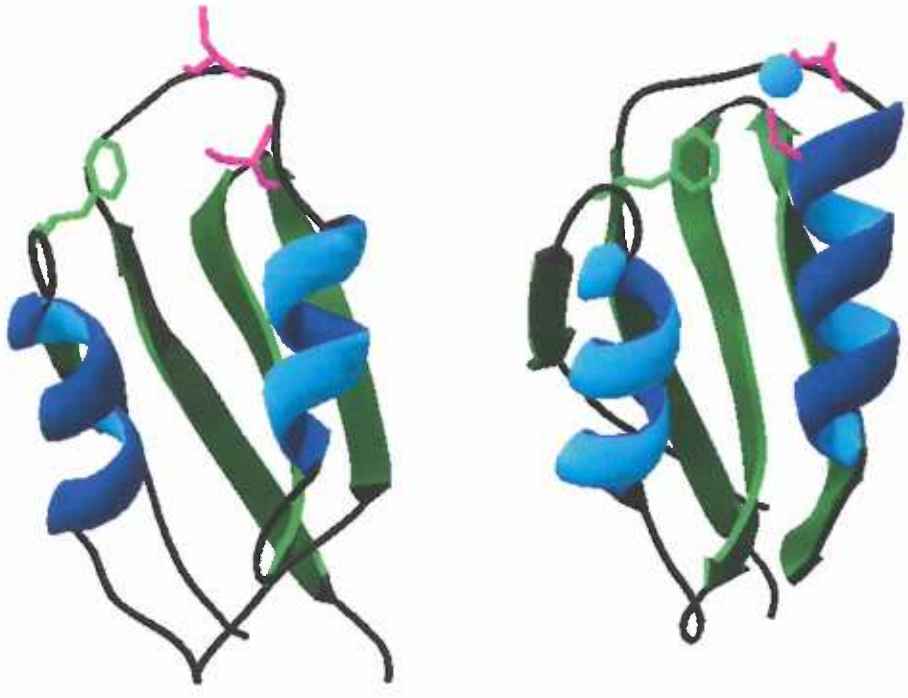

Apo-N-MNKP2 **Cu-N-MNKP2**

Chapter 2

Metallochaperone Atox1 Transfers Copper to the N-Terminal Domain of the Wilson's Disease Protein and Regulates Its Catalytic Activity

Walker, J. M., Tsivkovskii, R., and Lutsenko, S. (2002) *J Biol Chem 277*, 27953-9.

2. 1: Summary

Copper is essential for growth and development of mammalian cells. The key role in the intracellular distribution of copper belongs to the recently discovered family of metallochaperones and to copper-transporting P-type ATPases. Mutations in the ATPase ATP7B, the Wilson's disease protein (WNDP), lead to intracellular accumulation of copper and severe hepatic and neurological abnormalities. Several of these mutations were shown to disrupt protein-protein interactions between WNDP and the metallochaperone Atox1, suggesting that these interactions are important for normal copper homeostasis. To understand the functional consequences of the Atox1-WNDP interaction at the molecular level, we produced recombinant Atox1 and characterized its effects on WNDP. We demonstrate that Atox1 transfers copper to the purified N-terminal domain of WNDP (N-WNDP) in a dose-dependent and saturable manner. A maximum of 6 copper atoms can be transferred to N-WNDP by the chaperone. Furthermore, incubation of copper-Atox1 with the full-length WNDP leads to stimulation of the WNDP catalytic activity, providing strong evidence for the direct effect of Atox1 on the function of this transporter. Our data also suggest that Atox1 can regulate the copper-occupancy of WNDP. Incubation with apo-Atox1 results in removal of copper from the metallated N-WNDP and apparent down-regulation of WNDP activity. Interestingly, at least one copper atom remains tightly bound to N-WNDP even in the presence of excess apo-Atox1. We suggest that this incomplete reversibility reflects the functional non-equivalency of the metal-binding sites in WNDP and speculate about the intracellular consequences of the reversible Atox1-mediated copper transfer.

2. 2: Introduction

Copper is a trace element that has a dual role in human physiology. It is essential for normal cell metabolism serving as a cofactor to various enzymes involved in cellular processes as diverse as respiration, antioxidant defense, neurotransmitter biosynthesis, and iron homeostasis. At the same time excess copper is toxic to the cell, therefore the intracellular copper concentration is tightly controlled. Recent studies in yeast indicate that the amount of free copper in eucaryotic cells is negligible and that copper, after being transported into the cell, quickly becomes bound to various carriers (42). Among these carriers, the key role in further intracellular distribution of copper belongs to a recently discovered family of copper chaperones. These proteins temporarily sequester free copper while delivering it to specific target proteins throughout the cell (127-129).

Human copper chaperone Atox1 (also known as HAH1) is a small cytosolic protein that plays a key role in distribution of copper to the cell secretory pathway. In yeast, the Atox1 ortholog, Atx1, was shown to facilitate copper delivery to the copper-transporting P-type ATPase Ccc2, which then transports copper into the late Golgi compartment (41, 64). In mammalian cells, Atox1 was proposed to bring copper to the copper-transporting ATPases ATP7A and ATP7B, or the Menkes disease protein (MNKP) and the Wilson's disease protein (WNDP), respectively. MNKP and WNDP then utilize the energy of ATP hydrolysis to either translocate the metal into the lumen of the *trans*-Golgi network for incorporation into copper-dependent enzymes or to export excess copper out of the cell. Deletion of the Atox1 gene in mice leads to intracellular accumulation of copper and decreased activity of secreted copper-dependent enzymes,

such as tyrosinase, supporting the proposed role of Atox1 as a metal donor for the copper-transporting ATPases (82).

Although the important role of Atox1 for mammalian copper homeostasis was clearly demonstrated (82), the experimental data directly linking functions of the human chaperone Atox1 and the copper-transporting ATPases MNKP and WNDP are still lacking. Recent studies from several laboratories provided experimental evidence for physical interactions between Atox1 and the N-terminal domains of MNKP and WNDP (71, 83, 84). In addition, several mutations found in Wilson's disease patients were shown to disrupt the ability of WNDP to interact with Atox1, suggesting that this interaction was essential for normal copper homeostasis (83). Whether the protein-protein interactions lead to transfer of copper from Atox1 to either WNDP or MNKP has not yet been demonstrated. Most importantly, it remains unknown whether transfer of copper from the chaperone to the copper-transporting ATPases has a direct effect on activity of these transporters.

To address these important issues, we generated recombinant Atox1 and examined whether Atox1 can transfer copper to the N-terminal domain of WNDP (N-WNDP). We also determined the effect of Atox1 on the catalytic activity of WNDP using the full-length membrane-bound transporter. Finally, we characterized the reversibility of the Atox1-mediated transfer of copper and demonstrated that Atox1 can regulate the copper-occupancy and activity of WNDP. In this work, we focused on the functional interactions between Atox1 and WNDP; however our conclusions are likely to be applicable, at least in general, to the transfer of copper from Atox1 to MNKP, which is highly homologous to WNDP.

2. 3: Materials and Methods

Cloning, Expression, and Purification of Atox1. The Atox1 cDNA was excised from the previously generated pET24b-Atox1 plasmid using *NdeI* and *EcoRI* endonucleases and cloned into the pTYB12 vector (New England Biolabs) to produce the pTYB12-Atox1 construct (for detailed description of the construct see Figure 2. 1 and the Results section). This construct, encoding the fusion protein composed of Atox1, intein, and a chitin-binding domain, was then transformed into the *E. coli* strain BL21 (DE3).

The expression of the Atox1-containing fusion was induced with 0.5 mM isopropyl-β-D-thiogalactopyranoside (Roche) for 18 hours at room temperature. The cells were then harvested by centrifugation and resuspended in lysis buffer (25 mM Na_2HPO_4, 150 mM NaCl, pH 7.5) containing one Complete EDTA-free protease inhibitor mixture tablet (Roche). The cells were passed through a French Press (Sim-Aminco) at 16,000 psi and the lysate was cleared by centrifugation at 30,000 x *g* for 30 minutes. The soluble fraction of the lysate was passed through a chitin-bead column (New England Biolabs), allowing the Atox1-fusion to bind to the resin via its chitin-binding domain. The resin was then washed with 30 column volumes of lysis buffer. To induce the intein-mediated cleavage the beads were incubated in 50 mM dithiothreitol (DTT), 25 mM Na_2HPO_4, pH 8.15, 150 mM NaCl, for 40 hours at room temperature. Atox1 was then collected in elution fractions and dialyzed against lysis buffer at 4°C overnight to remove DTT. Protein concentration was measured using the Bradford assay (130) and protein purity was determined by a 15% Laemmli gel (131). The identity of Atox1 was confirmed by mass-spectrometry and by immunochemistry using an Atox1-

specific antibody (Figure 2. 6). The yield of purified soluble Atox1 was ~ 2 mg of protein from a liter of cell culture.

Preparation of the copper-bound Atox1. $CuCl_2$ was mixed with glutathione at a 1:10 molar ratio and the mixture was then added to Atox1 at copper to protein ratio of 1:1. Following a 10 min incubation at room temperature, Atox1 was extensively dialyzed against lysis buffer and the stoichiometry of the copper-Atox1 complex was determined by a bicinchoninic acid (BCA) assay, where absorbance of a Cu(I)-BCA complex was monitored at 562 nm (132), or by atomic absorption (both methods produced very similar results). Electron paramagnetic resonance (EPR) measurements were carried out on one of the samples, which had a typical copper-binding stoichiometry of 0.8 Cu/Atox1. EPR spectra were recorded on a Bruker E500 X-Band EPR spectrometer with a Super X microwave bridge and a Super High Q resonator. The instrument was equipped with a liquid nitrogen flow cryostat. No Cu^{2+} signal was detected, suggesting that copper bound to Atox1 was in the reduced Cu^{1+} form (Figure 2. 7).

Transfer of copper from Atox1 to the N-terminal domain of WNDP (N-WNDP). N-WNDP used in this study was a fusion of the first 606 amino acid residues of WNDP and the maltose binding protein. N-WNDP was expressed and purified using affinity chromatography on amylose resin as described earlier (105). For copper-transfer experiments, N-WNDP bound to amylose resin (New England BioLabs) was washed with 30 column volumes of assay buffer (20 mM Bis-Tris-propane pH 7.0, 200 mM KCl, 5 mM $MgCl_2$) and then incubated with 100 μM DTT for 10 minutes at room temperature. After an additional wash with 10 column volumes of assay buffer various amounts of soluble copper-bound Atox1 in assay buffer were added to the resin and incubated with

N-WNDP for 10 minutes at room temperature. (The amount of N-WNDP bound to the amylose resin was determined from a preliminary analytical purification of a portion of the lysate). Atox1 was then washed off the resin with assay buffer, followed by elution of N-WNDP with 10 mM maltose in the assay buffer. The protein concentration of each sample was measured using the Bradford assay and the amount of copper bound to each protein was estimated using the BCA assay.

The presence of Atox1 in the N-WNDP elution fractions was examined by quantitative Western blot analysis. From the elution fractions, 2 μg of total protein were run on a Tris-Tricine gel (133) in parallel with known amounts of purified Atox1 used to generate a calibration curve. The proteins were transferred to a Immobilon-P membrane (Millipore) and then immunostained using polyclonal anti-Atox1 antibody at 1:20,000 dilution. The amount of Atox1 in the fractions was quantified by densitometry (Bio-Rad) and compared to the calibration curve.

Reverse Copper Transfer from N-WNDP to Atox1. N-WNDP was loaded with copper *in vivo* by growing the N-WNDP-expressing cells in the presence of 500 μM $CuCl_2$, as previously described (105). Copper-loaded N-WNDP was bound to amylose resin and washed as described above. The increasing amounts of apo-Atox1 were then added to the resin and the mixture was incubated for 10 minutes at room temperature. Atox1 was washed off the resin followed by elution of N-WNDP with the maltose-containing buffer, and the amount of copper bound to N-WNDP and Atox1 was analyzed. In addition, the accessibility of the cysteines in N-WNDP after removal of copper by apo-Atox1 was examined using chemical labeling with the residue-specific fluorescent reagent 7-diethylamino-3-(4'-maleimidylphenyl)-4-methylcoumarin (CPM) (Molecular

Probes). A sixty-fold molar excess of CPM was added to N-WNDP and the reaction mixture was incubated for 2.5 minutes at room temperature in the dark. The reaction was quenched with an excess of β-mercaptoethanol, and the CPM-labeled protein was electrophoresed on a 10% SDS-PAGE. The intensity of labeling was quantified using densitometry of fluorescent bands. The gels were then stained with Coomassie Blue, and the amount of protein in the N-WNDP bands was determined by a second round of densitometry. The fluorescence intensity was then normalized to the N-WNDP protein levels.

The effect of the copper-Atox1 complex on the catalytic activity of WNDP. The full-length WNDP was expressed in *Sf9* cells using the baculovirus-mediated infection, and the membrane fraction containing WNDP was isolated as previously described (100). Apo-Atox1 and copper-bound Atox1 were prepared as described above and were dialyzed overnight against the assay buffer, containing 100 μM of freshly prepared reducing reagent tris-(2-carboxyethyl)phosphine hydrochloride (TCEP, Sigma), prior to incubation with WNDP.

For the Atox1-mediated reactivation of WNDP, 50 μg of total membrane protein was resuspended in 200 μl of ice-cold assay buffer, containing 100 μM TCEP. The copper chelator bathocuproine disulfonate (BCS, ICN Biomedicals) was added to a final concentration of 100 μM. After a 15 min incubation on ice, the membrane protein was pelleted by centrifugation at 20,000 x *g* for 5 min, and BCS was removed. The membrane pellets were resuspended in 200 μl assay buffer containing 100 μM TCEP, and the copper-Atox1 complex was added to the mixture at concentrations indicated in the legend to Figure 2. 3. After a 10 min incubation at room temperature, the samples

were placed on ice for 5 min, radioactive [γ-^{32}P]ATP (5 μCi, specific activity 20 mCi/μmol) was added to 1 μM final concentration, and the reaction mixture was incubated on ice for additional 4 min.

The reaction was stopped by addition of 50 μl of ice cold 1 mM NaH_2PO_4 in 50% trichloroacetic acid (TCA) and then centrifuged for 10 min at 20,000 x *g*. The protein pellet was washed once with ice-cold water, resuspended in 40 μl of sample buffer (5 mM Tris-PO_4, pH 5.8, 6.7M Urea, 0.4M DTT, 5% SDS) and loaded on the acidic version of a 7.5% Laemmli gel (134). After electrophoresis, the gels were fixed in 10% acetic acid for 10 min and dried on blotting paper. The dried gels were exposed either overnight to the Molecular Imaging screen CS (Bio-Rad) or for several hours at – 80°C to Kodak BioMax MS film, and the intensity of the bands was quantified using Bio-Rad Molecular Imager or Bio-Rad densitometer. Then, the dried gels were rehydrated, stained with Commassie Blue and the amount of protein in the WNDP-related bands was determined by a second round of densitometry. The ^{32}P-incorporation into WNDP was then normalized to the WNDP protein levels.

The results of the initial experiments with apo-Atox1 showed significant variability. This was most likely due to rapid oxidation of the apo-chaperone, since storage of apo-Atox1 decreased its effects on WNDP and N-WNDP, while subsequent treatment of apo-Atox1 with reducing reagent TCEP restored the chaperone function. To make the results reproducible additional treatment of apo-Atox1 with TCEP was carried out immediately before the reactions with either N-WNDP or the full-length WNDP.

Inactivation of the catalytic phosphorylation of WNDP by apo-Atox1. 50 μg of the membrane preparation containing WNDP was resuspended in 200 μl of the assay

buffer containing 100 μM TCEP, and apo-Atox1 was added to final concentrations indicated in the Figure 2. 5 legend. Following a 10 min incubation at room temperature, the membranes were sedimented by centrifugation at 20,000 x *g* for 5 min. The membrane pellets were then resuspended in 200 μl of assay buffer and incubated on ice for 5 min. Radioactive [γ-^{32}P]ATP (5 μCi, specific activity 20 mCi/μmol) was added to 1 μM final concentration and the analysis of catalytic phosphorylation of WNDP was carried out as described above. The generation and characterization of the D1027A mutant of WNDP, which lacks catalytic activity and was used in these experiments as a background control, had been described previously (100).

2. 4: Results

Expression and purification of Atox1. To simplify purification of Atox1 and to obtain the purified protein without a large affinity tag, we generated an expression construct for Atox1 using a pTYB12 vector. In this construct, Atox1 was fused with an intein and a chitin binding domain (CBD) (Figure 2. 1*A*). This enabled us to purify the expressed Atox1-CBD-intein fusion by affinity chromatography on chitin beads, and then excise Atox1 from the fusion through the intein-mediated protein cleavage, leaving CBD and intein associated with the beads. The procedure adds three amino acid residues to the amino terminus of Atox1.

Figure 2. 1*B* illustrates a typical experiment on expression and purification of Atox1. Induction of expression with isopropyl-β-D-thiogalactopyranoside leads to appearance of the 70 kDa protein (Figure 2. 1*B*, *lane 2*), consistent with the expression of the Atox1-CBD-intein fusion. The treatment of the fusion protein bound to chitin beads

with DTT releases highly pure Atox1 into the solution (Figure 2. 1*B*, *lane 5*). Judging from the ratio between the uncleaved Atox1 fusion and the CBD-intein fragment, which remains associated with the resin, the efficiency of the cleavage is ~80% (Figure 2. 1*B*, *lane 6*). The addition of the copper-glutathione complex to purified Atox1 (see "Materials & Methods") generates the metallated chaperone with a typical stoichiometry of 0.85 ± 0.1 copper atoms/Atox1.

Copper transfer from Atox1 to N-WNDP. To determine whether Atox1 can transfer copper to WNDP, we utilized purified N-WNDP bound to amylose resin and a soluble copper-Atox1 complex (Cu-Atox1). Cu-Atox1 was passed through the resin containing bound N-WNDP, the resin was washed, and N-WNDP was then eluted from the resin using the maltose-containing buffer (Figure 2. 2*A*). The amount of protein and copper in each elution fraction was analyzed. This protocol allowed for quick separation of Atox1 and N-WNDP and easy determination of copper bound to both proteins after the transfer reaction.

In agreement with our earlier results (105), control N-WNDP eluted from the amylose resin did not contain measurable amounts of copper. In contrast, when N-WNDP was first preincubated with Cu-Atox1 and then eluted, copper was detected in the N-WNDP-containing fractions (Figure 2. 2*A*, fractions 29 and 30), suggesting that copper was transferred from Atox1 to N-WNDP.

It was previously shown that Atox1 interacted with N-WNDP and that these interactions could be detected using a protocol similar to the procedure utilized for our transfer studies (84). Therefore it was possible that in our experiments copper co-eluted with N-WNDP as a result of association of Atox1 with N-WNDP and not because of

copper transfer. To eliminate this possibility, we examined the presence of Atox1 in the N-WNDP containing elution fractions. No Atox1 was detected in the N-WNDP containing fractions analyzed by gel electrophoresis and stained with Coomassie Blue. However, Atox1 was observed by immunostaining, indicating that small amounts of protein remained associated with N-WNDP after washes of the resin (Supplemental Figure 2. 6). The amount of Atox1 that co-elutes with N-WNDP was determined using quantitative Western blot analysis and purified Atox1 as a standard. These calculations indicate that Atox1 is present in the N-WNDP elution fractions at a molar ratio of ~0.1 Atox1/N-WNDP and can account for 5-10% total copper bound to N-WNDP (Supplemental Table 2. 1). Thus, we conclude that incubation of Atox1 with N-WNDP leads to a transfer of copper from the chaperone to its target.

To characterize the transfer reaction in more detail, the experiments were repeated using a wide range of molar ratios of Atox1, with a 0.85 ± 0.1 copper to protein stoichiometry, and N-WNDP. As shown in Figure 2. 2*B*, incubation of N-WNDP with increasing amounts of Cu-Atox1 leads to a dose-dependent and saturable transfer of copper to N-WNDP; up to 6 copper atoms per N-WNDP can be transferred when a 30-40 fold molar excess of Cu-Atox1 over N-WNDP is present. N-WNDP is known to contain six metal-binding sites, therefore it appears that Atox1 can deliver copper to all metal-binding sites in N-WNDP. A further increase in the amount of added Cu-Atox1 does not lead to additional binding of copper to N-WNDP consistent with the idea that the chaperone controls delivery of copper to specific sites.

In N-WNDP, copper is coordinated by Cys residues in the highly conserved GMTCxxC sequence motifs. Binding of copper to N-WNDP in a cell protects these Cys

residues against labeling with the fluorescent coumarine maleimide CPM (105). Similar decrease in fluorescent labeling of N-WNDP was observed following copper transfer from Cu-Atox1 to N-WNDP (Supplemental Figure 2. 8), suggesting that copper was transferred to Cys residues.

The effect of Atox1 on WNDP activity. Recently, we demonstrated that the full-length WNDP expressed in insect cells was catalytically active and was able to form a phosphorylated acyl-phosphate intermediate when incubated with ATP (100). This catalytic reaction is inhibited by the copper chelator bathocuproine disulfonate (BCS); addition of copper to the inhibited enzyme restores its activity. We utilized this assay to test whether Cu-Atox1 could reactivate the BCS-treated WNDP by transferring copper to the transporter. The membrane-bound WNDP was incubated with either apo-Atox1 or Cu-Atox1, [γ-^{32}P]ATP was then added and the ability of WNDP to form an acyl-phosphate intermediate was analyzed by measuring the amount of radioactivity associated with the WNDP band on an acidic polyacrylamide gel. As shown in Figure 2. 3*A*, addition of Cu-Atox1 to the BCS-treated WNDP leads to re-activation of the enzyme, indicating that Cu-Atox1 transfers copper to the WNDP metal-binding sites, which are essential for stimulation of its catalytic phosphorylation. The lack of WNDP reactivation by apo-Atox1 confirms that copper transfer, and not mere interaction with Atox1, is necessary for stimulation of the WNDP activity (Figure 2. 3*A*).

In the copper-transfer experiments shown in Figure 2. 2, purified N-WNDP was the only protein that could accept copper from Atox1. In contrast, in the membrane preparations used for the reactivation experiments, WNDP represents 2% or less of the total protein (our data). Thus, it was interesting to compare the ability of Atox1 to

transfer copper to purified N-WNDP with its ability to activate WNDP in the presence of a large excess of other proteins. To do that, the amount of WNDP in the membrane fraction was estimated using quantitative Western blot analysis. Then, Atox1 was added to the BCS-treated WNDP at the same molar ratios that were used previously for the copper-transfer experiments with purified N-WNDP.

As shown in Figure 2. 3*B*, the effect of copper-Atox1 on catalytic activity was dose-dependent and saturable with maximum reactivation reached in the presence of a 20-30 fold molar excess of Atox1 over WNDP. Thus, Atox1 was at least as efficient in activating WNDP in the presence of a large excess of unrelated proteins, as it was in transferring copper to purified N-WNDP. Also, we compared the efficiency of Cu-Atox1 in stimulation of the WNDP activity with respect to free copper. As shown in Figure 2. 3*B*, Cu-Atox1 activated WNDP with EC_{50} equal to 0.18 ± 0.07 μM. Free copper added in the presence of 100 μM ascorbate stimulated the WNDP phosphorylation with comparable $EC_{50} = 0.17 \pm 0.04$ μM. (The effective concentration of free copper required to activate WNDP in these experiments was lower than the previously reported value of 1.5 ± 0.6 μM (100). This difference is due to modification in the experimental conditions, i.e. the experiments described in this manuscript were carried out at pH 7.0 and room temperature, while previous studies were done at pH 6.0 on ice).

The reverse transfer of copper from N-WNDP to Atox1. It has been proposed that copper transfer from the chaperone to N-WNDP could be reversible (84). In fact, a reversible copper exchange was demonstrated using the yeast copper-chaperone Atx1 and a purified single metal-binding repeat of the copper-transporting ATPase Ccc2 (65). However, it remains unknown whether apo-Atox1 can remove copper from WNDP and

how the presence of the multiple copper-binding sites in this protein (a situation typical for the eucaryotic copper-ATPases) affects this process. To determine whether copper could be transferred from N-WNDP back to Atox1, N-WNDP loaded with 5-6 copper atoms in cell culture (105) was bound to amylose resin and then incubated with 30-40 fold molar excess of purified apo-Atox1.

As shown in Figure 2. 4*A*, addition of apo-Atox1 to the N-WNDP-containing resin leads to co-elution of the chaperone and copper, indicating that apo-Atox1 was able to strip copper from N-WNDP. However, some copper remained bound to N-WNDP suggesting that the reverse transfer was partial. To verify these conclusions, the experiments were repeated using a wide range of molar ratios of apo-Atox1 and copper-bound N-WNDP. As shown in Figure 2. 4*B*, addition of increasing amounts of apo-Atox1 to N-WNDP resulted in a saturable decrease in the amount of copper bound to N-WNDP. Interestingly, 3-4 copper atoms can be stripped from N-WNDP using a fairly small excess of apo-Atox1 over N-WNDP, whereas the remaining copper seems to be much less exchangeable. In fact, 1.11 ± 0.11 copper atoms remained associated with N-WNDP even after incubation with a large excess of apo-Atox1, suggesting that one metal-binding site had a much lower affinity for Atox1 or was much less exposed.

It was interesting to determine whether removal of copper by apo-Atox1 leaves the Cys residues in N-WNDP in the reduced state and thus available for subsequent loading with copper. To examine the accessibility of cysteines, we carried out the fluorescent labeling of N-WNDP before and after incubation of N-WNDP with increasing amounts of apo-Atox1. Copper bound to N-WNDP protects cysteine residues in the metal-binding sites against labeling with the fluorescent coumarine maleimide

CPM (Figure 2. 4*C*) (105). After incubation with apo-Atox1 copper is removed from N-WNDP; the decrease in copper binding is associated with the increase in the fluorescent labeling of Cys in N-WNDP (Figure 2. 4*C*). The availability of Cys residues for labeling with the fluorescent probe indicates that after copper is removed by the chaperone, these residues remain reduced and available for a new round of copper binding.

Apo-Atox1 down-regulates WNDP activity. We have previously proposed that copper binding to N-WNDP regulates the functional activity of WNDP (100). The ability of apo-Atox1 to remove copper from N-WNDP suggested that treatment of the fully active transporter with apo-Atox1 may decrease the copper-occupancy of WNDP and consequently reduce its catalytic activity. To test this hypothesis, the fully active membrane-bound WNDP was incubated with increasing concentrations of apo-Atox1, and subsequently, the chaperone was separated from WNDP by centrifugation. WNDP was resuspended in assay buffer and its ability to undergo catalytic phosphorylation was measured using [γ-^{32}P]ATP. As shown in Figure 2. 5, pre-incubation with apo-Atox1 leads to a concentration dependent and saturable reduction of the WNDP activity presumably due to reverse transfer of copper from the N-terminal domain of WNDP to Atox1. Interestingly, even after treatment with a large excess of apo-Atox1 WNDP retains significant portion of its activity (~50%), suggesting that the apo-Atox1 removes some but not all coppers from WNDP leading to down-regulation of the enzyme.

2. 5: Discussion

With this work, we began characterization of the biochemical processes important for distribution of copper from the cytosol to the secretory compartment of human cells.

We demonstrate that the previously reported interaction between Atox1 and N-WNDP leads to transfer of copper from the chaperone to the copper-transporting ATPase and that a maximum of six copper atoms can be transferred from Atox1 to N-WNDP.

Furthermore, we found that addition of increasing amounts of Atox1 to the full-length WNDP led to a concurrent stimulation of the catalytic activity of WNDP measured through the formation of the phosphorylated intermediate. Significantly, this effect was observed using fairly low concentrations of Atox1 ($EC_{50} \approx 200$ nM). The presence of a large excess of various proteins in the membrane preparation did not interfere with the transfer reaction, suggesting that Cu-Atox1 specifically targeted N-WNDP and activated the transporter.

Altogether, our results provide the first experimental demonstration of the direct effect of Atox1 on WNDP function and illustrate that Atox1 can indeed act as a physiological copper donor for this human copper-transporting ATPase. Although it is still technically difficult to make precise quantitation of how many copper atoms need to be transferred to the full-length WNDP to induce phosphorylation, it is clear that the Atox1-mediated copper transfer correlates with activation of WNDP. In a cell, such activation would most likely lead to copper transport from the cytosol into the secretory pathway of the cell.

It seems particularly interesting that Atox1 can not only deliver copper to N-WNDP but can also regulate its metal-occupancy through removal of copper. It is possible that in a cell, the ratio of copper-bound and apo-chaperones would fluctuate depending on how much copper is taken up by the cell and how much of it is exported or utilized. Our results suggest that apo-chaperone is not simply an inert carrier waiting to

be occupied by copper. Instead, apo-Atox1 can remove copper from N-WNDP and decrease the activity of the full-length transporter, suggesting that both metallated and apo forms of Atox1 may contribute to regulation of WNDP.

It has been previously shown that the metal-binding sites in N-WNDP are functionally non-equivalent (135). Only one of them is necessary to sustain the copper-transport activity of WNDP (101, 135), while the other metal-binding sites in N-WNDP are likely to be involved in regulation of the transporter. Our results provide further evidence of distinct properties of the metal-binding sites in N-WNDP. In experiments with apo-Atox1, one copper atom remained bound to N-WNDP even when the chaperone was present in a large excess, suggesting that certain metal-binding site in N-WNDP was unavailable for interactions with Atox1. This conclusion is in apparent contradiction with the results of the forward transfer experiments, in which all the binding sites in N-WNDP were filled by copper using the copper-Atox1 complex.

There are two possible explanations for these results. First, it is possible that in the forward reaction, one of the metal-binding sites in N-WNDP is filled with copper indirectly, i.e. copper is transferred to this site not from Atox1 but from another metal-binding site in N-WNDP. Alternatively, in apo-N-WNDP all metal-binding sites could be available for interactions with the chaperone, while in the copper-bound N-WNDP some sites could be less exposed. This interpretation would be consistent with the results of recent studies from DiDonato *et al*, who demonstrated that binding of copper to N-WNDP induced conformational transitions in this protein (109). Experiments are currently underway to understand the sequence of the events during copper-transfer to N-

WNDP and to identify the site(s) that can retain copper in the presence of excess apo-chaperone.

It is also interesting that incubation of WNDP with apo-Atox1 lowers the WNDP activity to a certain level but does not lead to full inactivation of the transporter. This finding is in contrast to our earlier results demonstrating that the copper chelator BCS can eliminate WNDP activity (100). Apo-Atox1 interacts quite efficiently with WNDP. A dose-dependent curve for the chaperone shows its half-maximum effect at concentration of 1.0 ± 0.24 μM (Figure 2. 5), while the half-maximum effect of BCS on the WNDP activity was observed only in the presence of 50 μM chelator (100). It appears that apo-Atox1, unlike BCS, strips copper only from some, presumably "regulatory" metal-binding sites in WNDP thus down-regulating the enzyme, whereas the site(s) essential for the WNDP activity remains inaccessible to apo-chaperone probably because of steric hindrances.

The ability of Atox1 to alter the copper occupancy of N-WNDP and the activity of WNDP in an asymmetric fashion may have important physiological consequences. In a cell, changes in copper-occupancy of WNDP were proposed to affect the intracellular localization (109, 135), posttranslational modification (114), and activity of WNDP (100). Thus, Atox1 may play a key role in these events by controlling the amount of copper bound to the transporter and hence contribute to the regulation of the intracellular localization or posttranslational modification of WNDP while keeping the transporter active at a wide range of copper concentrations.

2. 6: Acknowledgements

Dr. Ruslan Tsivkovskii did the catalytic phosphorylation experiments. We thank Dr. N. Blackburn and Dr. M. Ralle for polyclonal antibody against Atox1 and for help with the EPR analysis of the copper-bound Atox1, Dr. L. David and Dr. A. McCormack for mass-spectroscopy of purified Atox1.

Figure 2. 1.

Schematic representation of the Atox1 fusion protein (A) and expression and purification of Atox1 using the pTYB12-Atox1 construct (B). *A*, the Atox1 cDNA was inserted into pTYB12 plasmid to produce a fusion protein, in which the intein and CBD were fused to the amino terminus of Atox1 (Atox1-CBD-intein). The DTT-stimulated self-cleavage occurs between Asn and Ala in a linker region as indicated by an arrow. *B*, expression of the Atox1-fusion in *E.coli* was induced with isopropyl-β-D-thiogalactopyranoside. Non-induced cells (*lane 1*), induced cells (*lane 2*), the soluble fractions (*lane 3*), and insoluble fractions (*lane 4*) were prepared. The soluble fraction was applied to chitin beads, and after extensive washing, Atox1 was eluted from the beads with DTT (*lane 5*). The Atox1-CBD-intein and the CBD-intein moiety were then eluted from the beads with NaOH to estimate the efficiency of cleavage (*lane 6*).

Figure 2. 1.

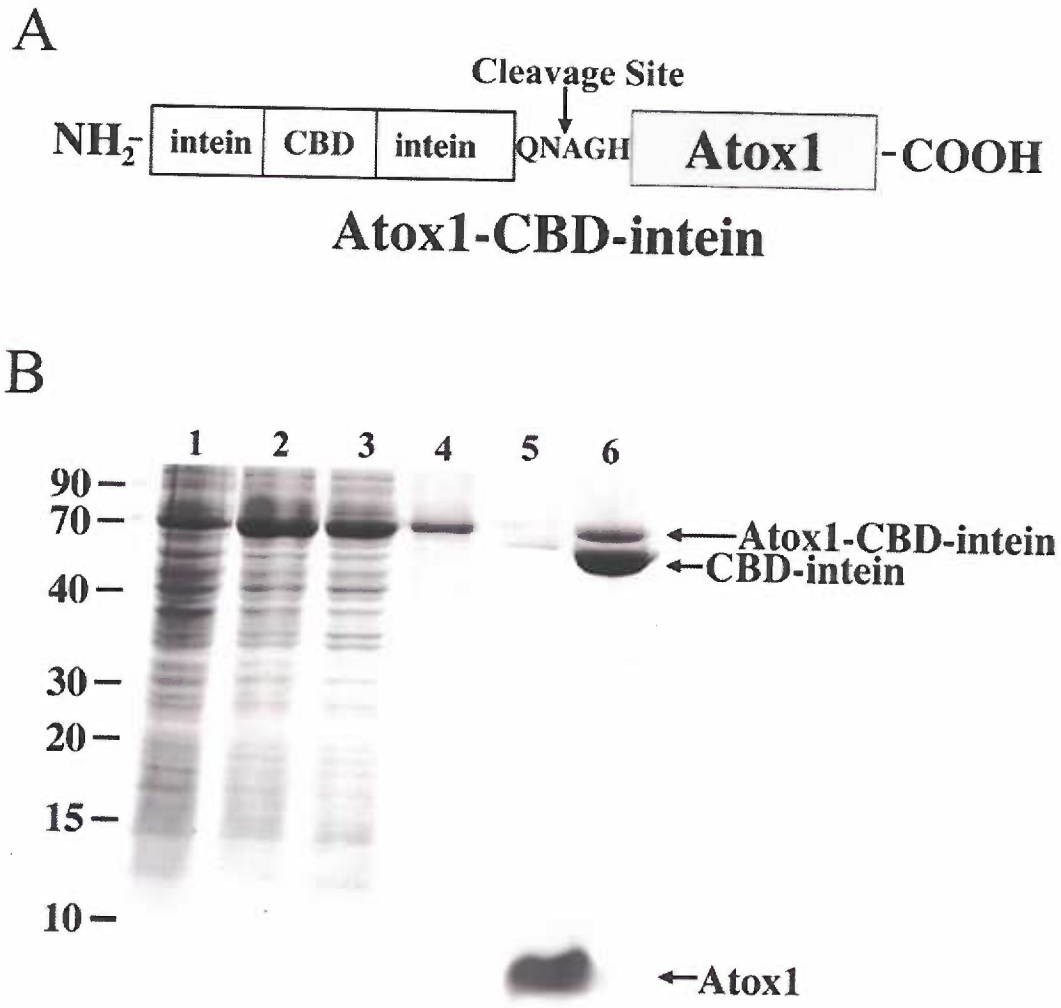
A
Cleavage Site
NH2-
intein
CBD
intein
QNAGH
Atox1
-COOH
Atox1-CBD-intein
B
1
2
3
4
5
6
90
70
40
30
20
15
10
Atox1-CBD-intein
CBD-intein
Atox1

Figure 2. 2.

Copper transfer from copper-Atox1 to N-WNDP. *A*, typical distribution of copper (□) and protein (●) in the elution fractions during a copper transfer experiment. The *arrows* indicate the time points at which chaperone (Cu-Atox1) or maltose-containing elution buffer were added to the N-WNDP containing resin. *B*, dose-dependent transfer of copper from the chaperone to N-WNDP. The results of five experiments are shown; the solid curve is the theoretical hyperbolic curve generated using SigmaPlot software, the R^2-factor is 0.90.

Figure 2. 2.

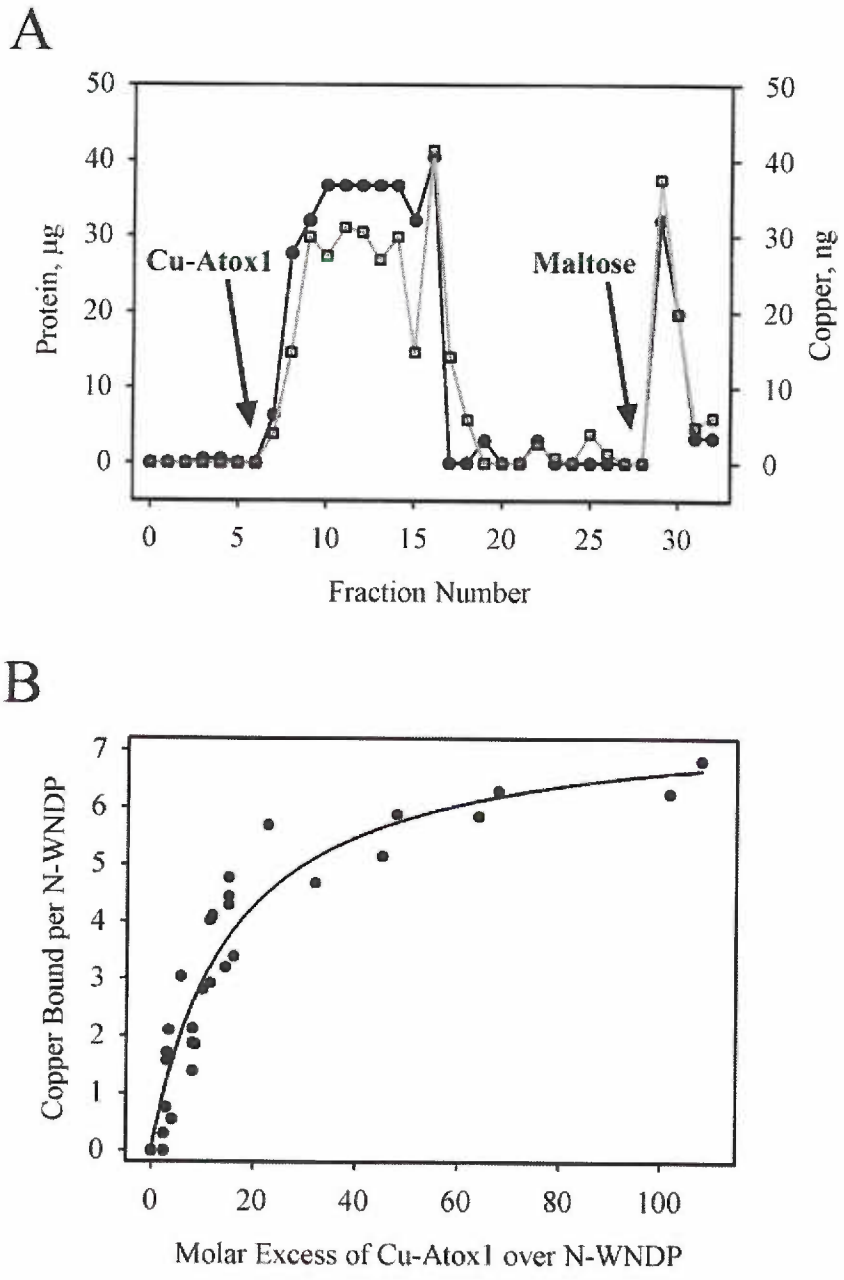
A
Protein, µg
Copper, ng
Cu-Atox1
Maltose
Fraction Number
B
Copper Bound per N-WNDP
Molar Excess of Cu-Atox1 over N-WNDP

Figure 2. 3.

The effect of Atox1 on catalytic activity of WNDP. *A*, WNDP was treated with or without BCS as described in the experimental procedures. BCS was then removed by centrifugation, WNDP was resuspended in the assay buffer and the same amounts of apo-Atox1 or Cu-Atox1 were added to the BCS-pretreated sample. The catalytic activity of WNDP was monitored by measuring the amount of radioactive acylphosphate intermediate as described in the text. Autoradiogram of a typical gel is shown. *B*, activation of the WNDP catalytic phosphorylation by Cu-Atox1 (●) and by free copper (Δ). The average of the densitometry data for five independent experiments is shown.

Figure 2. 3.

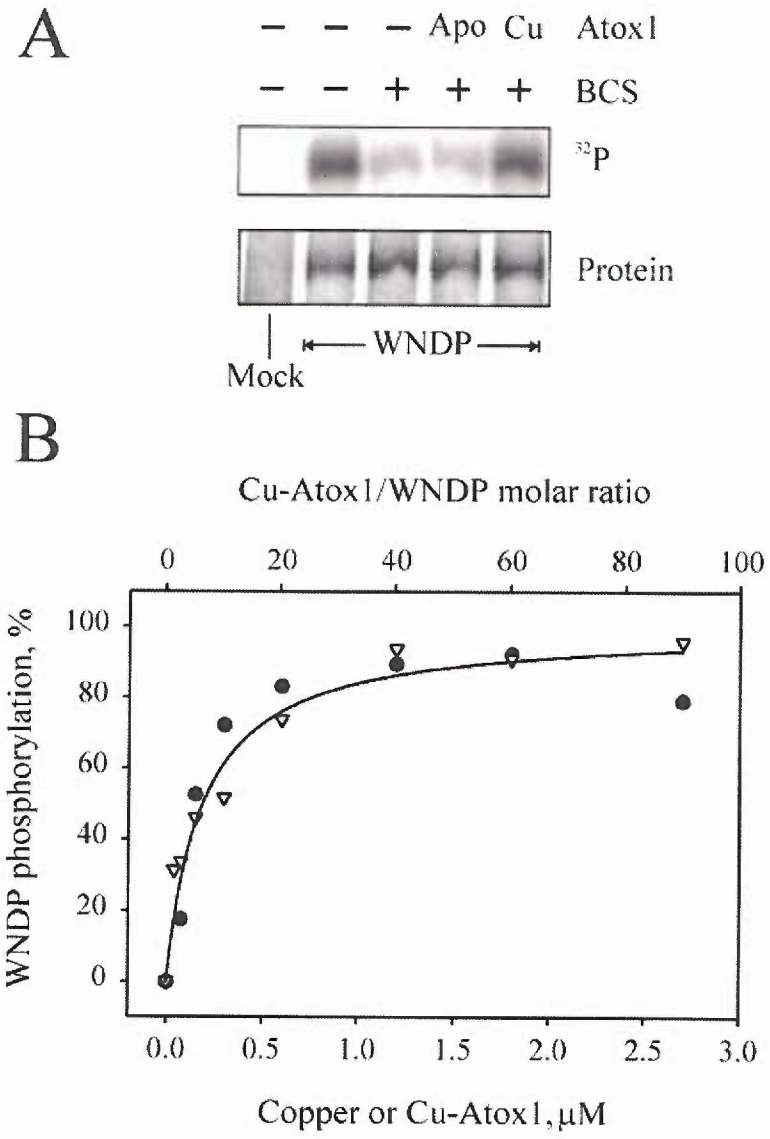
A
– – – Apo Cu Atox1
– – + + + BCS
^{32}P
Protein
Mock
WNDP
B
Cu-Atox1/WNDP molar ratio
0 20 40 60 80 100
WNDP phosphorylation, %
100
80
60
40
20
0
0.0 0.5 1.0 1.5 2.0 2.5 3.0
Copper or Cu-Atox1, μM

Figure 2. 4.

Apo-Atox1 removes copper from N-WNDP. *A*, metallated N-WNDP was bound to amylose resin and extensively washed. Apo-Atox1 was then passed through the resin, the resin was further washed, and N-WNDP was eluted with the maltose-containing buffer. The amount of copper (□) and protein (●) in each elution fraction was measured. Additions of the chaperone and the maltose-containing elution buffer are indicated by the arrows. *B*, dose-dependent effect of apo-Atox1 on the amount of copper that remains bound to N-WNDP. The average of five independent experiments is shown; the solid line is the theoretical hyperbolic curve with a R^2-factor of 0.99. *C*, copper was removed from N-WNDP as in *B* using increasing amounts of apo-Atox1. N-WNDP eluted from the resin was labeled with fluorescent reagent CPM and electrophoresed on a 10% Laemmli gel.

Figure 2. 4.

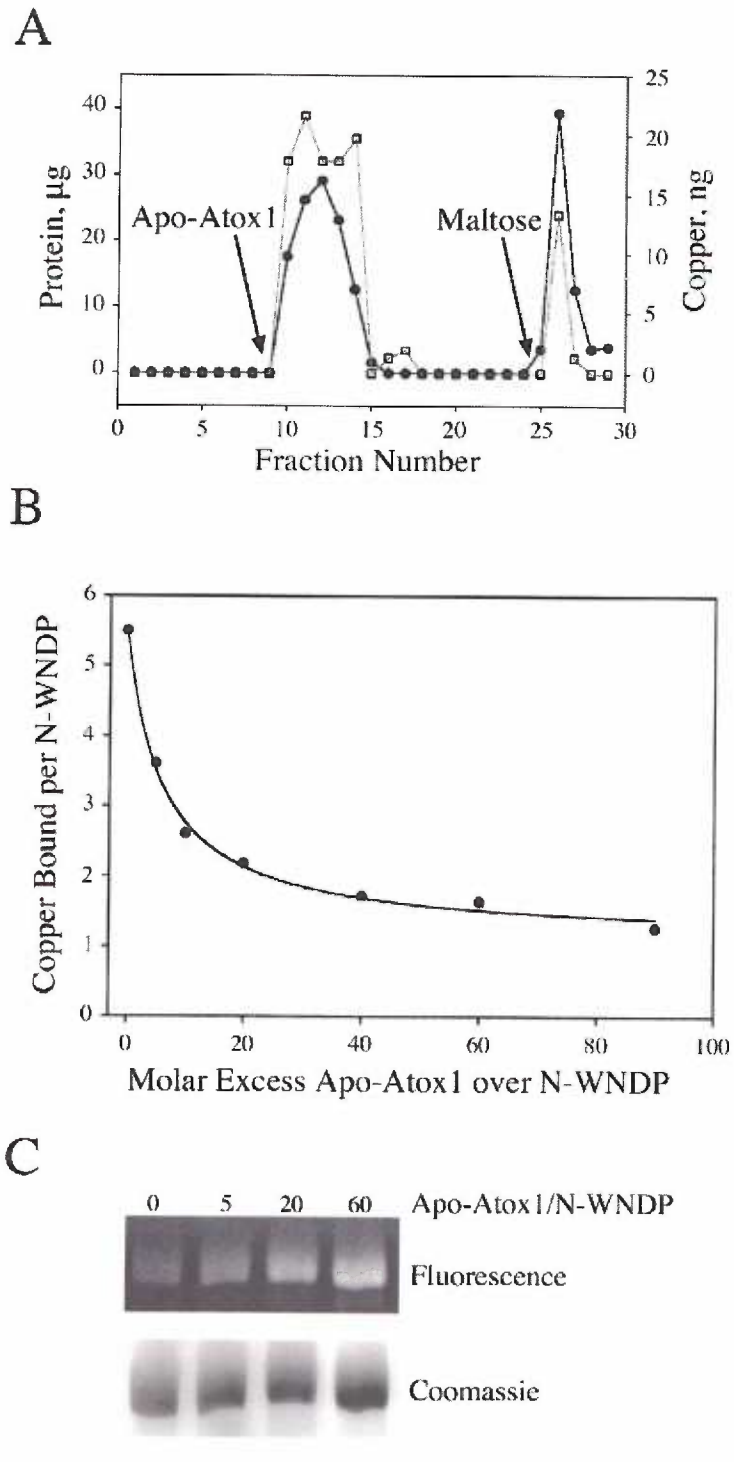
A
Protein, µg
Copper, ng
Apo-Atox1
Maltose
Fraction Number
B
Copper Bound per N-WNDP
Molar Excess Apo-Atox1 over N-WNDP
C
0
5
20
60
Apo-Atox1/N-WNDP
Fluorescence
Coomassie

Figure 2. 5.

Apo-Atox1 decreases catalytic activity of WNDP. *A*, WNDP or the D1027A mutant were incubated with apo-Atox1 added at indicated molar ratios (*top X-axis*). After centrifugation, apo-Atox1 was removed, and the pelleted WNDP was resuspended in the assay buffer. The catalytic activity of WNDP was analyzed by measuring the amount of radioactive acylphosphate intermediate of WNDP on an acidic gel. Autoradiogram of a typical gel is shown. *B*, the average of the densitometry data for four independent experiments.

Figure 2. 5.

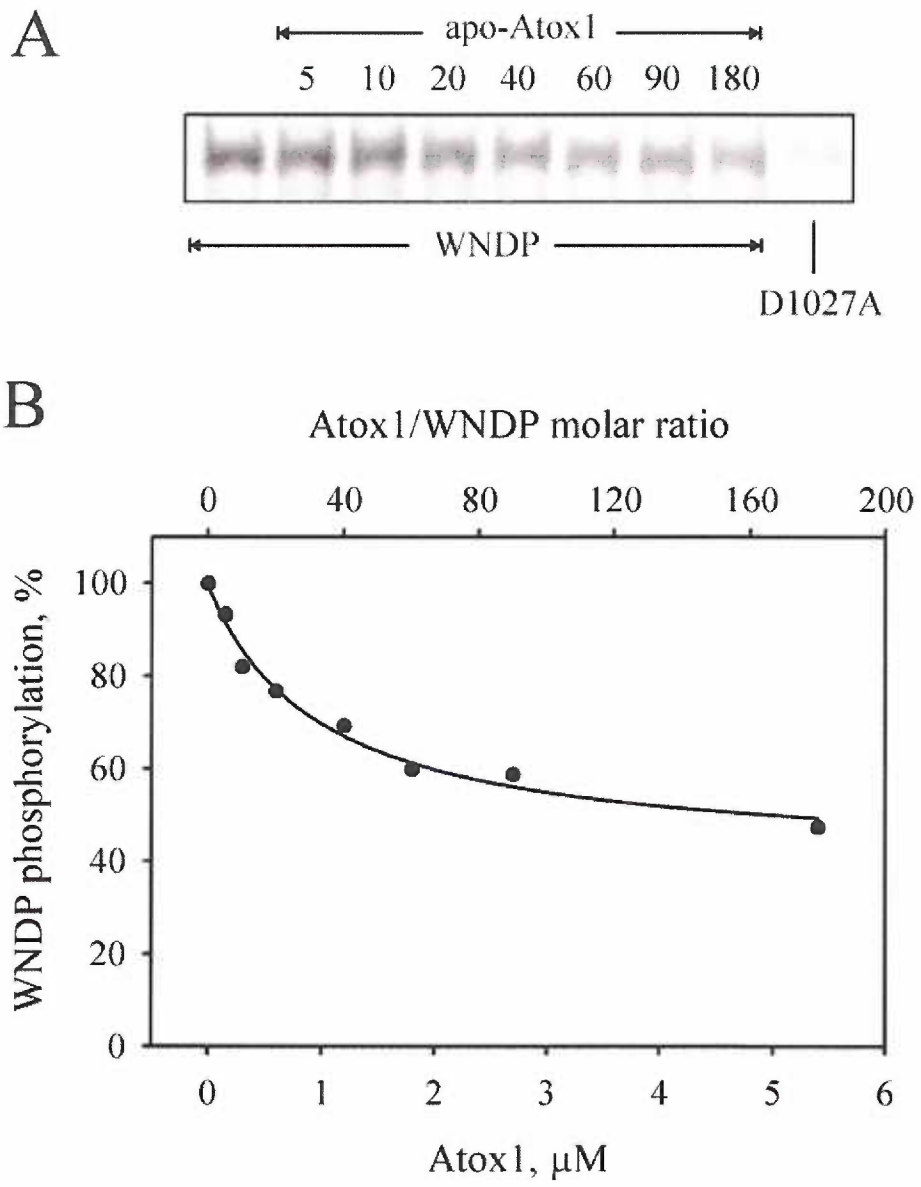
A
apo-Atox1
5 10 20 40 60 90 180
WNDP
D1027A
B
Atox1/WNDP molar ratio
0 40 80 120 160 200
WNDP phosphorylation, %
100
80
60
40
20
0
0 1 2 3 4 5 6
Atox1, μM

2. 7: Supplemental Data

Quantitation of Atox1 in N-WNDP elution fractions. To determine the amount of Atox1 present in the elution fractions after copper transfer to N-WNDP, western blot analysis was done on the elution fractions from two separate transfer experiments. Different amounts of purified recombinant Atox1 were run on the gel in parallel and utilized to generate a calibration curve. The goal of this experiment was to determine whether or not the amount of Atox1 remaining in the elution fraction would account for the amount of copper observed in the same fractions. The Figure 2. 6 shows Atox1 present in the elution fractions and Table 2. 1 summarizes the amount of Atox1 present in each fraction compared to the total amount of copper present. These results indicate that Atox1 associated with N-WNDP can only account for about 5-10% of the total amount of copper present in the fraction. This result suggests that most of the copper was bound to N-WNDP as a result of direct copper transfer.

Copper binds to Atox1 as Cu(I). To determine the redox state of copper when bound to Atox1, electron paramagnetic resonance spectroscopy measurements were carried out.. EPR spectroscopy monitors the presence of unpaired electrons in solution resulting in a signal for Cu(II) in solution but not for Cu(I). Atox1 was purified and loaded with copper using the copper-glutathione complex. The sample with a total bound copper concentration of 90 μM was analyzed by Dr. Martina Ralle and the Cu-Atox1 scan (Figure 2. 7*A*) had very little signal. (The example of signal produced by a standard sample containing 200 μM Cu(II) in complex with EDTA is showen in Figure 2. 7*B*). Using a series of copper-EDTA standards, the Cu-Atox1 sample was then estimated to

contain less than 10 μM Cu(I). This result showed that incubation of Atox1 with copper-glutathione complex results in a binding of copper to Atox1 in a reduced Cu(I) form.

Fluorescence labeling of N-WNDP following copper transfer. To determine whether copper was transferred to the metal binding site CxxC motifs, N-WNDP was incubated with the cysteine directed fluorescent label coumarin maleimide. This fluorescent reagent reacts with reduced cysteines and our lab has previously shown that copper binding to the CxxC motif protects those cysteines from labeling (105). Using coumarin maleimide as a probe for copper binding, the elution fractions of N-WNDP were labeled in the absence of Atox1 or after copper transfer from Atox1. Each reaction contained 2 μg eluted N-WNDP. The N-WNDP was incubated with a 50 fold molar excess of the fluorescent reagent coumarin maleimide in the dark for 2.5 min. The labeling reaction was quenched with the addition of excess β-mercaptoethanol and the samples were separated on a 7.5% Laemmli gel. The fluorescence was monitored under UV-light and the gel stained with Coomassie Blue. The experiment shows that copper transfer to N-WNDP results in a reduction in fluorescence suggesting that copper binding is protecting the cysteines from labeling (Figure 2. 8).

Table 2. 1. Quantitation of the Atox1 contribution to the total copper bound to N-WNDP after transfer.

Molar Excess Cu-Atox1/N-WNDP	Atox1 Present (pmol)	Total Copper (pmol)	Atox1/Copper %
3	2.1	16.9	12.4
15	4.2	63.6	6.6

Figure 2. 6.

Quantitation of Atox1 in elution fractions after copper transfer. Using 10 ng and 50 ng purified Atox1 as standards, 2 μg of elution fraction from a control experiment in the absence of Atox1 or with 3:1 and a 15:1 molar ratio Cu-Atox1 over N-WNDP were separated on a 15% Laemmli gel and transferred to PVDF membrane. The blot was probed with antibodies against Atox1 and the band intensities quantified by densitometry.

Figure 2. 6.

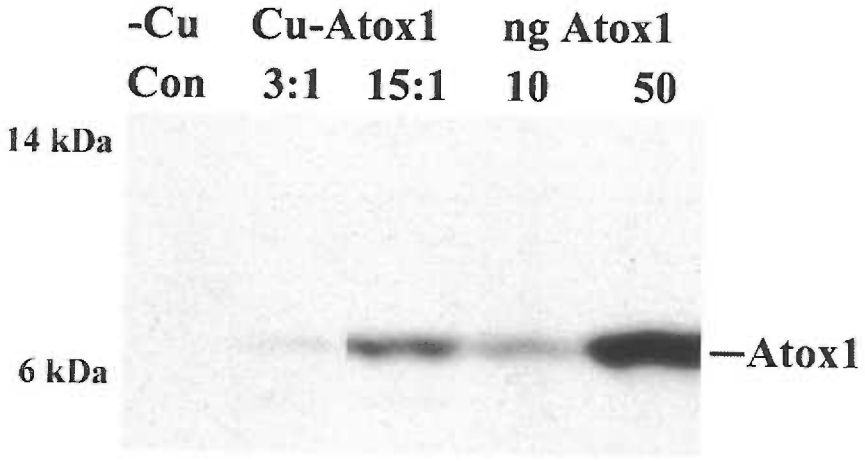

Figure 2. 7.

Copper-glutathione complex loads Atox1 with Cu(I). Electron paramagnetic resonance spectroscopy was used to determine the fraction of Cu(I) bound to Atox1 by monitoring Cu(II) signal in solution. *A,* scan showing a copper-Atox1 sample after loading with the copper-glutathione complex. *B,* a scan showing 200 μM Cu(II)-EDTA control sample.

Figure 2. 7.

A)

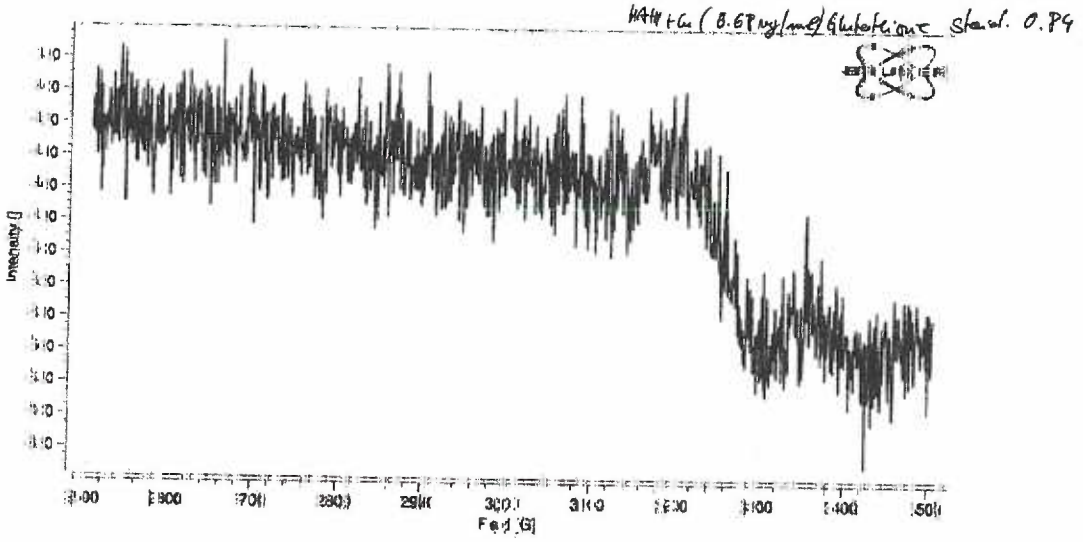

< 10 μM Cu^{2+}

B)

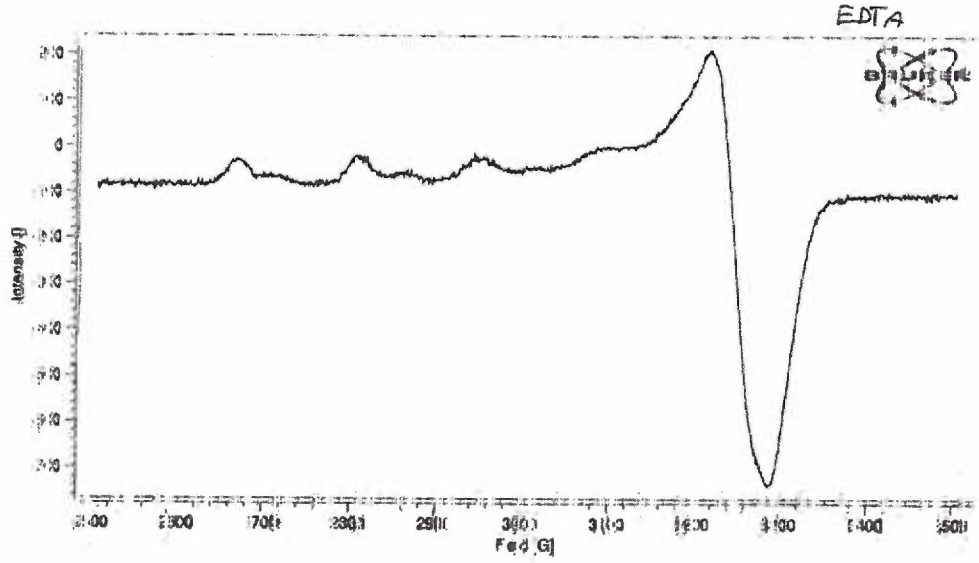

200 μM Cu^{2+}

Figure 2. 8.

Fluoresecent labeling of N-WNDP after copper transfer. Copper free (-Cu), *E. coli* copper bound N-WNDP (+Cu) or N-WNDP following copper transfer was labeled with coumarin maleimide and visualized under UV-light following gel electrophoresis. The gel was stained with Coomassie Blue.

Figure 2. 8.

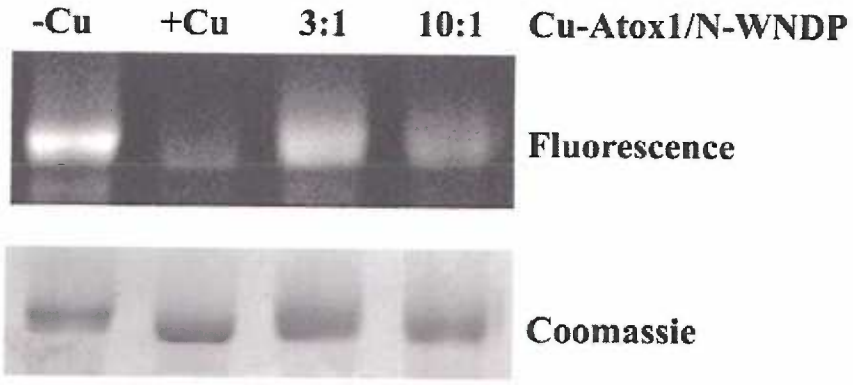

Chapter 3

The N-terminal Metal-binding Site 2 of the Wilson's Disease Protein Plays a Key Role in the Transfer of Copper from Atox1

Walker, J. M., Huster, D., Ralle, M., Morgan, C. T., Blackburn, N. J., and Lutsenko, S. (2004) *J Biol Chem 279*, 15376-84.

3. 1: Summary

The Wilson's disease protein (WNDP) is a copper-transporting ATPase regulating distribution of copper in the liver. Mutations in WNDP lead to a severe metabolic disorder, Wilson's disease. The function of WNDP depends on Atox1, a cytosolic metallochaperone, which delivers copper to WNDP. We demonstrate that the metal-binding site 2 (MBS2) in the N-terminal domain of WNDP (N-WNDP) plays an important role in this process. The transfer of one copper from Atox1 to N-WNDP results in selective protection of the metal-coordinating cysteines in MBS2 against labeling with a cysteine-directed probe. Such selectivity is not observed when free copper is added to N-WNDP. Similarly, site-directed mutagenesis of MBS2 eliminates stimulation of the catalytic activity of WNDP by the copper Atox1 complex but not by free copper. The Atox1 preference towards MBS2 is likely due to specific protein-protein interactions and is not due to unique surface exposure of the metal-coordinating residues or higher copper-binding affinity of MBS2 compared to other sites. Competition experiments using a copper chelator revealed that MBS2 retained copper much better than Atox1 and this may facilitate the metal transfer process. X-ray absorption spectroscopy of the isolated recombinant MBS2 demonstrated that this sub-domain coordinates copper with a linear bis-cysteinate geometry, very similar to that of Atox1. Therefore, non-coordinating residues in the vicinity of the metal-binding sites are responsible for the difference in the copper binding properties of MBS2 and Atox1. The intramolecular changes that accompany transfer of a single copper to N-WNDP are discussed.

3. 2: Introduction

Copper is essential for cell growth and development as a cofactor of cytochrome c oxidase, copper,zinc-dependent superoxide dismutase, ceruloplasmin, lysyl oxidase, and other important metabolic enzymes. However, abnormally elevated copper disrupts cell metabolism, presumably by stimulating the production of reactive oxygen species. Toxic effects of copper are evident in patients with Wilson's disease, a genetic disorder characterized by accumulation of copper in tissues and severe hepatic and neurological problems (136). To regulate the intracellular copper concentration, cells have developed a sophisticated network of copper-trafficking proteins that includes the copper-transporting ATPases and metallochaperones (113, 127, 128).

The Wilson's disease protein (WNDP) is a copper-transporting P-type ATPase that plays a key role in copper distribution in the liver, kidney, and the brain. WNDP utilizes the energy of ATP hydrolysis to transport the metal into the secretory pathway for incorporation into such copper-dependent enzymes as ceruloplasmin and to export excess copper from the cell (104). WNDP and other eucaryotic copper-ATPases are unique among the P-type ATPases, because they do not bind copper directly from the cytosol (where the amounts of free copper are extremely low (42)), but receive the metal ion from a small cytosolic protein called a metallochaperone through direct protein-protein interactions (41, 71, 84, 125).

Atox1 (previously known as HAH1) serves as a metallochaperone for WNDP. Several mutations in WNDP originally found in Wilson's disease patients were shown to disrupt the Atox1-WNDP interaction (83) suggesting that Atox1 is required for WNDP function. In agreement with this prediction, we demonstrated that Atox1 directly

transfers copper to WNDP and that copper delivery results in stimulation of the WNDP catalytic activity (125). Conversely, apo-Atox1 can strip copper from WNDP leading to inhibition of WNDP (125). Therefore, Atox1 can regulate the functional activity of WNDP by modulating the amount of copper bound to the protein.

Although the role of Atox1 in copper delivery to WNDP seems clear, the molecular details of this intriguing process remain uncertain. WNDP contains a large N-terminal domain (N-WNDP) with six metal-binding sub-domains (MBS) that have homologous sequences (Figure 3. 1) and a very similar βαββαβ fold (118, 120). Each MBS includes a conserved GMxCxxC sequence, which is situated in the exposed loop. It has been shown that N-WNDP binds up to six Cu^{+} ions and that copper is coordinated by the two cysteines of the GMxCxxC sequence (105, 109, 137). Atox1 contains a similar copper-binding motif, MxCxxC (Figure 3. 1), and binds one Cu^{+} per protein (79, 80). Interestingly, Atox1 has the same overall fold as the individual copper-binding sub-domains of N-WNDP (124). This similarity in structure and the presence of complimentary charges at the surface of Atox1 and some of the N-terminal MBS of the copper-transporting ATPases led to the suggestion that Atox1 docks to MBS and transfers copper via ligand exchange (118, 138). The crystallographic structure of Atox1, in which one copper bridges two Atox1 monomers, provides an attractive model for such a copper-transfer intermediate (124).

Despite considerable progress in the structural characterization of Atox1 and individual MBSs, it is still unknown how copper migrates within N-WNDP after transfer from Atox1. In fact, even the first step of this process is poorly understood. For example, we do not know whether Atox1 docks randomly to any MBS and transfers copper with

equal efficiency, or there is a specific and unique entry pathway in the N-WNDP for copper. It is also unclear what happens after copper is transferred to N-WNDP. Previous studies demonstrated that while six MBS of N-WNDP are structurally similar their functions are distinct. MBS5 and MBS6 are important for copper delivery to the intramembrane copper-binding site(s) (135) and appear to control the affinity of these sites for the metal (117). In contrast, MBSs1-4 do not affect the affinity of the intramembrane sites, but may regulate the access of copper to these sites and modulate the enzyme turnover (117).

Interestingly, the fragment of N-WNDP including MBS1-4, but not the MBS5 and MBS6-containing fragment, was shown to interact with the copper-bound Atox1 (84). Thus, taken together, the experimental data suggest that copper translocation through N-WNDP towards the intramembrane portion is likely to involve several MBS and represent a multi-step process. To better understand the molecular mechanism of this process, here we characterized the consequences of the Atox1-mediated transfer of a single copper ion to WNDP. We demonstrate that Atox1 selectively delivers copper to MBS2 and that this step is essential for further migration of copper to the intramembrane copper-binding sites of WNDP.

3. 3: Materials and Methods

Recombinant proteins. Expression and purification of Atox1 were carried out using a published protocol (125). Briefly, the recombinant Atox1 was expressed in *E.coli* as an intein fusion and purified from a soluble fraction of cell lysate using affinity chromatography on chitin beads (New England Biolabs). Following washes with 25 mM

Na_2HPO_4, 150 mM NaCl, pH 7.5 (Buffer A), Atox1 was cleaved from the fusion protein and eluted from the resin by incubation with 50 mM DTT in 25 mM Na_2HPO_4, 150 mM NaCl, pH 8.15. The protein was then dialyzed into buffer A and used for copper binding and transfer experiments. The copper-bound form of Atox1 (Cu^+-Atox1) was generated by incubation of apo-Atox1 with equimolar amount of a copper-glutathione complex as described (125) and dialyzed into buffer A. The protein concentration of Cu^+-Atox1 was determined by Bradford assay (130) and the amount of bound copper was measured using a bicinchoninic acid (BCA) assay (132) or atomic absorption spectroscopy (Shimadzu AA-6650G). The typical stoichiometry of the Cu^+-Atox1 complex was 0.8-0.95 copper per protein; the reducing state of copper was verified by EPR spectroscopy (Figure 2. 8).

The expression and purification of the N-WNDP-maltose binding protein fusion (abbreviated here as N-WNDP for simplicity) was described previously (105). Briefly, to maintain solubility, the recombinant N-WNDP fusion was co-expressed with thioredoxin in *E.coli* and purified using affinity chromatography on amylose resin (New England Biolabs). N-WNDP was washed with buffer A and eluted from the resin with buffer A containing 10 mM maltose.

To produce the recombinant metal-binding sub-domain 2 (MBS2, residues 141-212 of WNDP), the corresponding segment of the ATP7B cDNA was amplified using the following primers, forward: 5′ CATATGCAGGAGGCTGTGGTC 3′ and reverse: 5′ GTCGACTTAGCTCTTGATGGCAGC 3′. The primers were designed such that 5′ *Nde1* and 3′ *Sal1* restriction sites were incorporated into the MBS2 PCR product. The PCR fragment was cloned into the pTYB12 IMPACT expression vector (New England Biolabs) to produce the pTYB12-MBS2 expression plasmid and the sequence fidelity

was verified by automated DNA sequencing. *E. coli* ER2566 cells were transformed with the pTYB12-MBS2-intein plasmid, and the expression of the MBS2 fusion was induced by isopropyl-β-D-thiogalactopyranoside added to a final concentration of 500 μM at 25°C for 20 hrs. The MBS2 was purified from the soluble fraction using the protocol described above for Atox1 and was dialyzed into 25 mM Na_2HPO_4 pH 7.5, 150 mM NaCl. The copper-bound form of MBS2 was generated by incubation of apo-MBS2 with equimolar amount of a copper-glutathione complex and dialyzed into 20 mM Na_2HPO_4, 150 mM NaCl, pH 7.5 for copper competition experiments.

Copper transfer experiments. Prior to copper transfer experiments, the purified N-WNDP bound to amylose resin was reduced by incubating with 100 μM tris(2-carboxyethyl)phosphine hydrochloride (TCEP, Sigma) for 10 minutes. After a wash with 3 resin volumes of buffer A, apo-Atox1 or Cu^+-Atox1 were added and incubated with N-WNDP for 10 minutes. To remove the chaperone, the resin was washed extensively with 10 volumes of buffer A, and N-WNDP was eluted with buffer A containing 10 mM maltose. The protein concentration and the copper stoichiometry were measured in the eluted samples of N-WNDP as described above. For copper binding in the absence of Atox1, N-WNDP was incubated with increasing concentrations of $CuCl_2$ (Sigma) dissolved in 25 mM Na_2HPO_4 pH 7.5, 150 mM NaCl containing freshly prepared 200 μM ascorbate (Fisher). Under these conditions all copper is present in the reduced form (our data). The time of incubation and subsequent washes and elution steps were the same as for experiments with Cu^+-Atox1.

Chemical labeling and proteolysis of N-WNDP. 273 pmol (30 μg) of apo-N-WNDP, N-WNDP pre-incubated with apo-Atox1, or N-WNDP with one copper

transferred from Atox1 were incubated with a 50-fold molar excess of the cysteine-directed reagent 7-diethylamino-3-(4′-maleimidylphenyl)-4-methylcoumarin (CPM, Molecular Probes) for 2.5 minutes in the dark at room temperature. The reaction was quenched with a 10 fold molar excess of β-mercaptoethanol over CPM. The fluorescently labeled N-WNDPs were then proteolyzed with the TPCK-treated bovine pancreas trypsin (Sigma) added to protein at a 1:2000 (w/w) ratio for 3 hours at room temperature (supplemental Figure 3. 9); the reaction was stopped with the addition of 2 mM 4-(2-aminoethyl)benzenesulfonyl fluoride (AEBSF, ICN Biomedicals). (Under these conditions the maltose binding protein part of the N-WNDP fusion protein is not proteolyzed but the N-WNDP portion of the fusion is fragmented). The proteolyzed N-WNDP fragments were separated on a 15% Tris-Tricine gel (133) and the separation of the CPM-labeled peptides was monitored under UV light using a Gel-Doc system (Bio-Rad). The protein fragments were then either stained with Coomassie R250 or transferred to PVDF membrane (Millipore) at 185 mA for 40 minutes in 10% methanol, 10 mM CAPS, pH 11.0 and stained with Coomassie R250. The fluorescent and coomassie-stained patterns of the peptides from the apo- and copper-bound N-WNDP were compared. For N-terminal sequence analysis, the membrane was rinsed with water and dried; the bands were cut out and submitted to the sequencing facility.

Surface labeling of N-WNDP was performed by incubating 273 pmol of apo-N-WNDP with 0, 1, and 2 mole equivalents of CPM in buffer A. The reaction was quenched with β-mercaptoethanol. The labeled samples were then digested with trypsin and analyzed by Tris-Tricine gel electrophoresis as described above.

Comparison of the copper-binding characteristics of MBS2 and Atox1 using competition with the copper chelator BCA. Copper-bound Cu^+-Atox1 and Cu^+-MBS2 were diluted with 20 mM NaH_2PO_4, 150 mM NaCl, pH 7.5 buffer containing freshly prepared 40 μM ascorbate to obtain 7.5 μM concentration of the copper-containing complex. The proteins were then incubated with increasing concentrations of BCA for 10 minutes. The formation of the BCA-Cu(I) complex was monitored spectrophotometrically at 562 nm with a Beckman DU 640B spectrophotometer. A solution containing 7.5 μM $CuCl_2$, 40 μM ascorbate, 20 mM NaH_2PO_4, 150 mM NaCl, pH 7.5 was used as a control.

XAS Data Collection and Analysis. For the XAS experiments, the reconstitution of MBS2 with copper was performed in an inert atmosphere using an anaerobic chamber to prevent the oxidation of cysteine residues. Prior to metal reconstitution, a 10-fold molar excess of DTT was added to MBS2 on ice and the mixture was incubated for 10 min. The protein was then dialyzed overnight under argon into a buffer containing 50 mM HEPES and 10% acetonitrile at pH 7.5. Copper was added as a tetra-acetonitrile complex, $[(CH_3CN)_4Cu(I)]PF_6$, dissolved in the same buffer to an equimolar ratio to the protein. The Cu^+-MBS2 was then dialyzed in successive steps of 12 hours each against 50 mM HEPES, 10% acetonitrile, pH 7.5; 50 mM HEPES, 5% acetonitrile, pH 7.5; 50 mM HEPES, pH 7.5. The copper content was monitored by atomic flame absorption spectroscopy (Varian AA-5). The protein was then concentrated using a modified ultrafree centrifugation system (Millipore, MWCO 3,500 Da). Final concentrations were 140 μM in copper and 220 μM in MBS2 with copper stoichiometry of 0.7. The sample was sealed and stored at -80°C.

XAS data were collected at the Stanford Synchrotron Radiation Laboratory (SSRL) (beamline 9-3, 3.0GeV, 50-100mA). A bend Rh- coated mirror positioned upstream of the fully tuned Si220 monochromator was used to cut off all energy above 12 keV. Cu^{+}-MBS2 was analyzed in fluorescence mode using a Canberra 30 element array detector and was cooled down to 10K using a liquid He flow cryostat (Oxford Instruments). The energy was calibrated by simultaneously measuring a Cu metal foil and assigning the first inflection (139) point of the copper edge to 8980.3 eV. For Cu^{+}-MBS2, 10 scans were collected to k = 12.8 $Å^{-1}$.

Data reduction and analysis were performed using the EXAFSPAK computer suite (140). Theoretical phase and amplitude functions were calculated using FEFF 8.2 (139). The inspected raw data were averaged, background subtracted, and normalized. The EXAFS data were simulated by curve fitting in the OPT module of EXAFSPAK using a non-linear Marquadt algorithm, where the difference between the experimental and the calculated model is minimized. The following parameters were refined: ΔE_0 (a small energy correction at k = 0, ranging, from -5 to -20 eV), *Ri* (the distance between the central absorber and atom i), and σ^2 (the Debye-Waller factor, defining the mean square deviation of *Ri)*. A goodness-of-fit (F_w) parameter was displayed at the end of each cycle was used to evaluate the merit of the fit. F_w is defined as:

$$F_w = \sum \frac{k^6 (Data - Model)^2}{k^6 (Data)^2}$$

Preparation and Expression of mMBS2-WNDP in Insect Cells. The generation of the plasmid encoding the full-length 4.4-kilobase WNDP cDNA (pFastBacDual-wild-

type (wt-WNDP) and expression in *Spodoptera frugiperda* cells *(Sf9)* was previously described (100). The WNDP variant of MBS2, where both cysteines within the metal-binding motif GMTCQSC were substituted by alanines (mMBS2-WNDP), was generated using overlap PCR with the pFastBacDual-WNDP plasmid as a template. In the first amplification step, two fragments using forward primer (A) 5'-GCCTGGGAACCAGCAATGAAG-3', and reverse (mutagenesis) primer 5'-CTGACAGCGGACTGGGCGGTCATGCCCTCCACCC-3', and forward (mutagenesis) primer 5'-GCATGACCGCCCAGTCCGCTGTCAGCTCCATTGAAGG-3' along with reverse primer (B) 5'-GTCGACTTAGGCTCCATCAGGAAGAGA-3', were generated. The obtained fragments were then joined in the second PCR amplification step using primers A and B. The resulting product was sub-cloned into pCR-Blunt II TOPO vector (Invitrogen) and upon digestion with the restriction endonucleases Apa I and Afl II, the fragment was inserted into the pFastBacDual-WNDP vector. The presence of the anticipated mutations was verified by automated DNA sequencing. The resulting construct was then incorporated into the bacmid using the Bac-to-Bac kit (Invitrogen) and previously described protocols (28). After a three day infection with baculovirus, the *Sf9* insect cells were harvested and the total membrane fractions were prepared as previously described (100, 141). The protein concentration in the total membrane fraction was determined by Lowry (142).

Catalytic phosphorylation of WNDP and mMBS2-WNDP from γ-[^{32}P]ATP upon incubation with copper or Cu^{+}-Atox1. Catalytic phoshporylation of WNDP and mMBS2-WNDP was analyzed using previously described protocol (100). Briefly, 50 μg of total membrane protein was resuspended in 200 μl of 100 μM TCEP, 20 mM bis-Tris

propane, pH 7.0, 200 mM KCl, 5 mM $MgCl_2$ and then incubated on ice with 250 μM of copper chelator bathocuproine disulfonate (BCS, ICN Biomedicals) for 30 min to inhibit catalytic phosphorylation. The chelator was then removed by centrifugation and the pellets were washed with 20 mM bis-Tris propane, pH 7.0, 200 mM KCl, 5 mM $MgCl_2$ (phosphorylation buffer). The membranes were resuspended in phosphorylation buffer containing 100 μM ascorbate, 100 μM TCEP followed by addition of increasing concentrations of $CuCl_2$ or Cu^+-Atox1. After a 10 min incubation at room temperature, γ-[^{32}P]ATP (specific activity 25 mCi/μmol) was added to a final concentration of 1 μM and the reaction was incubated on ice for 4 min. The reaction was stopped by the addition of 50 μl of ice-cold 1 mM NaH_2PO_4 in 50% trichloroacetic acid and then centrifuged for 10 min at 20,000 x *g*. The protein pellet was washed, resuspended in 40 μl of 5 mM Tris-PO_4, pH 5.8, 6.7 M urea, 0.4 M dithiothreitol, 5% SDS and loaded on an acidic 7.5% polyacryalmide gel (134). After electrophoresis, the gels were fixed in 10% acetic acid for 10 min and dried on blotting paper. The dried gels were exposed either to the Molecular Imaging screen CS (Bio-Rad) or at -80 °C to Kodak BioMax MS film. The intensity of the bands was quantified using a Bio-Rad Molecular Imager GS-525. The dried gels were rehydrated, stained with Coomassie Blue R250, and the amount of protein in the WNDP-related bands was determined by densitometry. The incorporation of ^{32}P into WNDP was normalized to the WNDP protein levels.

3. 4: Results

The Atox1-mediated transfer of copper to N-WNDP selectively protects cysteines in MBS2 against labeling with CPM. Previously, we demonstrated that Atox1

transferred copper to N-WNDP, stimulating the catalytic activity of WNDP (125). To better understand the molecular details of this process, we sought to determine whether Cu^{+}-Atox1 delivered copper to a specific site on N-WNDP. Our approach is outlined in Figure 3. 2*A*. Apo-N-WNDP was incubated either with Cu^{+}-Atox1 to transfer one copper (125) or with apo-Atox1 as a control. Following copper transfer and subsequent removal of Atox1, the cysteine residues in N-WNDP were labeled with the fluorescent reagent CPM. Copper binding to N-WNDP protects the metal-coordinating cysteines in N-WNDP from labeling with CPM (105), therefore the difference in the intensity of fluorescent labeling can be utilized for identification of the copper-bound MBS.

To facilitate identification of the copper-bound MBS we also developed a protocol for limited proteolytic digestion of N-WNDP. MBSs in N-WNDP are thought to be compactly folded sub-domains (12,13) connected by fairly long linkers (with the exception of MBS5 and MBS6, which are linked by a very short sequence). Therefore, it was expected that under mild conditions, the proteolytic digestion would occur within the linkers leaving the MBSs intact. Indeed, treatment of labeled N-WNDP with low amounts of trypsin (1:2000 w/w) produced a series of the 8-16 kDa fragments that were stable to proteolysis for a period of about 3 hours (the predicted mass for individual MBS without the linker sequence is approximately 8 kDa). The tryptic fragments were separated by gel electrophoresis and the fluorescence intensities of the peptide bands from the apo- and copper-bound N-WNDP were compared (Figure 3. 2).

If Atox1 transfers copper to a more than one site in N-WNDP, one would expect to see a partial decrease in fluorescence of several fragments. However, if Atox1 delivers copper to a preferential site, only one band should be protected against the labeling

(Figure 3. 2*A*). As shown in Figure 3. 2*B*, there was a major reduction in the fluorescence of a single 8 kDa band in a sample derived from the copper-bound N-WNDP compared to a control apo-N-WNDP or to apo-N-WNDP pre-incubated with apo-Atox1. The fluorescence of other bands was affected only slightly or not affected at all. Importantly, there was no change in the intensity of Coomassie staining of the 8 kDa band indicating that the decrease in fluorescence was due to protection against the labeling with CPM and not due to loss of protein.

The peptides were transferred to the PVDF membrane and the 8 kDa fragment was identified using N-terminal amino-acid sequencing. In three independent experiments, the same N-terminal sequence NH_2-SLPAQEA was obtained. This sequence is identical to the Ser^{136}-Ala^{142} segment of N-WNDP, which is located in the loop between MBS1 and MBS2. The apparent molecular mass of 8 kDa indicates that this fragment contains only one metal-binding motif GMTCxxC, MBS2, since the next GMxCxxC site is 133 residues away and, if included, would generate a 15 kDa fragment. Consistant with these conclusions, we identified a cleavage site Arg^{232}-Ala^{238} between MBS2 and MBS3 (our data). Thus, copper transfer to N-WNDP causes a selective loss of fluorescence in MBS2, suggesting that MBS2 could be a site that preferentially accepts copper from Atox1.

Cysteines in MBS2 are not unique with respect to their surface exposure or affinity for copper. The selectivity towards MBS2 during copper transfer reaction suggested that the properties of this MBS were unique. For example, the cysteine residues of MBS2 could be the most exposed and hence the most likely residues to receive copper from Cu^+-Atox1, or MBS2 could have the highest affinity for copper

among the metal-binding sites in N-WNDP. In this latter case, copper can be delivered by Atox1 to other sites and then migrate to MBS2.

To evaluate the surface exposure of various metal binding sites, we examined the reactivity of the cysteine residues in N-WNDP using brief labeling with limited amounts of CPM, a fairly bulky reagent. As shown in Figure 3. 3, even when CPM is sub-stoicheometric with respect to cysteines, multiple bands were fluorescently labeled. Therefore, judging by their chemical reactivity, several MBS in N-WNDP appeared to be similarly exposed (Figure 3. 3). This conclusion was further confirmed using a cysteine-directed reagent with different chemistry, MTSEA-biotin (our data, not shown).

To test whether MBS2 is the site with the highest affinity for copper, transfer experiments were repeated using free copper added in the presence of the reducing reagents, such as ascorbate or glutathione. In this case, binding of one copper to N-WNDP results in the decreased fluorescence of several fragments, including MBS2 (Figure 3. 4). This result suggests that not only are several sites available for copper binding, but also the apparent affinities of these MBSs for the metal are not significantly different. Since neither the exposure nor affinity of MBS2 for copper appear to be unique, it seems likely that specific protein-protein interactions with Atox1 are essential for delivery of copper to the preferential site.

Binding of a single copper induces conformational change in N-WNDP. Interestingly, the transfer of one copper leads to a small but reproducible change in the proteolytic pattern of N-WNDP. As seen in Figures 3. 2*C* and 3. 4, although a single 16-kDa band is observed in the apo-N-WNDP sample, the digestion of the copper-bound N-WNDP results in a 16 kDa doublet (Figure 3. 2*C*) and is often accompanied by an

increase in the intensity of the 14 kDa band (Figure 3. 4). The N-terminal amino-acid sequencing revealed that the 14 kDa fragment began with the sequence NH_2-NQVQGTC. This sequence corresponds to a segment Asn^{352}-Cys^{358} located in the loop prior to MBS4. The next cleavage site is Ala^{484}, located prior to MBS5. The predicted molecular weight of the Asn^{352}-Arg^{483} fragment is 14 kDa. Therefore, the 14 kDa fragment includes the entire MBS4 and the linker sequences between MBS4 and MBS5, but does not include MBS5. The two bands of the 16 kDa doublet have the same N-terminal sequence NH_2-AVAPQKC corresponding to the segment Ala^{484}-Cys^{490}. Thus, the 16 kDa doublet encompasses the MBS5 and MBS6 region, and the difference in mobility of the two bands within the doublet is a result of different cleavage at their C-termini. Overall, it appears that the binding of one copper to N-WNDP leads to a change in the conformation of N-WNDP, exposing new sites for cleavage with trypsin.

The difference in copper-binding characteristics of MBS2 and Atox1. Why is copper transferred from Atox1 to MBS2? To address this question we compared the ability of Atox1 and MBS2 to retain copper in the presence of the specific copper chelator BCA. Atox1 and MBS2 were expressed using the same expression system, purified, and loaded with copper under identical conditions (see "Materials and Methods" for details). The copper-bound Atox1 or MBS2 were then incubated under reducing conditions with increasing concentrations of BCA and redistribution of copper between each protein and BCA was monitored spectrophotometrically (copper-BCA complex has maximum absorbance at 562 nm).

There was a marked difference between Atox1 and MBS2 in these experiments (Figure 3. 5). A 45-fold molar excess of BCA over copper-bound Atox1 caused complete

redistribution of copper from Atox1 to the chelator. In contrast, only 10% of copper was removed from MBS2 under the same conditions, suggesting that either the affinity of MBS2 for copper was significantly higher than that of Atox1 or the dissociation rate of copper from MBS2 was much slower. This difference in copper retention could either be due to a difference in copper coordination by these two proteins (two-coordinate versus three-coordinate, for example) or due to a difference in the local environment of metal-binding sites To examine these possibilities we used X-ray absorption spectroscopy (XAS).

MBS2 coordinates copper with a linear bis-cysteinate geometry, very similar to that of Atox1. We have shown recently that Atox1 binds copper with a linear bis-cysteinate coordination geometry (80). The extended X-ray absorption spectroscopy fine structure studies of MBS2 yielded a similar result. EXAFS of MBS2 was dominated by strong Cu-S backscattering out to k=12.8Å^{-1} (Figure 3. 6*A*, *inset a*) in agreement with the key role of the cysteine residues of the GMTCxxC motif in Cu^+ coordination. The Fourier Transform (FT) revealed a strong feature at R ~ 2 Å and several less intense features centered around R + Δ = 3.5 Å and 4.3 Å, respectively (Figure 3. 6*A*). The 2 Å feature was fitted with 2 x Cu-S at 2.16Å (1). When the outer shells were included in the refinement the F_w value improved slightly (Table 3. 1). The best fit was obtained with 2 x Cu-S at 2.16 Å, 2 x Cu-C at 3.38 Å and multiple scattering (MS) paths for Cu-S1-Cu-S2-Cu at 4.32 Å (Table 3. 1). As suggested by Penner-Hahn and coworkers, the Cu-S-Cu-S-Cu multiple scattering is very sensitive to the S-Cu-S angle and can only be observed if the angle is > 175° (143). Thus, observing this scattering path is an indication of an almost linear S-Cu^+-S coordination. The linear Cu^+-coordination in

MBS2 was confirmed by comparing the pre-edge features at 8983 eV for MBS2 to that of a synthetic linear S-Cu^{+}-S complex; which were found very similar in their shape and intensity (Figure 3. 6*A*, *inset b*).

Overall, the data and the refinement results for Atox1 and MBS2 are very similar (Table 1, Figure 3. 6*B*). The differences in intensity of the Fourier Transform and EXAFS can be traced to a small variation in the Debye-Waller factor for the first shell and can be explained by differences in the static disorder of the Cu-S bond, i.e the Cu-S bond in Atox1 is more ordered than in MBS2. We conclude that the difference in the apparent affinity for copper is likely due to the local environment in MBS2 compared to Atox1 rather than distinct metal coordination.

Mutation of MBS2 disrupts Atox1-mediated stimulation of catalytic activity of WNDP. The experiments with differential labeling of N-WNDP (Figure 3. 2) suggested that MBS2 was the site receiving copper from Atox1. However, these experiments did not exclude the possibility that copper binding protects MBS2 against fluorescent labeling indirectly. In addition, previous experiments using yeast-complementation assay demonstrated that mutation of the cysteines in MBS2 to serines did not disrupt the ability WNDP to transport copper across the membrane (135). Therefore, to independently test whether MBS2 is required for copper transfer from Atox1 to the full-length WNDP, both copper-coordinating cysteines in MBS2 of the full-length WNDP were mutated to alanines, a mutation that is expected to inactivate metal-binding more efficiently than cysteine to serine substitution. The generated mMBS2-WNDP was expressed in *Sf9* cells and the catalytic activity of the mutant in the presence of copper or copper-Atox1 was characterized using the protocol developed for the wild-type WNDP

(100). In this procedure, the ability of WNDP to form a catalytic phosphorylated intermediate is first inhibited by removing copper with the copper chelator BCS. The reactivation is then monitored upon the addition of free copper or a copper-Atox1 complex. Since the formation of a catalytic intermediate critically depends on binding of copper to the intramembrane binding site(s) of WNDP, the disruption of copper delivery from the cytosol to the membrane site(s) would result in the inactivation of catalytic phosphorylation.

The membrane fraction containing the full-length WNDP and mMBS2-WNDP mutant were isolated from *Sf9* cells and treated with BCS to inhibit their activity. The subsequent addition of free copper in the presence of ascorbate reactivated the wild-type WNDP and the mMBS2-WNDP mutant in a very similar manner and to the same level (Figure 3. 7*A*). This result indicated that (a) copper was able to reach the intramembrane copper-binding site despite the mutation at MBS2 and (b) under these conditions the mutant had activity similar to wild-type WNDP. In contrast, when Cu^{+}-Atox1 was used as a metal donor, there was a drastic difference between reactivation of wild-type WNDP and mMBS2-WNDP (Figure 3. 7*B*). Even the large excess of Cu^{+}-Atox1 could not stimulate the catalytic activity of mMBS2-WNDP suggesting that MBS2 was essential for the initial steps of copper delivery from Atox1 to the catalytically essential intramembrane sites.

3. 5: Discussion

The current work was undertaken to understand the molecular mechanisms underlying copper transport by WNDP. Specifically, the described experiments focus on

transfer of copper from Atox1 to the N-terminal domain of WNDP (N-WNDP), the first step of a poorly understood journey of copper from the cytosol to the intramembrane copper-binding site(s) of WNDP. Our results suggest that the chaperone delivers copper specifically to MBS2 of N-WNDP. The involvement of MBS2 in the Atox1-mediated copper transfer is consistent with the earlier yeast two-hybrid data showing interactions of Atox1 with the MBS1-4 fragment and the lack of interactions with the MBS 5-6 containing fragment (84).

The importance of MBS2 for copper transfer led us to examine the properties of this site in more detail. The labeling with CPM suggests that with respect to solvent exposure, MBS2 is not unique and that other MBS can potentially accept copper from Atox1. Indeed, when present in excess, Atox1 metallates all six MBSs in N-WNDP (125). This earlier observation seems at odds with our current results showing that mutation of a single MBS2 in the full-length WNDP abolishes the Atox1-mediated delivery of copper (Figure 3. 7). There are two possible explanations of this apparent contradiction. First, it could be that Atox1 can only dock to MBS2 via specific protein-protein interactions, and copper then migrates from MBS2 to other MBSs. In this case, all N-terminal metal-binding sites can be loaded via MBS2 and the mutation of MBS2 would disrupt this process. This explanation seems unlikely since we observed no redistribution of copper from MBS2 to other copper-binding sites in N-WNDP. In fact, unless interactions of MBS2 with other domains in the full-length WNDP facilitate copper dissociation from MBS2, this site appears to retain copper remarkably well (Figure 3. 5).

The following alternative explanation better accommodates the experimental data. It seems likely that the folding of N-WNDP and its interaction with other domains of WNDP, such as the ATP-binding domain (144), limit accessibility of the N-terminal MBSs to Atox1 (which is bulkier than the chemical probe) and make the delivery of copper to these MBSs strongly dependent on initial binding of copper to MBS2. In this scenario, copper transfer to MBS2 may trigger a change in the conformation of N-WNDP, allowing Atox1 sufficient access to other MBSs. This hypothesis is consistent with our observation that the binding of a single copper to N-WNDP is accompanied by appearance of new tryptic sites during proteolysis (Figures 3. 2*C*, 3. 4). Also circular dichroism experiments of N-WNDP showed subtle changes in the overall fold upon copper binding (109).

Our experiments further suggest that the affinity of several metal binding sites in N-WNDP for copper are comparable and higher that that of Atox1. In the competition experiments, MBS2 displayed a much better retention of copper than Atox1 suggesting that under equilibrium copper is likely to redistribute to this site. It is clear that the difference in properties of MBS2 and Atox1 is not due to copper coordination. The EXAFS experiments demonstrate that MBS2 binds Cu^{+} with linear coordination and the distance between the sulfurs in the cysteine residues to the copper was 2.16 Å. This distance is the same as the distance between Cu^{+} and the cysteines of Atox1 (80). Therefore, the local protein environment plays an important role in stability of the copper-bound form of Atox1 and MBS2.

The high-resolution structure of MBS2 of WNDP is not yet available, but this sub-domain is homologous to MBS2 and MBS4 of the Menkes disease protein (58%

identity to MBS2), the structures of which were determined by NMR (*118, 120*). The NMR experiments revealed some structural features that could account for the difference in the retention of copper by MBS2 and Atox1. In MBS2 of either Menkes disease protein or WNDP, there is a conserved phenylalanine that lies within the loop adjacent to the cysteines at the MBS (Figures 3. 1 and 3. 8*A*). It was proposed that the hydrophobic residue in close proximity to the binding site would stabilize bound copper (120), a hypothesis that is consistent with our results. Dameron and co-workers showed that such stabilization can be accomplished not only by phenylalanine but also by other hydrophobic residues, for example isoleucine (120). The equivalent position in Atox1 is occupied by a charge residue, lysine 60 (Figures 3. 1 and 3. 8*A*). The electrostatic repulsion between the lysine residues and the positively charged copper may lead to the decrease in the apparent copper-binding affinity for Atox1 compared to MBS2.

Our experiments suggest that the selective transfer of copper from Atox1 to MBS2 is a result of specific protein-protein interactions. Such specific interactions can be facilitated by the presence of a negatively charged patch at the surface of MBS2, which is complimentary to the positively charged surface of Atox1 (Figure 3. 8*B*). While this complementation may play a role in attracting and positioning Atox1 with respect to MBS2, the interactions between MBS2 and Atox1 are most likely not tight, since in our experiments we were unable to detect stoichiometric amounts of bound Atox1 after incubation with N-WNDP (Figure 2. 6). It is also clear that the charge distribution at the surface of MBS2 is not unique for this sub-domain (Figure 3. 8*B*), and consequently the key role of MBS2 in the Atox1-mediated copper transfer is likely due to specific location of this site in N-WNDP.

If all the metal-binding sites in N-WNDP have a comparable affinity for copper, why doesn't copper migrate from MBS2 to other metal-binding sites? While available data do not allow us to unambiguously answer this question, it seems that extremely poor dissociation of copper from MBS2 is a likely reason for this result. The strong retention of copper by MBS2 also reinforces our conclusion that binding of copper to MBS2 is likely to work as a switch allowing subsequent loading of other sites, rather than a specific entrance for copper. The experiments testing this model are currently underway in our laboratory.

In summary, we demonstrated the specific role of the N-terminal metal-binding site 2 of WNDP in the first step of the Atox1-mediated delivery of copper to N-WNDP. This first step appears to involve specific protein-protein interactions between the donor and acceptor and is likely to be facilitated by the difference in the copper-binding affinity of the Atox1/MBS2 pair. We speculate that binding of copper to MBS2 works as a switch, which opens the access of the chaperone to other metal-binding sites in WNDP.

3. 6: Acknowledgements

Dominik Huster generated the mMBS2-WNDP construct and performed the catalytic phosphorylation experiments with the mutant and WT-WNDP. Martina Ralle and Ninian Blackburn did XAS and EXAFS analysis of Atox1 and MBS2. Clinton Morgan generated the MBS2-intein construct and helped with the copper competition experiments. We thank Drs. Deb McMillen and Jan Pohl for N-terminal amino acid sequencing and Dr. James E. Penner-Hahn for making available the XAS data on the bis-2,3,5,6-tetramethylbenzene-thiolate Cu(I) model complex. We are grateful to members of the

Lutsenko laboratory for critical reading of the manuscript and useful discussions and to Minsun Hong and David Murray for help with the preparation of Figure 3. 8.

Table 3. 1. Data and refinement calculations from EXAFS of MBS2 and Atox1.

1st Shell			Outer Shell				F_w
Scatterer	Distance (Å)	Debye-Waller Factor ($Å^2$)	Scatterer	Distance (Å)	Debye-Waller Factor ($Å^2$)	Cu-S-X angle (°)	
MBS-2							
2 x Cu-S	2.16 (1)	0.006					0.42
2 x Cu-S	2.16 (1)	0.006	2 x Cu-C Cu – S MS[a]	3.38 (1) 4.32 (1)	0.013 0.010	114 180	0.40
Atox1[b]							
2 x Cu-S	2.16 (1)	0.004					0.29
2 x Cu-S	2.16 (1)	0.004	2 x Cu-C Cu – S MS[b]	not detected 4.32 (1)	not detected 0.002	not detected 180	0.25

[a] Multiple scattering (MS) distances were fixed; only Debye-Waller factors were refined.

[b] Data from previously published sample (80).

Figure 3. 1.

Sequence alignment of the six MBS of N-WNDP and Atox1. The residues conserved in metal-binding sites are shown as a consensus on top of the alignment. The residues conserved in Atox1 and MBSs are indicated by a larger bold font. The residues marked with the star (*) are located in close proximity to the metal-coordinating cysteines in the folded structure (see also Figure 3. 8).

Figure 3. 1.

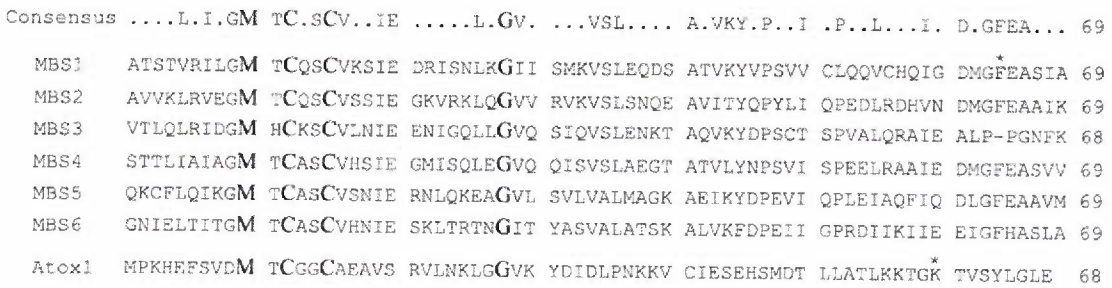
Consensus ....L.I.GM TC.SCV..IE .....L.GV. ...VSL.... A.VKY.P..I .P..L...I. D.GFEA... 69
MBS1 ATSTVRILGM TCQSCVKSIE DRISNLKGII SMKVSLEQDS ATVKYVPSVV CLQQVCHQIG DMGFEASIA 69
MBS2 AVVKLRVEGM TCQSCVSSIE GKVRKLQGVV RVKVSLSNQE AVITYQPYLI QPEDLRDHVN DMGFEAAIK 69
MBS3 VTLQLRIDGM HCKSCVLNIE ENIGQLLGVQ SIQVSLENKT AQVKYDPSCT SPVALQRAIE ALP-PGNFK 68
MBS4 STTLIAIAGM TCASCVHSIE GMISQLEGVQ QISVSLAEGT ATVLYNPSVI SPEELRAAIE DMGFEASVV 69
MBS5 QKCFLQIKGM TCASCVSNIE RNLQKEAGVL SVLVALMAGK AEIKYDPEVI QPLEIAQFIQ DLGFEAAVM 69
MBS6 GNIELTITGM TCASCVHNIE SKLTRTNGIT YASVALATSK ALVKFDPEII GPRDIIKIIE EIGFHASLA 69
Atox1 MPKHEFSVDM TCGGCAEAVS RVLNKLGGVK YDIDLPNKKV CIESEHSMDT LLATLKKTGK TVSYLGLE 68

Figure 3. 2.

Identification of MBS that accepts copper from Cu^{+}-Atox1. *A*, schematic representation of two possible outcomes of the experiment on copper transfer and subsequent fluorescent labeling. The *two left panels* show the change in the pattern of the CPM-labeled peptides if transfer is directed to the specific site (*Ordered*) or to any MBS (*Random*). The *right panel* shows the protein pattern (*Coomassie*), which remains unaltered in both cases. *B*, the actual result of the experiment. The fluorescence pattern is shown on the *left panel*; the Coomassie R250 staining is on the *right*. The *arrow* indicates the differentially labeled 8-kDa band corresponding to MBS2 (see "Results" for details). *C*, a separate gel showing a typical change in the tryptic cleavage of the 16 kDa band and no change in total fluorescence following transfer of one copper.

Figure 3. 2.

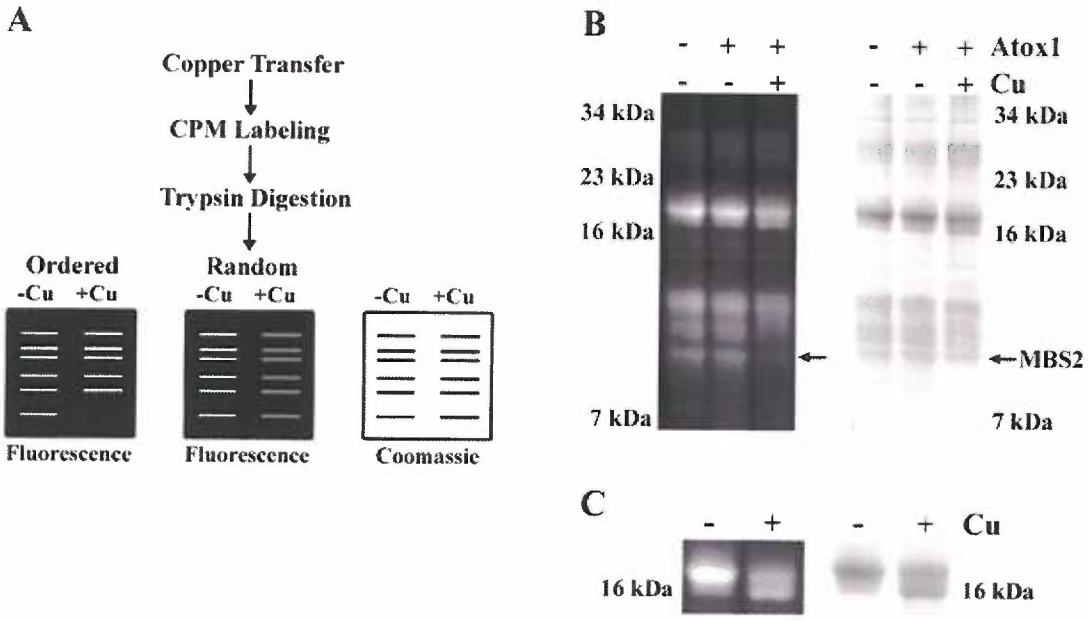
A
Copper Transfer
CPM Labeling
Trypsin Digestion
Ordered
-Cu +Cu
Random
-Cu +Cu
-Cu +Cu
Fluorescence
Fluorescence
Coomassie
B
- + + - + + Atox1
- - + - - + Cu
34 kDa
23 kDa
16 kDa
7 kDa
34 kDa
23 kDa
16 kDa
MBS2
7 kDa
C
- + - + Cu
16 kDa
16 kDa

Figure 3. 3.

Surface labeling of N-WNDP with CPM. N-WNDP was incubated in the absence or presence of 1 and 2 mol equivalent of CPM. The protein was proteolyzed, and the labeling of various fragments analyzed (*Fluorescence*). The same gel was then stained with Coomassie R250.

Figure 3. 3.

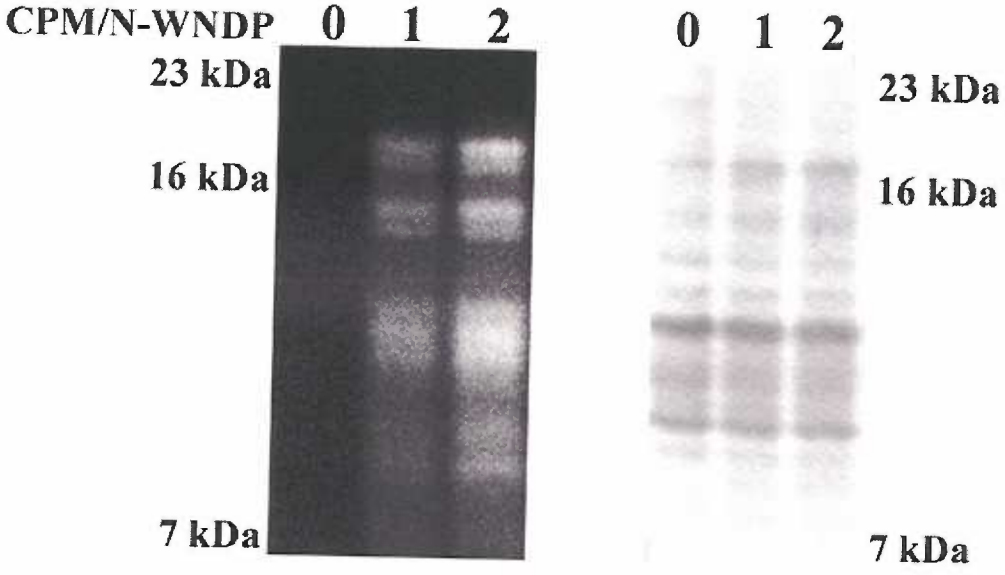

Figure 3. 4.

Comparison of selectivity of protection against CPM labeling after transfer of one copper to N-WNDP using various copper donors. Copper was added to N-WNDP in the presence of ascorbate or as a complex with glutathione or Atox1 to obtain binding of approximately one copper per N-WNDP in each case. The N-WNDP was then CPM-labeled and proteolyzed, and the fluorescent patterns were compared. Each *lane* contains the same amount of protein.

Figure 3. 4.

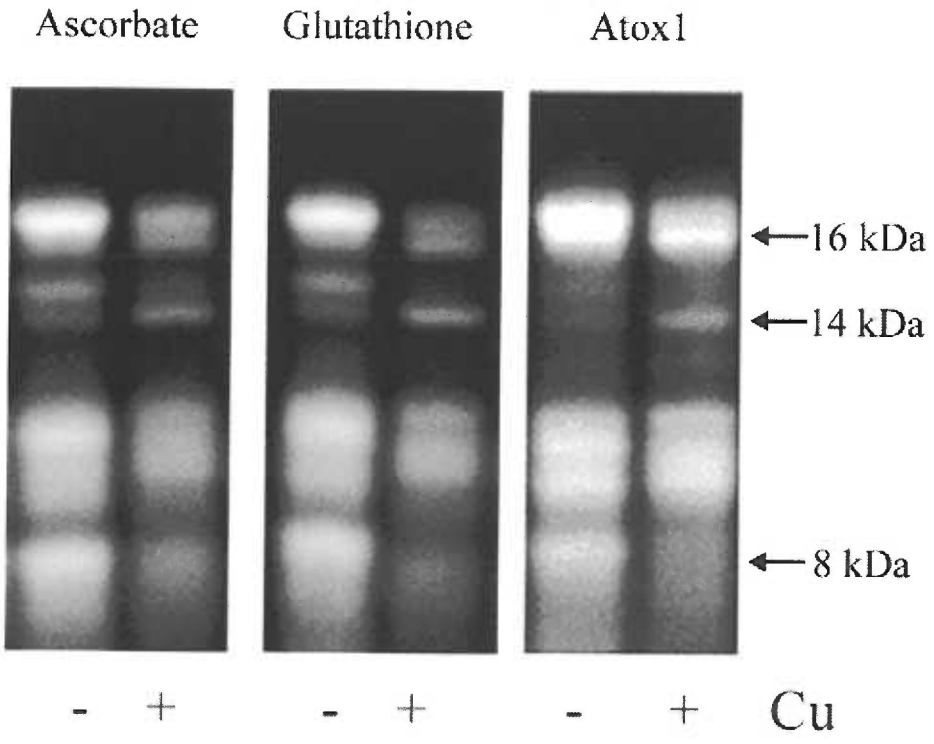

Figure 3. 5.

Copper retention by MBS2 and Atox1 in the presence of the high affinity copper chelator BCA. The purified copper complexes with MBS2 (●) and Atox1 (▲) were incubated with increasing concentrations of the copper chelator BCA. The amount of copper redistributed from the protein to BCA was determined by comparing the absorbance to the standard. The initial amount of copper-bound protein was taken as 100%, and the amount of copper redistributed to BCA was substracted.

Figure 3. 5.

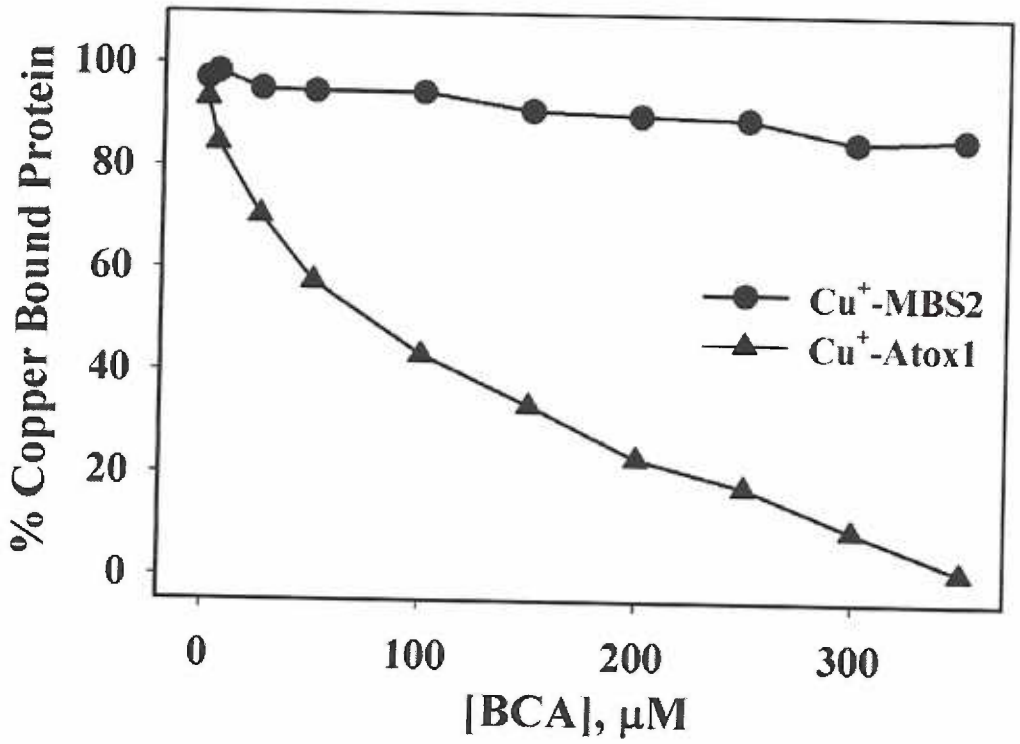
% Copper Bound Protein
100
80
60
40
20
0
0
100
200
300
[BCA], μM
Cu+-MBS2
Cu+-Atox1

Figure 3. 6.

EXAFS analysis of the copper-MBS2 complex (*left*) and comparison of copper-MBS2 with copper-Atox1 (*right*). *Left*, Fourier transform data (*black*) and fits (*red*) are shown for MBS2. *Inset a* shows the data (*black*) and fit (*red*) of the EXAFS data. *Inset b* shows an overlay of the pre-edge region for MBS2 (*black*) and the Cu(I) bis-2,3,5,6-tetramethylbenzenethiolate complex (*red*). *Right*, comparison of XAS data for MBS2 (*black*) and Atox1 (*red*) (*inset*, comparison of the EXAFS data). The first shell in the Fourier transform and the EXAFS data for Atox1 are slightly more intense than for MBS2, originating from a lower Debye-Waller factor for the Cu-S bond for Atox1. Because the Debye-Waller factor is a measure for static disorder of a given bond we can assume that the Cu-S bond in Atox1 is more rigid than the Cu-S bond in MBS2.

Figure 3. 6.

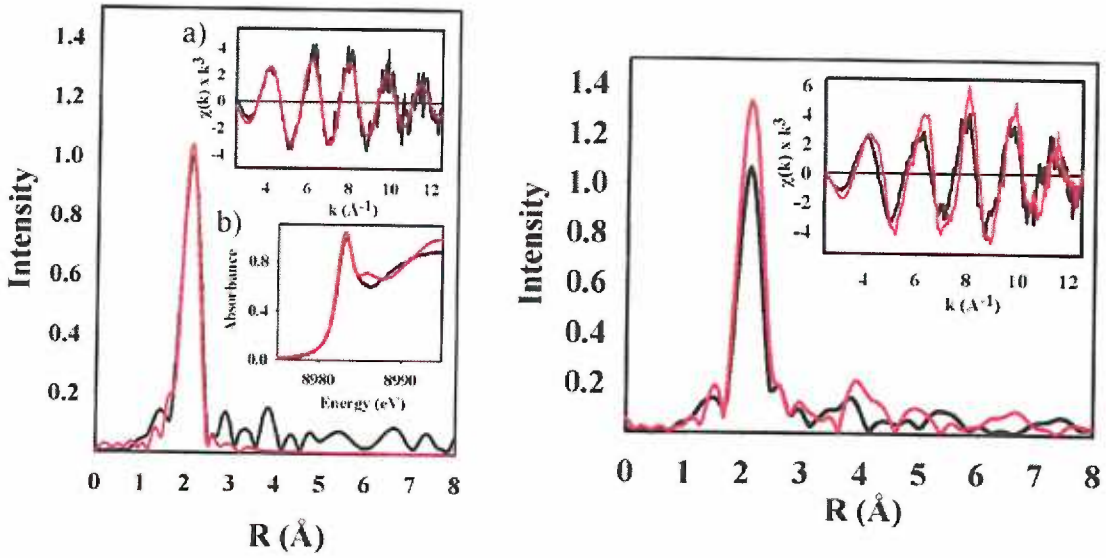

Figure 3. 7.

Stimulation of catalytic phosphorylation of WNDP and the mMBS2-WNDP mutant by free copper (*A*) and by Cu^{+}-Atox1 (*B*). An autoradiogram of a typical gel (*top*) and the normalized densitometry data (*bottom*) demonstrate formation of the catalytic phosphorylated intermediate for WNDP (●) and mMBS2-WNDP (○) in the presence of increasing concentrations of copper (*A*) or Cu^{+}-Atox1 complex (*B*). The amount of the phosphorylated intermediate is graphed as a percentage of the catalytic activity prior to treatment with copper chelator BCS. *WT*, wild type.

Figure 3. 7.

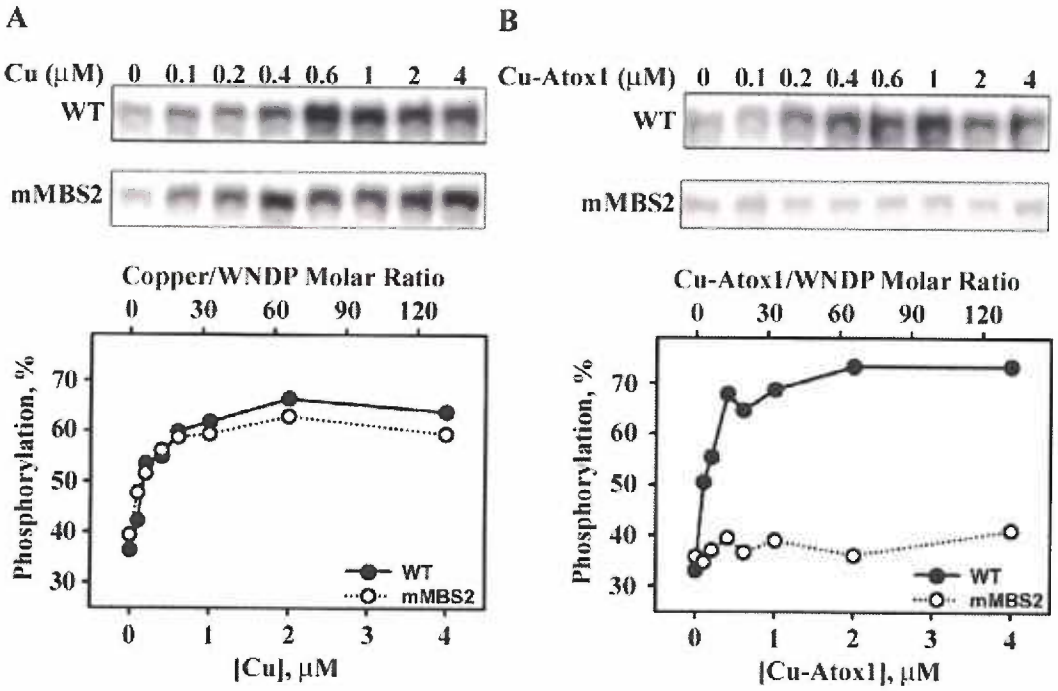
A
Cu (μM) 0 0.1 0.2 0.4 0.6 1 2 4
WT
mMBS2
Copper/WNDP Molar Ratio
0 30 60 90 120
Phosphorylation, %
70
60
50
40
30
WT
mMBS2
0 1 2 3 4
[Cu], μM
B
Cu-Atox1 (μM) 0 0.1 0.2 0.4 0.6 1 2 4
WT
mMBS2
Cu-Atox1/WNDP Molar Ratio
0 30 60 90 120
Phosphorylation, %
70
60
50
40
30
WT
mMBS2
0 1 2 3 4
[Cu-Atox1], μM

Figure 3. 8.

Comparison of the local environment of the metal-coordinating cysteines in MBS2 and Atox1 (*A*) and surface charge distribution on all MBS and Atox1 (*B*). *A*, the copper-coordinating cysteines in the GMxCxxC motif are shown in *yellow*, the residues in close proximity to this motif (Phe in MBS2 and Lys in Atox1) are shown in *green*. *B*, the negative charges on the surface of MBSs and Atox1 are indicated by *red* color, the positive charges are in *blue*. The figure was generated with the program MOLMOL (145).

Figure 3. 8.

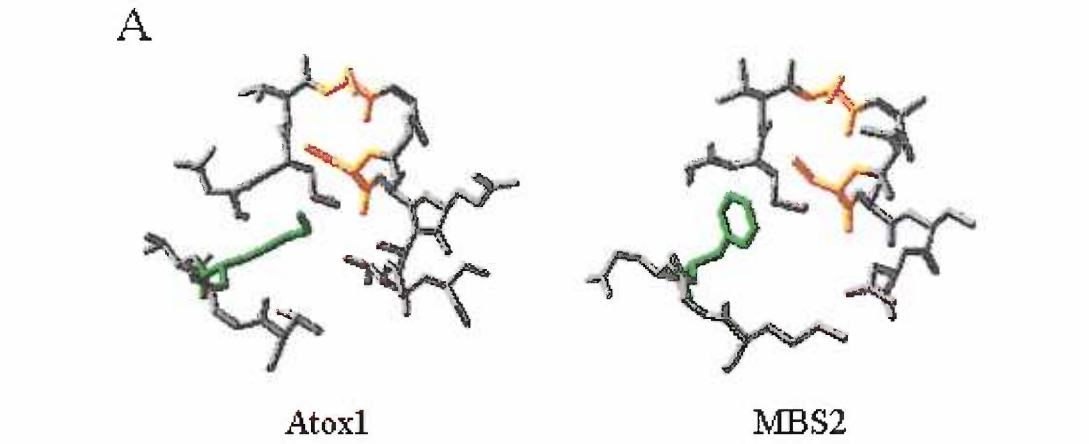

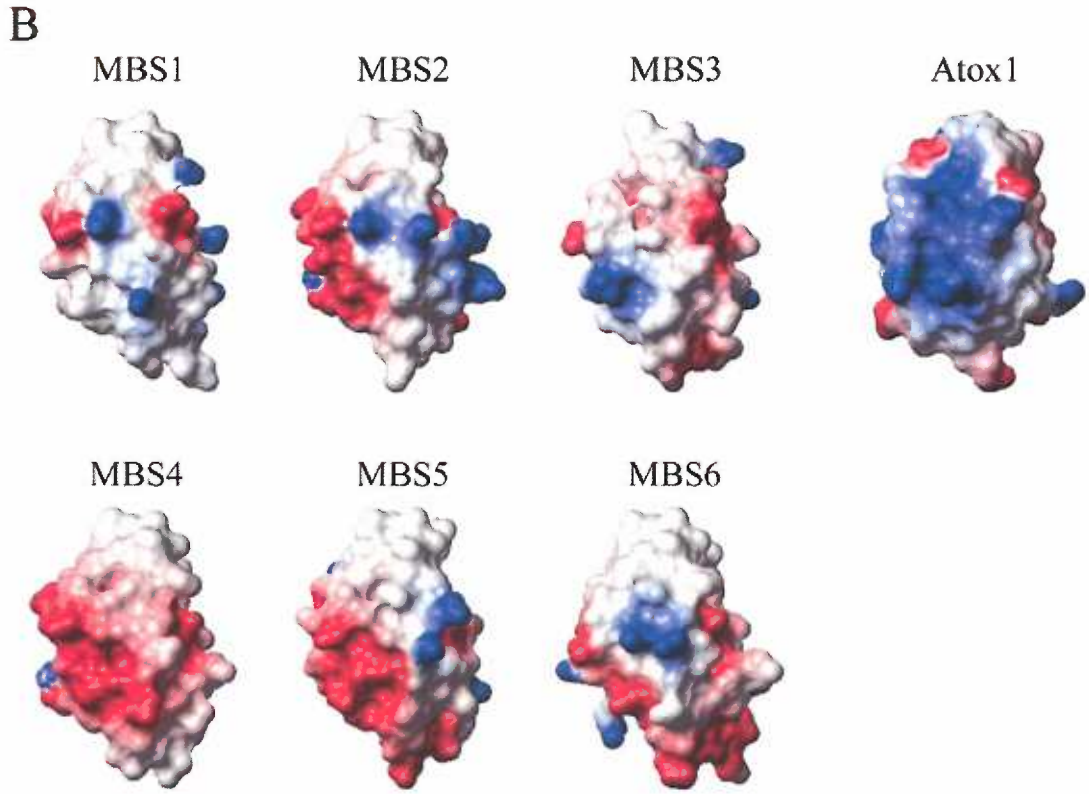

3. 7: Supplemental Data

Optimization of the proteolysis time with trypsin. To optimize conditions for limited proteolysis of N-WNDP with tripsin, a time course experiment was performed.. The goal was to determine the time needed for partial proteolysis of N-WNDP where the metal binding sites would be intact but the loop regions between the metal binding sites would be cleaved. In this case, the predicted lengths of the metal binding sites after cleavage with trypsin would be between 8-kDa and 15-kDa. This wide molecular weight range would allow for better separation on a 15% Tris-tricine gel and ease of identification of the metal binding sites by sequencing. The figure shows the proteolysis of 30 μg of N-WNDP incubated with at 1:2000 w/w ratio of protein to trypsin for several time points (Figure 3. 9). The reactions were stopped with the addition of 2 mM 4-(2-aminoethyl) benzenesulfonyl fluoride and the fragments were separated on a 15% Tris Tricine gel. At the 3 h time point the partially proteolyzed fragments of N-WNDP are stable and within the range of the predicted molecular weight masses of the metal binding sites. Subsequent sequencing of several bands confirmed that the cleavage sites were in the loop regions between the metal binding sites.

Figure 3. 9.

Time course for partial proteolysis of N-WNDP with trypsin. N-WNDP was incubated with in the absence or presence of trypsin for 0.5, 1, 1.5, 2 or 3 hours. The digests were separated on a Tris-tricine gel and stained with Coomassie R250.

Figure 3. 9.

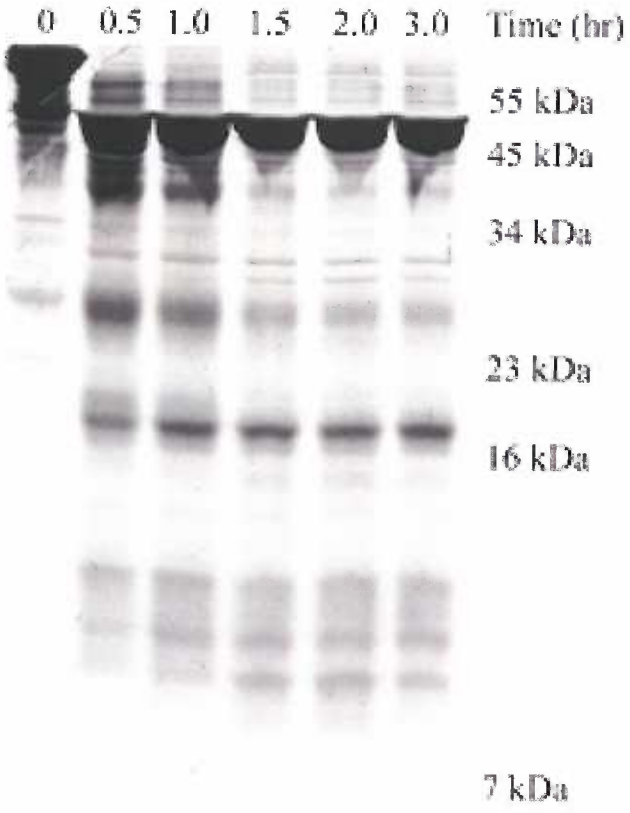

Chapter 4

Summary and Conclusions

Copper is an essential nutrient required for cellular function. It is an important component of several key metabolic enzymes located in various compartments; however, copper can also be toxic to the cell when left unbound. A novel class of proteins, called metallochaperones have two distinct roles. They protect the cell from the toxic effects of copper but also distribute copper to copper-dependent proteins. Many aspects of this copper transfer mechanism have been studied. Research presented in this dissertation concentrates on the molecular mechanisms of copper transfer from the metallochaperone Atox1 to the Wilson disease protein.

Atox1-mediated copper transfer and regulation of WNDP activity. Using biochemical and biophysical techniques, we demonstrated that Atox1 directly transfers copper to N-WNDP (Figures 2. 2, A. 1). Atox1-mediated copper transfer results in a stimulation of WNDP catalytic activity (Figure 2. 3) suggesting that Atox1 acts as a physiological partner for WNDP. In these *in vitro* experiments copper transfer and stimulation of WNDP catalytic activity occurred with an excess of Atox1. This observation has implications for understanding of Atox1-mediated transfer under the actual cellular conditions. If Atox1 is present in a large excess over WNDP in the cell, then Atox1 might act alone as the physiological partner. In contrast, if the ratio of Atox1 and WNDP is equal or there is, in fact, more WNDP compared to Atox1, this result suggests that there might be another helper protein involved in the Atox1-WNDP interaction. The ratio of Atox1 to WNDP in the cell, however, has yet to be determined but preliminary quantitative RT-PCR experiments and western blot analysis (data not shown) suggest a 3-4 fold excess of Atox1 over WNDP in the cell.

The results in this dissertation also demonstrated a role for Atox1 in the regulation of the Wilson disease protein activity. Huffman and O'Halloran had previously shown that incubation of yeast apo-Atx1 could remove copper from the isolated MBS1 of Ccc2p (65) suggesting that reversible transfer between the metallochaperone and an isolated MBS was possible. The question that we addressed was whether apo-Atox1 could remove copper from full-length N-WNDP with six metal binding sites and whether or not this reverse transfer affected WNDP activity.

The incubation of apo-Atox1 with *E. coli* copper-bound N-WNDP resulted in the stripping of copper from five of the six metal-binding sites on N-WNDP (Figure 2. 4). This process coincided with a reduction in WNDP catalytic activity (Figure 2. 5). Interestingly, apo-Atox1 could not decrease WNDP activity to the same level as incubation with the copper chelator BCS. This suggests that the last site on N-WNDP is not only unavailable to Atox1, but is also responsible for the minimal WNDP activity. The identification of this last site still remains to be determined.

The physiological role of apo-Atox1 in the cell deserves further characterization. Changes in the cellular copper concentration have been documented to result in specific changes to WNDP. These changes include trafficking to a vesicular compartment, protein modifications, and increased activity. An important question that remains to be addressed is whether fluctuations in the cellular copper concentration affect the ratio of apo-Atox1 compared to Cu-Atox1. This question has implications for the understanding of the cellular consequences to copper elevation.

Molecular mechanism of Atox1-mediated copper transfer to WNDP. We next addressed the molecular mechanism of copper transfer to the Wilson disease protein, in

particular, the first step of transfer. Data from the copper transfer experiments showed that Atox1 could load all six metal-binding sites of N-WNDP (Figure 2. 3). Furthermore, Atox1 preferentially loaded MBS2 with copper (Figure 3. 2). This first step is essential for Atox1-mediated copper delivery to the intramembrane site(s) as mutation of the copper binding cysteines in MBS2 abolishes Atox1-stimulated WNDP activity (Figure 3. 7).

The unique orientation of MBS2 within the entire N-WNDP best explains the reason for MBS2 acting as the preferential site for copper delivery from Atox1. Chemical labeling of N-WNDP with a cysteine-directed fluorescent reagent demonstrated that several MBS are exposed to the solvent (Figure 3. 3). Additionally, incubation of free copper in solution or bound to glutathione resulted in copper binding to multiple metal-binding sites including MBS2 (Figure 3. 4). This result suggested that the copper-binding affinity of the various MBS are comparable and in agreement with the isothermal calorimetry data for the metal-binding sites of N-WNDP (81). The fact that under these circumstances copper is still preferentially bound to MBS2 indicates that the accessibility or interaction of Atox1 with MBS2 is preferred over the other MBS.

If Atox1 delivers copper first to MBS2 then how do the other metal-binding sites become occupied with copper? Competition experiments between the copper chelator bicinchonic acid and MBS2 demonstrated that once copper binds to MBS2, it is not easily removed from the coordinating cysteines in the CxxC motif (Figure 3. 5). The observed conformational changes resulting from copper binding to MBS2 suggest that copper binding to this preferential site triggers changes in N-WNDP, which then allow access of Atox1 to other sites. The homology modeling experiments in Appendix I

suggest that Cu-Atox1 can interact favorably with multiple metal-binding sites including MBS2, MBS4, and MBS5 (Figure A. 6, A. 7).

The results presented in this dissertation allow us to propose a model for copper delivery from the cytosol to the intramembrane sites of human copper-transporting ATPases. The first step in this process involves Atox1-mediated copper transfer to MBS2. Copper binding to MBS2 induces several molecular events. First, the copper coordinating cysteines in MBS2 reorient as seen in Figure 1. 5, occluding copper. The change in the position of the copper-binding site in MBS2 triggers conformational changes in neighboring metal-binding sites that can be visualized by a change in the proteolytic pattern of the N-terminal domain (Figure 3. 2). The most significant changes are observed in proximity to MBS5,6 suggesting that these two sites become reoriented and ready to accept copper from Atox1. The binding of copper to MBS5,6 can then be transferred from MBS5,6 to the intramembrane portion of WNDP.

How this conformational switch is induced in response to copper binding to MBS2 is a fascinating question, which will be addressed in detail when structural information on N-WNDP becomes available. However, our results provide the first clues. The data described in Appendix I suggests that the cysteines in MBS3 are in close proximity to the cysteines of MBS2 and might function to keep the MBS2 cysteines reduced and available for copper binding (Figures A. 2, A. 3). Mutation of the cysteines to alanines of either MBS2 or MBS3 results in a phenotype whereby only two or three metal-binding sites of N-WNDP are loaded with copper (Table A. 1). This observation suggests that MBS2 and MBS3 work together to enable complete copper binding to N-WNDP. Mutation of the MBS2,3 pair resulted in the expected copper binding to the

remaining four MBS suggesting that MBS2 and MBS3 work together to regulate copper loading of the N-WNDP.

In conclusion, during the work on this dissertation several new observations related to the copper transfer mechanism have been made and new protocols were developed. The expression system for generating non-tagged Atox1 was set-up and a protocol for loading the human metallochaperone Atox1 with Cu(I) using the physiologically relevant molecule glutathione was developed. An *in vitro* copper transfer assay was also developed which demonstrated that Cu(I)-bound Atox1, alone, directly transfers copper to N-WNDP. Using this copper transfer assay, it was also shown that apo-Atox1 can regulate the copper occupancy on N-WNDP and modulate WNDP activity. The dissertation also documents the development of a fluorescence labeling and partial proteolysis procedure, which allows detection of copper binding to metal-binding sites in N-WNDP and conformational changes. Using this protocol, we describe the molecular mechanisms of Atox1-mediated copper transfer that involves delivery of copper to the preferential site, MBS2, of the Wilson disease protein, and demonstrate that this step is essential for further copper translocation to the intramembrane portion of the transporter. Furthermore, our recent research suggests the importance of MBS3 in facilitating Atox1-mediated copper transfer to the other five MBS on N-WNDP. Together, these findings represent an important step in the understanding of copper metabolism in the cell.

Appendix I

The Role of Metal-binding Site 3 in Copper Delivery to the Wilson Disease Protein

AI. 1: Introduction

Our studies have shown that Atox1 transfers copper to MBS2, the preferential site, and subsequently to all five other metal-binding sites. The experiments in Chapter 3 also began to characterize the molecular mechanisms involved in Atox1-mediated copper transfer to MBS2 by characterizing the copper coordination and retention in MBS2 and Atox1. We also found that copper binding to MBS2 induced specific conformational changes in other parts of N-WNDP suggesting a mechanism for further Atox1-mediated copper transfer to the other MBS. The information on the 3-dimensional orientation of the six MBS in N-WNDP would be extremely helpful for understanding of how copper migrates through N-WNDP. Such information is currently unavailable, however the experiments described in this Appendix revealed functional interactions between the MBS within N-WNDP, which could be critical for the overall copper-binding process.

The first hint that metal-binding sites within WNDP interact came from our initial copper transfer experiments using a recombinant HisTagged version of Atox1, Atox1-HT. (These experiments were performed prior to the experiments involving the intein Atox1 protein described in Chapters 2 and 3). These studies showed that incubation of copper-Atox1-HT resulted in the transfer of 1-1.5 copper atoms to N-WNDP and that copper was transferred preferentially to MBS2. However, in marked contrast to the experiments with the intein construct, in which transfer of 6 coppers to N-WNDP was repeatedly observed (Chapter 2), incubation of N-WNDP with increasing concentrations of Atox1-HT did not to lead to a copper-binding stoichiometry beyond 1.5 suggesting that the further transfer was somehow blocked. Furthermore, the N-WNDP proteolysis after transfer of one copper from Atox1-HT revealed the decreased

availability of the MBS3 cysteines for labeling with the fluorescent reagent CPM, in addition to protection of MBS2. This result suggested that the there was something about the copper Atox1-HT complex that affected the MBS3 cysteines and abrogated further copper transfer. Utilization of a different Atox1 construct and, more importantly, a different method of copper binding to Atox1 (see below for details) helped us to improve the efficiency of copper transfer and better understand the possible reasons for partial transfer by Atox1-HT. These initial results led to the additional experiments described in Appendix I, which altogether allow us to propose a model with MBS3 and MBS2 acting in concert as the switch, which facilitates copper delivery to the other MBS in N-WNDP.

AI. 2: Materials and Methods

Cloning, Expression and Purification of recombinant proteins. To generate the expression construct for His-tagged Atox1, Atox1 cDNA was amplified using polymerase chain reaction and oligonucleotides designed to introduce an *NdeI* restriction site 5' and an *EcoRI* restriction site 3' of the Atox1 coding region. The Atox1 insert was cloned into the pET24b (+) vector (Novagen) using these two cloning sites and the plasmid was transformed into the *E. coli* strain BL21 (DE3). Expression of Atox1-HT was induced with 0.5 mM isopropyl-1-thio-β-D-galactopyranoside (Roche) for 2.5 hours at room temperature. The cells were then harvested by centrifugation and resuspended in 25 mM Tris-HCl, 150 mM NaCl, and pH 7.5. The cells were lysed twice at 16,000 psi with a French Press and the lysate cleared by centrifugation at 30,000 x g for 30 minutes. The soluble fraction was incubated with 10 mM DTT for 10 minutes at room temperature and then dialyzed against lysis buffer at 4 °C for six hours. The dialyzed lysate was

passed over Ni-NTA resin (Qiagen) to bind Atox1-HT to the resin and sequester the His-Tag prior to copper binding.

The resin was washed with six column volumes of 25 mM Tris-HCl, 150 mM NaCl, 45 mM imidazole, pH 7.5 and Atox1-HT was either loaded with copper (see below) or just eluted with 25 mM Tris-HCl, 150 mM NaCl, 150 mM imidazole pH 7.5. When 25 mM $NaPO_4$ was used instead of 25 mM Tris-HCl in each buffer, similar purity and copper-binding stoichiometry of Atox1-HT were obtained. The protein-containing elution fractions were pooled and dialyzed against lysis buffer at 4° C overnight to remove the imidazole. Protein concentration was measured using the Bradford assay (130) and the protein purity was determined using 15 % SDS-PAGE (131).

To produce the recombinant metal-binding site 2 and metal-binding site 3, the corresponding segment of the *ATP7B* cDNA was amplified using the following primers, MBS2 (forward) 5′-CATATGCATGTGGTCACCCTC-3′ and MBS2 (reverse) 5′-GTCGACTTAGGCTCCATCAGGAAGAGA-3′ (reverse); MBS3 (forward) 5′-CATATGCATGTGGTCACCCTC-3′ and MBS3 (reverse) 5′-GTCGACTTAGGCTCCATCAGGAAGAGA-3′. The primers were designed such that 5′ *Nde1* and 3′ *Sal1* restriction sites were incorporated into the MBS2 and MBS3 PCR products. The PCR fragments were cloned into the pTYB12 IMPACT expression vector (New England Biolabs) to produce the pTYB12-MBS2 and the pTYB12-MBS3 expression plasmids and the sequence fidelity was verified by automated DNA sequencing. *E. coli* ER2566 cells were transformed with the pTYB12-MBS2 and pTYB12-MBS3 plasmids. The expression of the MBS2 and MBS3 fusion proteins was induced by isopropyl-β-D-thiogalactopyranoside added to a final concentration of 500

μM at 25°C for 20 hrs. The MBS2 and MBS3 proteins were purified from the soluble fraction using the protocol for Atox1 (Chapter 2 Materials and Methods) and then dialyzed into 25 mM Na_2HPO_4 pH 7.5, 150 mM NaCl. The copper-bound form of MBS2 and MBS3 was generated by incubation of apo-MBS2 and apo-MBS3 with an equimolar amount of copper-glutathione complex and dialyzed into 20 mM Na_2HPO_4 pH 7.5, 150 mM NaCl for further experiments.

To generate the N-WNDP constructs with mutations in metal-binding sites, site-directed mutagenesis was performed using the N-WNDP coding sequence in the pMAL-c2 vector as a template. The mMBS2 N-WNDP mutant, where the CxxC motif of MBS2 was mutated to AxxA, was generated using the mutagenesis primers 5′-GCATGACCGCCCAGTCCGCTGTCAGCTCCATTGAAGG-3′ (forward) and 5′-CTGACAGCGGACTGGGCGGTCATGCCCTCCACCC-3′ (reverse) with the QuikChange II XL site-directed mutagenesis kit (Stratagene). To generate the mMBS3 N-WNDP mutant with the CxxC motif mutated to AxxA, mutagenic primers 5′-GGAATGCATGCTAAGTCTGCCGTCTTGAATATT-3′ (forward) and 5′-CAAGACGGCAGACTTAGCATGCATTCCATCTATTC-3′ (reverse) were utilized. The mMBS23 N-WNDP mutant was produced using mMBS2 N-WNDP as a template and the MBS3 mutagenic primers. The presence of mutations was verified by automated DNA sequencing. The N-WNDP mutant plasmids were transformed into *E. coli* BL21 (DE3) cells and the corresponding proteins were expressed and purified using protocols described in Chapter 2 (Materials and Methods). The amount of copper bound to purified proteins was determined by atomic absorption in Chapter 3 (Materials and Methods).

Loading of Atox1-HT with copper. Copper was added to Atox1 while Atox1-HT was bound to the Ni-NTA resin and the His-tag sequestered, using a five fold molar excess of $CuCl_2$ over Atox1-HT. The resin was washed with three column volumes of lysis buffer followed by elution and subsequent dialysis. After dialysis, the protein concentration was measured and the amount of copper bound to Atox1-HT was determined using a bicinchoninic acid (BCA) assay, where absorbance of a Cu(I)-BCA complex was monitored at 562 nm (132). Under these condition, the stoichiometry of copper-binding to Atox1 was 0.4-0.6. The copper transfer experiments between Atox1-HT and N-WNDP were done using the same protocol as described in Chapter 2 (Materials and Methods).

Chemical labeling and proteolysis of N-WNDP. The CPM labeling and trypsin proteolysis shown in Figures A. 2, 3, 5 were performed as described in Chapter 3 (Materials and Methods). Briefly, 30 μg of N-WNDP was labeled with a 50 mol excess of CPM, the labeling reaction was quenched with an excess of β-mercaptoethanol. The N-WNDP was partially proteolyzed with trypsin for 3 hours at room temperature, the reaction stopped with the protease inhibitor AEBSF; the fragments were separated on a Tris-tricine gel, and transferred to PVDF membrane for identification by Edman sequencing.

The proteolysis experiment described in Figure A.4 had a different order of CPM labeling and trypsin addition. Here, 30 μg of N-WNDP was first proteolyzed with trypsin for 3 hours at room temperature and the reaction stopped with the addition of AEBSF. The fragments were then labeled with CPM, separated on a Tris-tricine gel, and transferred to PVDF membrane for Edman sequencing.

Homology modeling of Atox1 with the MBS of N-WNDP. The ".pdb" file for each of the six MBS of N-WNDP was generated by threading the MBS sequence through the N-MNKP2 structure using the web-based PredictProtein server (http://cubic.bioc.columbia.edu/ predictprotein/). The generated "pdb" file of each MBS was used for further modeling studies.

The homology modeling of Atox1 in complex with the individual metal-binding sites of N-WNDP was generated based on the dimeric crystal structure of copper-bound Atox1 (PDB code 1FEE). Using the program Swiss PDB Viewer (http://www.expasy.org/spdbv/), the N-WNDP metal-binding site ".pdb" files were modeled over the Atox1 structure using the Magic Fit command and the model was improved using the Iterative Magic Fit command. The ".pdb" file for each Atox1-MBS complex was modified to remove the Atox1 monomer which the MBS were to replace in the model complex. This new copper-bound Atox1-MBS complex was refined using the Crystallography and NMR System (http://cns.csb.yale.edu/v1.1/). The ".pdb" file was input into the model_minimize.inp program which generates a new model based on the geometry of the input structure in the absence of crystallographic information. The program eliminates residue clashes within the model and the conjugate gradient minimization functions to achieve the lowest energy based on the original parameters. The input parameters used included a triclinic crystal cell with no symmetry interactions, 200 minimization steps, and a 13 Å nonbonded cutoff. The electrostatic surface potential for each energy minimized Atox1-MBS complex was visualized with the program MOLMOL (145).

AI. 3: Results

Inefficient copper transfer from Atox1-HT to N-WNDP. A series of copper transfer experiments were carried out prior to the experiments described in Chapter 2 using a wide range of ratios between Atox1-HT and N-WNDP. When a large excess of copper bound Atox1-HT over N-WNDP was used, only 1.5-1.6 copper atoms were transferred from Atox1-HT to N-WNDP. The inefficient transfer from Atox1-HT was perplexing as N-WNDP contained six MBS and had previously been shown to bind six copper atoms both in *E. coli* and *in vitro* (*105, 109*). This result suggested two distinct possibilities. One possibility was that copper transfer from Atox1 to N-WNDP required an additional protein to facilitate copper binding to all six sites. This is unlikely as the results in Chapter 2 demonstrate, Atox1, alone, can transfer copper to all six sites.

The other possible reason for inefficient transfer involved the oxidation of one or more metal-binding sites in N-WNDP during incubation with the copper-Atox1-HT complex. As was originally suggested (79) and subsequently directly shown in our experiments (80, 125), Atox1 binds Cu(I). In the early experiments with Atox1-HT, however, copper was added to resin-bound Atox1-HT as Cu(II). This apparently resulted in the two-step process of copper binding to Atox1. First, one Atox1-HT protein reduces Cu(II) to Cu(I) resulting in an oxidized protein and allowing a second Atox1-HT molecule to bind the reduced Cu(I).

This mechanism explains the 0.4-0.6 copper binding stoichiometry routinely observed with Atox1-HT and is consistent with our EPR data showing the majority of bound copper in a Cu(I) state. It is also consistent with the results of CPM labeling, where binding of ~0.5 copper per Atox1 resulted in a two fold higher protection of Cys

residues than was expected based on this stoichiometry. Thus, we concluded that following the loading of Atox1 with Cu(II), the Atox1-HT sample is likely to contain copper-bound protein along with the oxidized protein. Under these circumstances Atox1-HT only transferred at most 1.5-1.6 copper suggesting that other sites were unavailable for transfer.

Copper transfer to the preferential site involves MBS3. Utilization of Atox1-HT for copper transfer produced important results. The copper-bound Atox1-HT preferentially transferred copper to MBS2 (Figure A. 1), similarly to later experiments using non-tagged Atox1 suggesting that the HisTag did not affect the selectivity of copper transfer. We hypothesized that the steps after initial copper transfer to MBS2 were altered by incubation with the copper-Atox1-HT complex and that inactivation of further transfer was likely due to oxidation of other metal-binding sites. In agreement with this hypothesis we found MBS3 among the fragments protected against CPM labeling as the result of transfer of one copper. We also realized that the mechanistic significance of the experiments with the His-Tagged Atox1 is somewhat limited, since copper was added to the protein as Cu(II) and oxidative effects may not be physiologically relevant.

We therefore turned our attention to the intein system that allowed Atox1 to bind Cu(I) and load the six MBS on N-WNDP with copper. In addition to the experiments described in Chapters 2 and 3 we decided to look more closely at the role of MBS3 in copper transfer. CPM labeling experiments revealed that MBS3 was protected from labeling in the apo N-WNDP samples likely due to unusual cysteine reactivity or sterical hindrances. Furthermore, no labeling of MBS3 was also observed after copper transfer

(Figure A. 2*A*). The inability to label the cysteines in MBS3 with CPM either before or after transfer caused us to modify the protocol for labeling and proteolysis. In the original protocol, N-WNDP was first labeled with CPM and then proteolyzed. The drawback with this protocol was that the protein folding may have prevented access of label to MBS3.

To address this problem, the order of labeling and proteolysis was changed. N-WNDP was first proteolyzed and then labeled with CPM. As Figure A. 3*B* shows, the new protocol resulted in the change of the overall fragmentation pattern of N-WNDP suggesting that CPM labeling affected proteolysis. More importantly, though, CPM labeling after proteolysis resulted in distinct effects on the labeling of both MBS2 and MBS3.

The cysteines in MBS2 became unavailable to labeling even in MBS2 from apo N-WNDP suggesting that these cysteines become rapidly oxidized during proteolysis (Figure A. 3*B*). (This result was supported by the observation that the cysteines in recombinant MBS2 became quickly oxidized during storage (our data)). The marked difference in the labeling of MBS2 cysteinses in folded and unfolded N-WNDP suggest that the local environment around the MBS2 cysteines in the intact N-WNDP keeps these cysteines reduced and available for copper loading from Atox1.

The other obvious and opposite change in labeling occurred with MBS3. The partial proteolysis of apo N-WNDP resulted in the relaxation and exposure of the MBS3 cysteines to CPM labeling suggesting that in the apo protein these cysteines were reduced and available for copper binding. Interestingly, the Atox1-mediated transfer of one copper to N-WNDP resulted in the selective loss of fluorescence of MBS3. This

observation suggested that either MBS3 was involved in copper coordination, or became oxidized, or a redistribution of copper from MBS2 to MBS3 occurred during proteolysis.

To test this latter possibility, isolated recombinant MBS2 and MBS3 were expressed, purified, and loaded with copper as described in the Materials and Methods. Copper binding affinities of these two proteins were compared in competition experiments using the copper chelator bicinchoninic acid (BCA). As shown in Figure A. 3, there was a complete redistribution of copper from MBS3 to BCA when a 45-fold molar excess of chelator was used. In contrast, MBS2 only lost 10% of its copper in these conditions. This result suggested that MBS2 was unlikely to lose copper during proteolysis and have the copper redistribute to MBS3.

A second possible explanation was that MBS3 helped coordinate the copper bound to MBS2 or became oxidized when copper binds to MBS2. Which of these explanations was correct was tested by acid precipitating the proteolyzed copper-bound fragments, resuspending the fragments, and labeling with CPM. If copper binds between MBS2 and MBS3, then acid precipitation should release the copper from both proteins and make them available for labeling. If MBS3 was oxidized, then acid precipitation would not allow for the later accessibility of the MBS3 Cys for CPM label. Although the data are preliminary, these experiments demonstrated that the MBS3 cysteines were CPM-labeled after precipitation while the MBS2 cysteines were still unlabeled (data not shown) raising a question about the initial copper binding state of MBS2. At this point it became clear that both MBS2 and MBS3 are affected by transfer of one copper and that independent methods would help to clarify their specific role in copper binding.

Mutation of metal-binding site 3 disrupts copper loading of N-WNDP. To test the hypothesis that the role of MBS3 is to act in concert with MBS2 as a regulator of further copper binding to N-WNDP, site-directed mutagenesis of MBS2, MBS3, and a MBS23 pair of N-WNDP was carried out. In these proteins, the CxxC metal-binding site sequence motifs were mutated to AxxA motifs.

The mutant N-WNDP proteins were expressed in *E. coli* grown in the presence of copper to allow for copper binding (105) and purified with yields and purity similar to WT N-WNDP. The copper binding properties were then characterized. The average copper stoichiometry from two independent experiments is shown in Table A. 1 and the results were surprising and quite interesting. Mutation of a single site, MBS2, resulted in N-WNDP with only two sites occupied by copper instead of the predicted five sites. Mutation of MBS3 also resulted in a lower amount of expected bound copper to N-WNDP as only about 3 sites were filled. Thus mutations of their MBS2 or MBS3 significantly impair copper transfer to other sites in N-WNDP. However, mutation of both MBS2 and MBS3 in the MBS2,3 construct alleviated this negative effect and resulted in the expected copper binding stoichiometry of four suggesting that MBS2 and MBS3 work together to regulate copper loading of the N-WNDP.

Partial proteolysis of the mutant N-WNDP proteins with trypsin revealed a change in the protein folding upon mutation of the cysteines in MBS3, an effect that was also observed in the MBS2,3 mutant (Figure A. 4*A,B*). This change in fragment size was most pronounced when the proteins were labeled with CPM prior to proteolysis although careful examination of the proteolytic pattern in the absence of CPM revealed the same effects (Figure A. 4*C*). A possible explanation for this change in folding is that the one

or both of the cysteines of CxxC motif of MBS3 were involved in a hydrogen bond. Disruption of the hydrogen bond destabilizes the entire N-WNDP resulting in a change in proteolysis. To test of this hypothesis it would be necessary to mutate both cysteines to serines or each cysteine individually and monitor the effects on proteolysis.

Atox1-MBS complexes show some favorable electrostatic interactions. The electrostatic surface potential of the individual metal-binding sites and Atox1 suggested that several MBS had favorable interacting surfaces (Figure. 3. 8). To better understand the structural basis of copper transfer from Atox1 to N-WNDP, a model of Atox1 interacting with each of the individual MBS was made using the copper-bound Atox1 crystal dimer structure (PDB code 1FEE) as a template (124). The complex structure was refined through energy minimization calculations resulting in a new structure with no amino acid clashes. The Table A. 2 shows the total energy of the two interacting proteins in each complex with the 1FEE crystal structure having the lowest total energy. The other Atox1-MBS complexes have similar energies with MBS1 having the highest and least favorable interaction.

In order to determine whether the electrostatic interactions in the homology models were complementary, the Atox1-MBS complexes were analyzed using the program MOLMOL (145). This program displays negative electrostatic surfaces in red and positive electrostatic surfaces in blue. A favorable interaction has negative and positive electrostatic surface areas between the interacting proteins on the same face of the complex but not necessarily adjacent to each other.

As seen in Figures A. 5,6, MBS4 shows very strong complementary electrostatic interactions, which is consistent with the recent yeast 2-hybrid data showing interaction

of Atox1 with isolated MBS2 and MBS4 (146). From the bottom view (Figure. A. 6) MBS5, MBS6, and MBS2 appear to have complementary surfaces suggesting favorable interactions and potential interaction with Atox1 when the metal-binding sites are properly oriented. In contrast, MBS1 has a repulsive, positively-charged surface with an asparagine residue pointed directly at the KTGK sequence motif of Atox1, which helps explain the high total energy of interaction. Finally, the Atox1-MBS3 complex does not produce a good fit at the interacting faces possibly due to the diproline motif in loop 5 (Figure 1. 5), suggesting that MBS3 might have a different role within the N-WNDP.

AI. 4: Summary

The results from this Appendix suggest that MBS2 and MBS3 work together to regulate the copper occupancy of the N-WNDP possibly through a cysteine-mediated redox function. The modeling experiments suggest that Atox1 can form favorable complexes with several MBS including MBS5 and MBS6, the two metal-binding sites involved in copper delivery to the intramembrane region of WNDP.

AI. 5: Acknowledgements

Clinton Morgan generated the recombinant MBS2-intein and MBS3-intein constructs and helped with the competition experiments. We also thank Dr. Maria Schumacher for help with the modeling experiments.

Table A .1. Mutant N-WNDP copper stoichiometry measurements.

E. coli copper-loaded protein	Copper Stoichiometry
WT N-WNDP	5.5
mMBS2 N-WNDP	2.0
mMBS3 N-WNDP	2.7
mMBS2,3 N-WNDP	4.6

Table A. 2. Calculated energies of interaction between the Atox1 dimer and the Atox1-MBS complexes. The refined energy minimization calculations of the copper-bound complex was computed for each Atox1-MBS pair and also for the control Atox1 dimer structure (PDB code 1FEE). The total number of interactions between all the amino acids in each complex, including the interacting surface, is shown in the table. The refined structure contains no amino acid clashes in the complex.

Table A. 2.

Atox1 complex	Control (1FEE)	MSB1	MSB2	MSB3	MSB4	MSB5	MSB6
Interactions (#)	111170	112622	113179	104510	107418	114040	113566
Overall E (kcal)	1684.4	2050.4	1952.4	1812.6	1935.7	1794.5	1969.4

Figure A. 1.

Proteolysis of labeled N-WNDP after copper transfer from Atox1-HT. The CPM fluorescence pattern of N-WNDP after transfer from copper-bound Atox1-HT, labeling with CPM, and trypsin proteolysis. The N-WNDP samples were separated on a Tris-tricine gel and visualized under UV-light. The left lane shows incubation of N-WNDP with copper-bound Atox1-HT while the right lane contains apo Atox1-HT. The dashed arrow shows the location of the MBS2 fragment.

Figure A. 1.

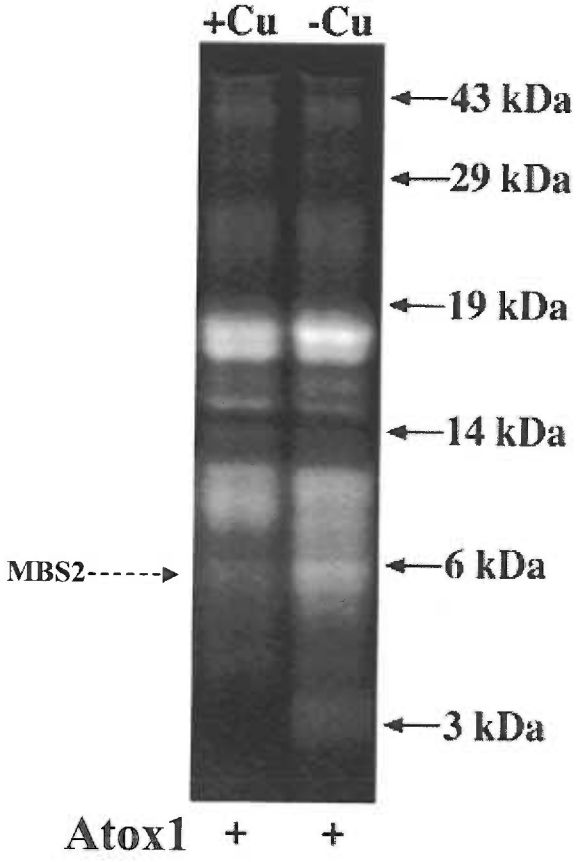

Figure A. 2.

Fluorescent labeling and proteolysis of N-WNDP after copper transfer from Atox1. Copper transfer to N-WNDP was done as described in Chapter 3 with transfer of one copper atom. *A,* N-WNDP was labeled with the fluorescent reagent CPM and proteolyzed with trypsin. The fragments were separated on a Tris-tricine gel with the fluorescence (*Left*) and Coomassie R250 staining (*Right*). The arrows indicate the location of MBS2 and MBS3 fragments. *B,* N-WNDP was proteolyzed with trypsin and subsequently labeled with the fluorescent reagent CPM. The fragments were separated on a Tris-tricine gel with the fluorescence (*Left*) and Coomassie R250 staining (*Right*). The arrows indicate the location of MBS2,MBS3 fragments, and Coomassie stained Atox1.

Figure A. 2.

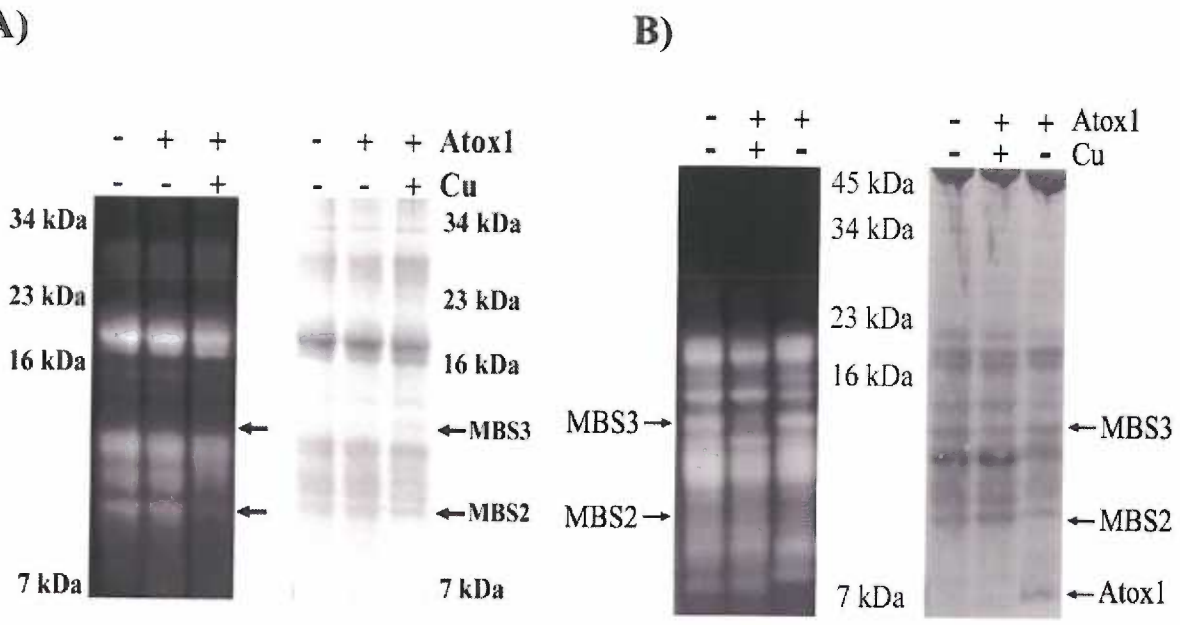
A)
B)
- + + - + + Atox1
- - + - - + Cu
34 kDa
23 kDa
16 kDa
MBS3
MBS2
7 kDa
34 kDa
23 kDa
16 kDa
MBS3
MBS2
7 kDa
- + +
- + -
45 kDa
34 kDa
23 kDa
16 kDa
MBS3
MBS2
7 kDa
- + + Atox1
- + - Cu
MBS3
MBS2
Atox1

Figure A. 3.

Copper retention by MBS2 and MBS3 in the presence of the high affinity copper chelator BCA. The purified copper complexes with MBS2 (●) and MBS3 (○) were incubated with increasing concentrations of the copper chelator BCA. The amount of copper redistributed from the protein to BCA was determined by comparing the absorbance to the standard. The initial amount of copper-bound protein was taken as 100%, and the amount of copper redistributed to BCA was subtracted.

Figure A. 3.

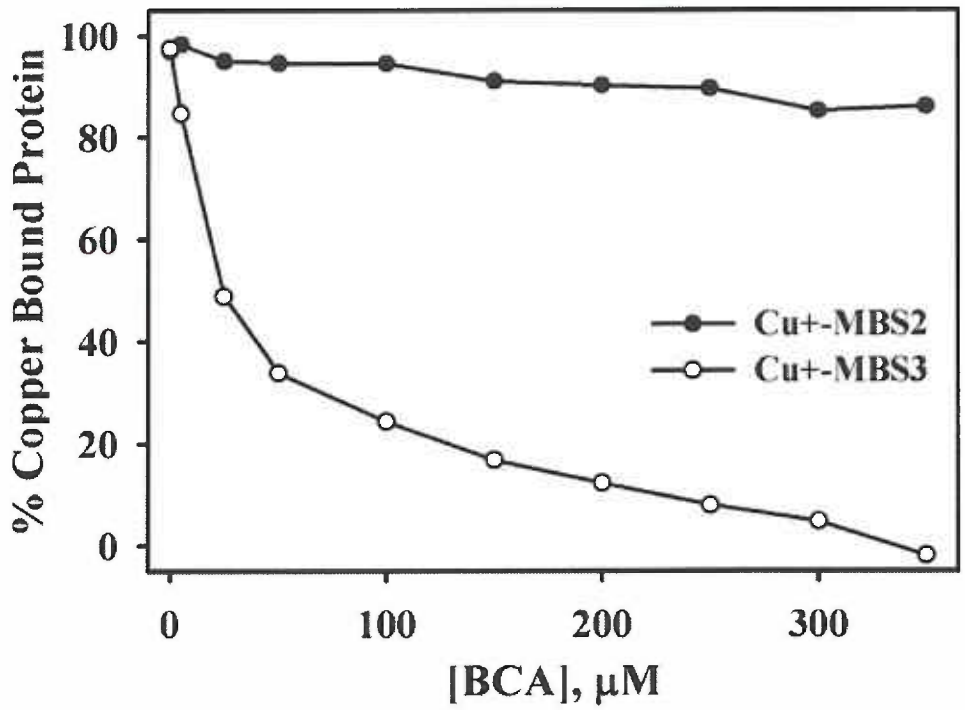
% Copper Bound Protein
100
80
60
40
20
0
0
100
200
300
[BCA], μM
Cu+-MBS2
Cu+-MBS3

Figure A. 4.

Proteolysis of mutant N-WNDP. *A,* wild-type and mutant N-WNDP was labeled with a 50 mol equivalent CPM, proteolyzed with trypsin and the fragments separated on a Tris-Tricine gel. The *left panel* shows the fluorescence pattern and the *right panel* shows the protein pattern after staining with Coomassie R250. *B,* wild-type and mutant N-WNDP were proteolyzed with trypsin and the fragments separated on a Tris-Tricine gel. The fragments were visualized after staining with Coomassie R250.

Figure A. 4.

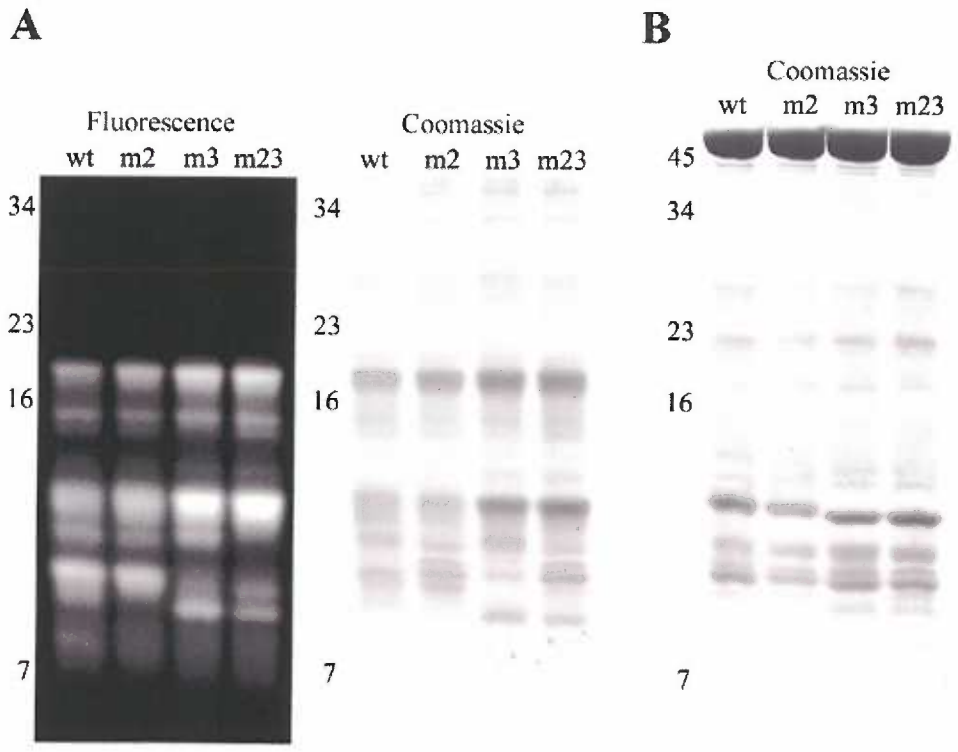
A
Fluorescence
wt m2 m3 m23
34
23
16
7
Coomassie
wt m2 m3 m23
34
23
16
7
B
Coomassie
wt m2 m3 m23
45
34
23
16
7

Figure A. 5.

Side view of the electrostatic surface potential for Atox1-MBS complexes. *A,* ribbon diagram shows the orientation of the two proteins in complex in panel *B*. The proteins were homology modeled onto the Cu-Atox1 crystal structure (1FEE) using the program Swiss-PdbViewer. The copper atom is shown in cyan. *B,* the surface charge distribution for each Atox1-MBS complex is shown with negative charges shown in red and positive charges shown in blue. The figure was generated with the program MOLMOL (145).

Figure A. 5.

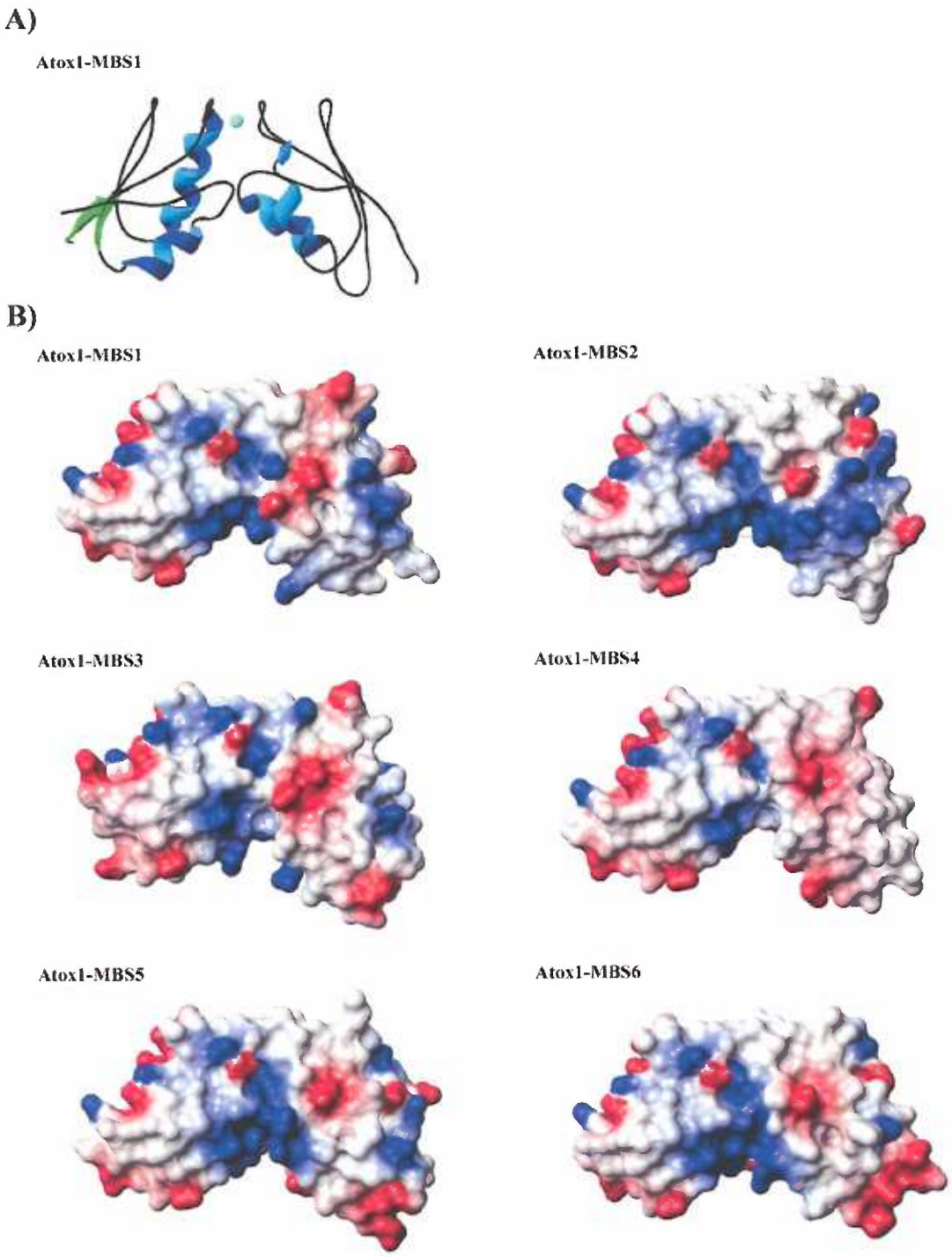
A)
Atox1-MBS1
B)
Atox1-MBS1
Atox1-MBS2
Atox1-MBS3
Atox1-MBS4
Atox1-MBS5
Atox1-MBS6

Figure A. 6.

Bottom view of the electrostatic surface potential for Atox1-MBS complexes. *A,* ribbon diagram shows the orientation of the Atox1 with a metal-binding site in complex in panel *B*. The proteins were homology modeled onto the Cu-Atox1 crystal structure (1FEE) using the program Swiss-PdbViewer. The copper atom is shown in cyan. *B,* the surface charge distribution for each Atox1-MBS complex is shown with negative charges shown in red and positive charges shown in blue. The figure was generated with the program MOLMOL (145).

Figure A. 6.

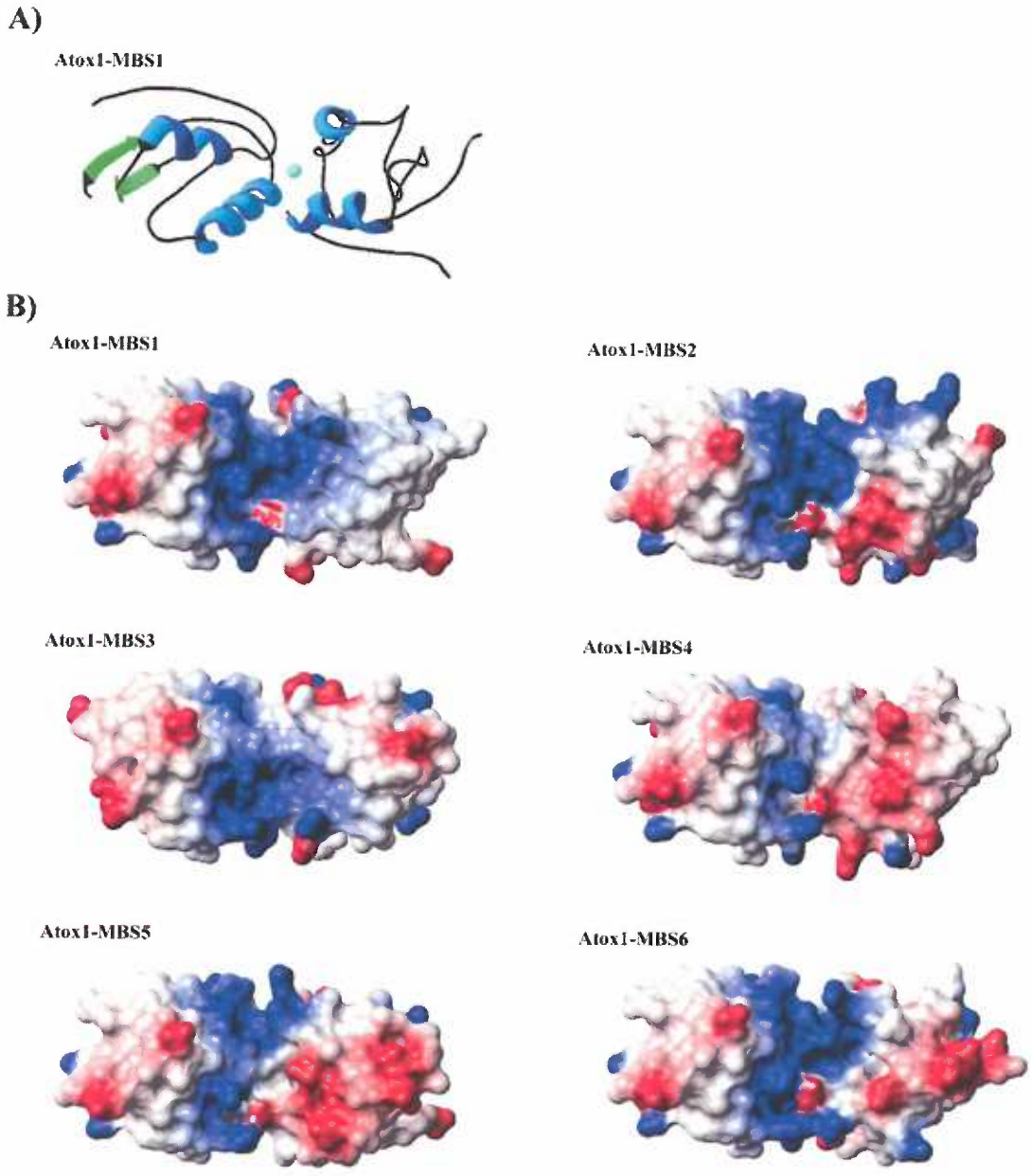
A)
Atox1-MBS1
B)
Atox1-MBS1
Atox1-MBS2
Atox1-MBS3
Atox1-MBS4
Atox1-MBS5
Atox1-MBS6

Appendix II

Atox1 Exists Predominantly as a Monomer in the Cell

Atox1 exists as a monomer in the soluble fraction of Hek293 cell. In Appendix II we addressed the question of whether Atox1 is a monomer or a dimer in the cell. The Atox1 crystal structure was solved as a homodimer where each monomer of Atox1 was coordinating the shared copper atom (124). Recently, experimental evidence using Biacore analysis has shown that recombinant Atox1 can form homodimers in solution upon the addition of Cu(II) (147). To address this question, the soluble fraction from Hek293 cells was isolated. Using gel filtration chromatography, the soluble fraction was passed over a calibrated Amersham Pharmacia Superose 12 10/300 GL column and the fractions collected. Western blot analysis for Atox1 was performed on all the fractions. The results in Figure A. 7 show the presence of monomeric Atox1 primarily in the 7 kDa protein fraction. A smaller portion of Atox1 appears to complex with a high molecular weight protein, possibly the recently identified interacting protein FKBP52 (148). These results suggest that Atox1 exists primarily as a monomer in Hek293 cells.

Figure A. 7.

Gel filtration chromatography for Atox1 in Hek293 cell lysates. *A,* the chromatogram shows the protein eluting from the gel filtration column with four calibrating standard proteins labeled. *B,* western blot analysis of several column fractions indicates the presence of Atox1 as a monomer and in a high molecular weight complex.

Figure A. 7.

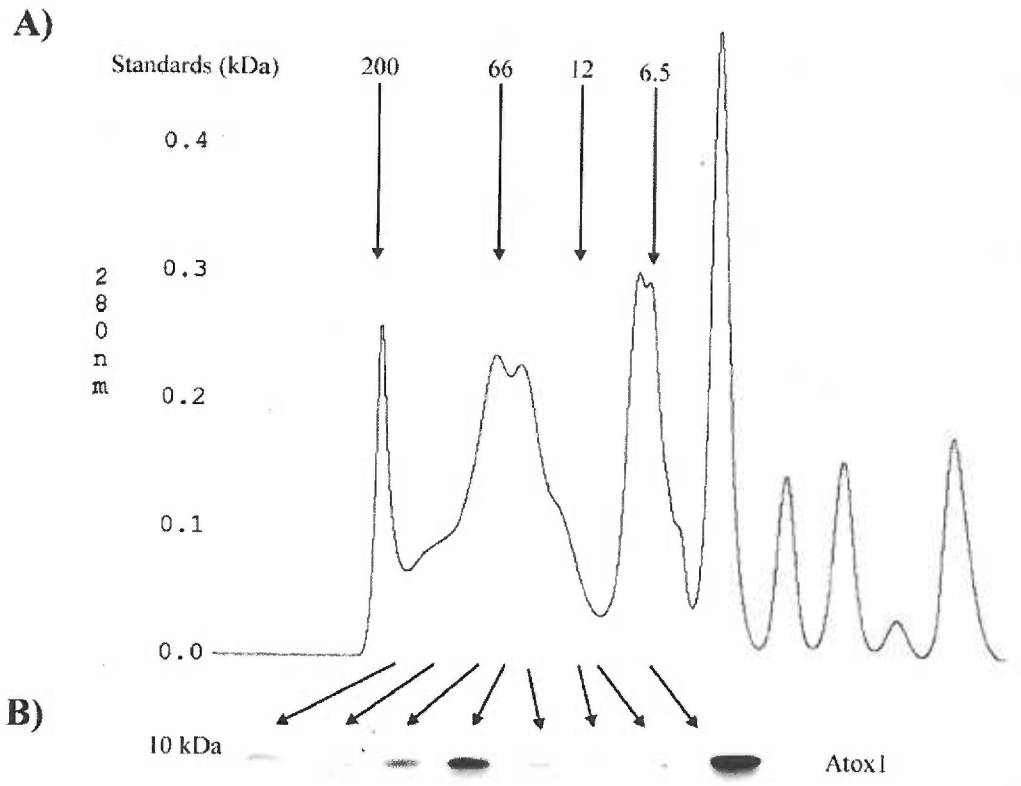

References:

1. Pena, M. M., Lee, J., and Thiele, D. J. (1999) A delicate balance: homeostatic control of copper uptake and distribution. *J Nutr 129*, 1251-60.
2. Carmichael, P. L., Hewer, A., Osborne, M. R., Strain, A. J., and Phillips, D. H. (1995) Detection of bulky DNA lesions in the liver of patients with Wilson's disease and primary haemochromatosis. *Mutat Res 326*, 235-43.
3. Nair, J., Carmichael, P. L., Fernando, R. C., Phillips, D. H., Strain, A. J., and Bartsch, H. (1998) Lipid peroxidation-induced etheno-DNA adducts in the liver of patients with the genetic metal storage disorders Wilson's disease and primary hemochromatosis. *Cancer Epidemiol Biomarkers Prev 7*, 435-40.
4. Gu, M., Cooper, J. M., Butler, P., Walker, A. P., Mistry, P. K., Dooley, J. S., and Schapira, A. H. (2000) Oxidative-phosphorylation defects in liver of patients with Wilson's disease. *Lancet 356*, 469-74.
5. Buiakova, O. I., Xu, J., Lutsenko, S., Zeitlin, S., Das, K., Das, S., Ross, B. M., Mekios, C., Scheinberg, I. H., and Gilliam, T. C. (1999) Null mutation of the murine ATP7B (Wilson disease) gene results in intracellular copper accumulation and late-onset hepatic nodular transformation. *Hum Mol Genet 8*, 1665-71.
6. Linder, M. C., and Hazegh-Azam, M. (1996) Copper biochemistry and molecular biology. *Am J Clin Nutr 63*, 797S-811S.
7. Wapnir, R. A. (1998) Copper absorption and bioavailability. *Am-J-Clin-Nutr 67*, 1054S-1060S.
8. Brewer, G. J., and Yuzbasiyan-Gurkan, V. (1992) Wilson disease. *Medicine (Baltimore) 71*, 139-64.

9. Linder, M. C. (1991) *Biochemistry of Copper*, Plenum Press, New York.

10. Vargas, E. J., Shoho, A. R., and Linder, M. C. (1994) Copper transport in the Nagase analbuminemic rat. *Am J Physiol 267*, G259-69.

11. Cordano, A. (1998) Clinical manifestations of nutritional copper deficiency in infants and children. *Am J Clin Nutr 67*, 1012S-1016S.

12. Uauy, R., Castillo-Duran, C., Fisberg, M., Fernandez, N., and Valenzuela, A. (1985) Red cell superoxide dismutase activity as an index of human copper nutrition. *J Nutr 115*, 1650-5.

13. Graham, G. G., and Cordano, A. (1969) Copper depletion and deficiency in the malnourished infant. *Johns Hopkins Med J 124*, 139-50.

14. Cordano, A., Placko, R. P., and Graham, G. G. (1966) Hypocupremia and neutropenia in copper deficiency. *Blood 28*, 280-3.

15. Danks, D. M. (1995) Disorders of copper transport. In *The metabolic and molecular basis of inherited disease* (Scriver, C. R., Beaudet, A. L., Sly, W. M., and Valle, D., Eds.) pp 2211-2235, McGraw-Hill, New York.

16. Wakai, S., Ishikawa, Y., Nagaoka, M., Okabe, M., Minami, R., and Hayakawa, T. (1993) Central nervous system involvement and generalized muscular atrophy in occipital horn syndrome: Ehlers-Danlos type IX. A first Japanese case. *J Neurol Sci 116*, 1-5.

17. Das, S., Levinson, B., Vulpe, C., Whitney, S., Gitschier, J., and Packman, S. (1995) Similar splicing mutations of the Menkes/mottled copper-transporting ATPase gene in occipital horn syndrome and the blotchy mouse. *Am J Hum Genet 56*, 570-6.

18. Kaler, S. G., Gallo, L. K., Proud, V. K., Percy, A. K., Mark, Y., Segal, N. A., Goldstein, D. S., Holmes, C. S., and Gahl, W. A. (1994) Occipital horn syndrome and a mild Menkes phenotype associated with splice site mutations at the MNK locus. *Nature Genet. 8*, 195-202.

19. Kaler, S. G. (1998) Diagnosis and therapy of Menkes syndrome, a genetic form of copper deficiency. *Am J Clin Nutr 67*, 1029S-1034S.

20. Menkes, J. H., Alter, M., Steigleder, G. K., Weakley, D. R., and Sung, J. H. (1962) A sex-linked recessive disorder with retardation of growth, peculiar hair, and focal cerebral and cerebellar degeneration. *Pediatrics 29*, 764-79.

21. Gillespie, J. M. (1973) Keratin structure and changes with copper deficiency. *Australas J Dermatol 14*, 127-31.

22. Danks, D. M., Cartwright, E., Stevens, B. J., and Townley, R. R. (1973) Menkes' kinky hair disease: further definition of the defect in copper transport. *Science 179*, 1140-2.

23. Mercer, J. F., Livingston, J., Hall, B., Paynter, J. A., Begy, C., Chandrasekharappa, S., Lockhart, P., Grimes, A., Bhave, M., and Siemieniak, D. (1993) Isolation of a partial candidate gene for Menkes disease by positional cloning. *Nat Genet 3*, 20-5.

24. Vulpe, C., Levinson, B., Whitney, S., Packman, S., and Gitschier, J. (1993) Isolation of a candidate gene for Menkes disease and evidence that it encodes a copper-transporting ATPase. *Nat Genet 3*, 7-13.

25. Chelly, J., Tumer, Z., Tonnesen, T., Petterson, A., Ishikawa-Brush, Y., Tommerup, N., Horn, N., and Monaco, A. P. (1993) Isolation of a candidate gene

for Menkes disease that encodes a potential heavy metal binding protein. *Nat Genet 3*, 14-9.

26. Bhave, S. A., Pandit, A. N., Pradhan, A. M., Sidhaye, D. G., Kantarjian, A., Williams, A., Talbot, I. C., and Tanner, M. S. (1982) Liver disease in India. *Arch Dis Child 57*, 922-8.

27. Prasad, R., Kaur, G., Nath, R., and Walia, B. N. (1996) Molecular basis of pathophysiology of Indian childhood cirrhosis: role of nuclear copper accumulation in liver. *Mol Cell Biochem 156*, 25-30.

28. Tanner, M. S. (1998) Role of copper in Indian childhood cirrhosis. *Am J Clin Nutr 67*, 1074S-1081S.

29. Wilson, S. A. K. (1912) Progressive lenticular degeneration: a familial nervous disease associated with cirrhosis of the liver. *Lancet 1*, 1115-1119.

30. Cunnings, J. N. (1948) The copper and iron content of the liver and brain in the normal and hepatolenticular degeneration. *Brain 71*, 410-417.

31. Scheinberg, H., and Gitlin, J. (1952) Deficiency of ceruloplasmin in patients with hepatolenticular degeneration (Wilson's disease). *Science 116*, 484-485.

32. Bull, P. C., Thomas, G. R., Rommens, J. M., Forbes, J. R., and Cox, D. W. (1993) The Wilson disease gene is a putative copper transporting P-type ATPase similar to the Menkes gene. *Nat Genet 5*, 327-37.

33. Yamaguchi, Y., Heiny, M. E., and Gitlin, J. D. (1993) Isolation and characterization of a human liver cDNA as a candidate gene for Wilson disease. *Biochem Biophys Res Commun 197*, 271-7.

34. Petrukhin, K., Lutsenko, S., Chernov, I., Ross, B. M., Kaplan, J. H., and Gilliam, T. C. (1994) Characterization of the Wilson disease gene encoding a P-type copper transporting ATPase: genomic organization, alternative splicing, and structure/function predictions. *Hum Mol Genet 3*, 1647-56.

35. Hsi, G., and Cox, D. W. (2003) A comparison of the mutation spectra of Menkes disease and Wilson disease. *Hum Genet*.

36. Gollan, J. L., and Gollan, T. J. (1998) Wilson disease in 1998: genetic, diagnostic and therapeutic aspects. *J Hepatol 28 Suppl 1*, 28-36.

37. Gitlin, J. D. (2003) Wilson disease. *Gastroenterology 125*, 1868-77.

38. Brewer, G. J. (2000) Recognition, diagnosis, and management of Wilson's disease. *Proc Soc Exp Biol Med 223*, 39-46.

39. Scheinberg, I. H., and Sternlieb, I. (1984) *Wilson's Disease*, Vol. 23, W. B. Saunders, Philadelphia.

40. Brewer, G. J. (2000) Wilson's Disease. *Curr Treat Options Neurol 2*, 193-204.

41. Pufahl, R. A., Singer, C. P., Peariso, K. L., Lin, S. J., Schmidt, P. J., Fahrni, C. J., Culotta, V. C., Penner-Hahn, J. E., and O'Halloran, T. V. (1997) Metal ion chaperone function of the soluble Cu(I) receptor Atx1. *Science 278*, 853-6.

42. Rae, T. D., Schmidt, P. J., Pufahl, R. A., Culotta, V. C., and O'Halloran, T. V. (1999) Undetectable intracellular free copper: the requirement of a copper chaperone for superoxide dismutase. *Science 284*, 805-8.

43. Lee, J., Pena, M. M., Nose, Y., and Thiele, D. J. (2002) Biochemical characterization of the human copper transporter Ctr1. *J Biol Chem 277*, 4380-7.

44. Eisses, J. F., and Kaplan, J. H. (2002) Molecular characterization of hCTR1, the human copper uptake protein. *J Biol Chem 277*, 29162-71.

45. Xiao, Z., and Wedd, A. G. (2002) A C-terminal domain of the membrane copper pump Ctr1 exchanges copper(I) with the copper chaperone Atx1. *Chem Commun (Camb)*, 588-9.

46. Tapia, L., Gonzalez-Aguero, M., Cisternas, M. F., Suazo, M., Cambiazo, V., Uauy, R., and Gonzalez, M. (2004) Metallothionein is crucial for safe intracellular copper storage and cell survival at normal and supra-physiological exposure levels. *Biochem J 378*, 617-24.

47. Horng, Y. C., Cobine, P. A., Maxfield, A. B., Carr, H. S., and Winge, D. R. (2004) Specific copper transfer from the Cox17 metallochaperone to both Sco1 and Cox11 in the assembly of yeast cytochrome C oxidase. *J Biol Chem 279*, 35334-40.

48. Maxfield, A. B., Heaton, D. N., and Winge, D. R. (2004) Cox17 is functional when tethered to the mitochondrial inner membrane. *J Biol Chem 279*, 5072-80.

49. Field, L. S., Luk, E., and Culotta, V. C. (2002) Copper chaperones: personal escorts for metal ions. *J Bioenerg Biomembr 34*, 373-9.

50. Hellman, N. E., and Gitlin, J. D. (2002) Ceruloplasmin metabolism and function. *Annu Rev Nutr 22*, 439-58.

51. Mercer, J. F. (2001) The molecular basis of copper-transport diseases. *Trends Mol Med 7*, 64-9.

52. Ogihara, N. L., Parge, H. E., Hart, P. J., Weiss, M. S., Goto, J. J., Crane, B. R., Tsang, J., Slater, K., Roe, J. A., Valentine, J. S., Eisenberg, D., and Tainer, J. A.

(1996) Unusual trigonal-planar copper configuration revealed in the atomic structure of yeast copper-zinc superoxide dismutase. *Biochemistry 35*, 2316-21.

53. Hart, P. J., Balbirnie, M. M., Ogihara, N. L., Nersissian, A. M., Weiss, M. S., Valentine, J. S., and Eisenberg, D. (1999) A structure-based mechanism for copper-zinc superoxide dismutase. *Biochemistry 38*, 2167-78.

54. Furukawa, Y., Torres, A. S., and O'Halloran, T. V. (2004) Oxygen-induced maturation of SOD1: a key role for disulfide formation by the copper chaperone CCS. *Embo J.*

55. Arnesano, F., Banci, L., Bertini, I., Martinelli, M., Furukawa, Y., and O'Halloran, T. V. (2004) The unusually stable quaternary structure of human Cu,Zn-superoxide dismutase 1 is controlled by both metal occupancy and disulfide status. *J Biol Chem 279*, 47998-8003.

56. Tainer, J. A., Getzoff, E. D., Beem, K. M., Richardson, J. S., and Richardson, D. C. (1982) Determination and analysis of the 2 A-structure of copper, zinc superoxide dismutase. *J Mol Biol 160*, 181-217.

57. Lamb, A. L., Wernimont, A. K., Pufahl, R. A., Culotta, V. C., O'Halloran, T. V., and Rosenzweig, A. C. (1999) Crystal structure of the copper chaperone for superoxide dismutase. *Nat Struct Biol 6*, 724-9.

58. Lamb, A. L., Torres, A. S., O'Halloran, T. V., and Rosenzweig, A. C. (2001) Heterodimeric structure of superoxide dismutase in complex with its metallochaperone. *Nat Struct Biol 8*, 751-5.

59. Eisses, J. F., Stasser, J. P., Ralle, M., Kaplan, J. H., and Blackburn, N. J. (2000) Domains I and III of the human copper chaperone for superoxide dismutase interact via a cysteine-bridged Dicopper(I) cluster. *Biochemistry 39*, 7337-42.

60. Schmidt, P. J., Kunst, C., and Culotta, V. C. (2000) Copper activation of superoxide dismutase 1 (SOD1) in vivo. Role for protein-protein interactions with the copper chaperone for SOD1. *J Biol Chem 275*, 33771-6.

61. Rae, T. D., Torres, A. S., Pufahl, R. A., and O'Halloran, T. V. (2001) Mechanism of Cu,Zn-superoxide dismutase activation by the human metallochaperone hCCS. *J Biol Chem 276*, 5166-76.

62. Field, L. S., Furukawa, Y., O'Halloran, T. V., and Culotta, V. C. (2003) Factors controlling the uptake of yeast copper/zinc superoxide dismutase into mitochondria. *J Biol Chem 278*, 28052-9.

63. Lin, S. J., and Culotta, V. C. (1995) The ATX1 gene of Saccharomyces cerevisiae encodes a small metal homeostasis factor that protects cells against reactive oxygen toxicity. *Proc Natl Acad Sci U S A 92*, 3784-8.

64. Lin, S. J., Pufahl, R. A., Dancis, A., O'Halloran, T. V., and Culotta, V. C. (1997) A role for the Saccharomyces cerevisiae ATX1 gene in copper trafficking and iron transport. *J Biol Chem 272*, 9215-20.

65. Huffman, D. L., and O'Halloran, T. V. (2000) Energetics of copper trafficking between the Atx1 metallochaperone and the intracellular copper transporter, Ccc2. *J Biol Chem 275*, 18611-4.

66. Dancis, A., Yuan, D. S., Haile, D., Askwith, C., Elde, D., Moehle, C., Kaplan, J., and Klausner, R. D. (1994) Molecular characterization of a copper transport

protein in S. cerevisiae: an unexpected role for copper in iron transport. *Cell 76*, 393-402.

67. Stearman, R., Yuan, D. S., Yamaguchi-Iwai, Y., Klausner, R. D., and Dancis, A. (1996) A permease-oxidase complex involved in high-affinity iron uptake in yeast. *Science 271*, 1552-7.

68. Askwith, C., Eide, D., Van Ho, A., Bernard, P. S., Li, L., Davis-Kaplan, S., Sipe, D. M., and Kaplan, J. (1994) The FET3 gene of S. cerevisiae encodes a multicopper oxidase required for ferrous iron uptake. *Cell 76*, 403-10.

69. De Silva, D. M., Askwith, C. C., Eide, D., and Kaplan, J. (1995) The FET3 gene product required for high affinity iron transport in yeast is a cell surface ferroxidase. *J Biol Chem 270*, 1098-101.

70. Klomp, L. W., Lin, S. J., Yuan, D. S., Klausner, R. D., Culotta, V. C., and Gitlin, J. D. (1997) Identification and functional expression of HAH1, a novel human gene involved in copper homeostasis. *J Biol Chem 272*, 9221-6.

71. Lockhart, P. J., and Mercer, J. F. (2000) Identification of the copper chaperone SAH in Ovis aries: expression analysis and in vitro interaction of SAH with ATP7B. *Biochim Biophys Acta 1490*, 11-20.

72. Naeve, G. S., Vana, A. M., Eggold, J. R., Kelner, G. S., Maki, R., Desouza, E. B., and Foster, A. C. (1999) Expression profile of the copper homeostasis gene, rAtox1, in the rat brain. *Neuroscience 93*, 1179-87.

73. Hiromura, M., and Sakurai, H. (1999) Molecular cloning of rat ATX1 homologue protein. *Biochem Biophys Res Commun 265*, 509-12.

74. Hamza, I., Klomp, L. W., Gaedigk, R., White, R. A., and Gitlin, J. D. (2000) Structure, expression, and chromosomal localization of the mouse Atox1 gene. *Genomics 63*, 294-7.

75. Nanji, M. S., and Cox, D. W. (1999) The copper chaperone Atox1 in canine copper toxicosis in Bedlington terriers. *Genomics 62*, 108-12.

76. Moore, S. D., Helmle, K. E., Prat, L. M., and Cox, D. W. (2002) Tissue localization of the copper chaperone ATOX1 and its potential role in disease. *Mamm Genome 13*, 563-8.

77. Liu, P. C., Koeller, D. M., and Kaler, S. G. (2003) Genomic organization of ATOX1, a human copper chaperone. *BMC Genet 4*, 4.

78. Boultwood, J., Strickson, A. J., Jabs, E. W., Cheng, J. F., Fidler, C., and Wainscoat, J. S. (2000) Physical mapping of the human ATX1 homologue (HAH1) to the critical region of the 5q- syndrome within 5q32, and immediately adjacent to the SPARC gene. *Hum Genet 106*, 127-9.

79. Hung, I. H., Casareno, R. L., Labesse, G., Mathews, F. S., and Gitlin, J. D. (1998) HAH1 is a copper-binding protein with distinct amino acid residues mediating copper homeostasis and antioxidant defense. *J Biol Chem 273*, 1749-54.

80. Ralle, M., Lutsenko, S., and Blackburn, N. J. (2003) X-ray absorption spectroscopy of the copper chaperone HAH1 reveals a linear two-coordinate Cu(I) center capable of adduct formation with exogenous thiols and phosphines. *J Biol Chem 278*, 23163-70.

81. Wernimont, A. K., Yatsunyk, L. A., and Rosenzweig, A. C. (2004) Binding of copper(I) by the Wilson disease protein and its copper chaperone. *J Biol Chem 279*, 12269-76.

82. Hamza, I., Faisst, A., Prohaska, J., Chen, J., Gruss, P., and Gitlin, J. D. (2001) The metallochaperone Atox1 plays a critical role in perinatal copper homeostasis. *Proc Natl Acad Sci U S A 98*, 6848-52.

83. Hamza, I., Schaefer, M., Klomp, L. W., and Gitlin, J. D. (1999) Interaction of the copper chaperone HAH1 with the Wilson disease protein is essential for copper homeostasis. *Proc Natl Acad Sci U S A 96*, 13363-8.

84. Larin, D., Mekios, C., Das, K., Ross, B., Yang, A. S., and Gilliam, T. C. (1999) Characterization of the interaction between the Wilson and Menkes disease proteins and the cytoplasmic copper chaperone, HAH1p. *J Biol Chem 274*, 28497-504.

85. Rosenzweig, A. C., Huffman, D. L., Hou, M. Y., Wernimont, A. K., Pufahl, R. A., and O'Halloran, T. V. (1999) Crystal structure of the Atx1 metallochaperone protein at 1.02 A resolution. *Structure Fold Des 7*, 605-17.

86. Portnoy, M. E., Rosenzweig, A. C., Rae, T., Huffman, D. L., O'Halloran, T. V., and Culotta, V. C. (1999) Structure-function analyses of the ATX1 metallochaperone. *J Biol Chem 274*, 15041-5.

87. Arnesano, F., Banci, L., Bertini, I., Huffman, D. L., and O'Halloran, T. V. (2001) Solution structure of the Cu(I) and apo forms of the yeast metallochaperone, Atx1. *Biochemistry 40*, 1528-39.

88. Anastassopoulou, I., Banci, L., Bertini, I., Cantini, F., Katsari, E., and Rosato, A. (2004) Solution structure of the apo and copper(I)-loaded human metallochaperone HAH1. *Biochemistry 43*, 13046-53.

89. Skou, J. C. (1957) The influence of some cations on an adenosine triphosphatase from peripheral nerves. *Biochim Biophys Acta 23*, 394-401.

90. Kuhlbrandt, W. (2004) Biology, structure and mechanism of P-type ATPases. *Nat Rev Mol Cell Biol 5*, 282-95.

91. Nucifora, G., Chu, L., Misra, T. K., and Silver, S. (1989) Cadmium resistance from Staphylococcus aureus plasmid pI258 cadA gene results from a cadmium-efflux ATPase. *Proc Natl Acad Sci U S A 86*, 3544-8.

92. Rensing, C., Mitra, B., and Rosen, B. P. (1997) The zntA gene of Escherichia coli encodes a Zn(II)-translocating P-type ATPase. *Proc Natl Acad Sci U S A 94*, 14326-31.

93. Odermatt, A., Suter, H., Krapf, R., and Solioz, M. (1993) Primary structure of two P-type ATPases involved in copper homeostasis in Enterococcus hirae. *J Biol Chem 268*, 12775-9.

94. Lutsenko, S., and Kaplan, J. H. (1995) Organization of P-type ATPases: significance of structural diversity. *Biochemistry 34*, 15607-13.

95. Yuan, D. S., Stearman, R., Dancis, A., Dunn, T., Beeler, T., and Klausner, R. D. (1995) The Menkes/Wilson disease gene homologue in yeast provides copper to a ceruloplasmin-like oxidase required for iron uptake. *Proc Natl Acad Sci U S A 92*, 2632-6.

96. Forbes, J. R., and Cox, D. W. (1998) Functional characterization of missense mutations in ATP7B: Wilson disease mutation or normal variant? *Am J Hum Genet 63*, 1663-74.

97. Tumer, Z., Moller, L. B., and Horn, N. (1999) Mutation spectrum of ATP7A, the gene defective in Menkes disease. *Adv Exp Med Biol 448*, 83-95.

98. Petris, M. J., Voskoboinik, I., Cater, M., Smith, K., Kim, B. E., Llanos, R. M., Strausak, D., Camakaris, J., and Mercer, J. F. (2002) Copper-regulated trafficking of the Menkes disease copper ATPase is associated with formation of a phosphorylated catalytic intermediate. *J Biol Chem 277*, 46736-42.

99. Voskoboinik, I., Mar, J., Strausak, D., and Camakaris, J. (2001) The regulation of catalytic activity of the menkes copper-translocating P-type ATPase. Role of high affinity copper-binding sites. *J Biol Chem 276*, 28620-7.

100. Tsivkovskii, R., Eisses, J. F., Kaplan, J. H., and Lutsenko, S. (2002) Functional properties of the copper-transporting ATPase ATP7B (the Wilson's disease protein) expressed in insect cells. *J Biol Chem 277*, 976-83.

101. Iida, M., Terada, K., Sambongi, Y., Wakabayashi, T., Miura, N., Koyama, K., Futai, M., and Sugiyama, T. (1998) Analysis of functional domains of Wilson disease protein (ATP7B) in Saccharomyces cerevisiae. *FEBS Lett 428*, 281-5.

102. Pedersen, P. A., Jorgensen, J. R., and Jorgensen, P. L. (2000) Importance of conserved alpha -subunit segment 709GDGVND for Mg2+ binding, phosphorylation, and energy transduction in Na,K-ATPase. *J Biol Chem 275*, 37588-95.

103. Tsivkovskii, R., Efremov, R. G., and Lutsenko, S. (2003) The role of the invariant His-1069 in folding and function of the Wilson's disease protein, the human copper-transporting ATPase ATP7B. *J Biol Chem 278*, 13302-8.

104. Lutsenko, S., and Petris, M. J. (2003) Function and regulation of the mammalian copper-transporting ATPases: insights from biochemical and cell biological approaches. *J Membr Biol 191*, 1-12.

105. Lutsenko, S., Petrukhin, K., Cooper, M. J., Gilliam, C. T., and Kaplan, J. H. (1997) N-terminal domains of human copper-transporting adenosine triphosphatases (the Wilson's and Menkes disease proteins) bind copper selectively in vivo and in vitro with stoichiometry of one copper per metal-binding repeat. *J Biol Chem 272*, 18939-44.

106. Jensen, P. Y., Bonander, N., Moller, L. B., and Farver, O. (1999) Cooperative binding of copper(I) to the metal binding domains in Menkes disease protein. *Biochim Biophys Acta 1434*, 103-13.

107. Ralle, M., Cooper, M. J., Lutsenko, S., and Blackburn, N. J. (1998) The Menkes Disease Protein Binds Copper via Novel 2-Coordinate Cu(I)-Cysteinates in the N-Terminal Domain. *J. Am. Chem. Soc. 120*, 13525-13526.

108. DiDonato, M., Narindrasorasak, S., and Sarkar, B. (1999) Expression, purification, and metal binding characteristics of the putative copper binding domain from the Wilson disease copper transporting ATPase (ATP7B). *Adv Exp Med Biol 448*, 165-73.

109. DiDonato, M., Hsu, H. F., Narindrasorasak, S., Que, L., Jr., and Sarkar, B. (2000) Copper-induced conformational changes in the N-terminal domain of the Wilson disease copper-transporting ATPase. *Biochemistry 39*, 1890-6.

110. Ralle, M., Lutsenko, S., and Blackburn, N. J. (2004) Copper transfer to the N-terminal domain of the Wilson disease protein (ATP7B): X-ray absorption spectroscopy of reconstituted and chaperone-loaded metal binding domains and their interaction with exogenous ligands. *J Inorg Biochem 98*, 765-74.

111. Hung, I. H., Suzuki, M., Yamaguchi, Y., Yuan, D. S., Klausner, R. D., and Gitlin, J. D. (1997) Biochemical characterization of the Wilson disease protein and functional expression in the yeast Saccharomyces cerevisiae. *J Biol Chem 272*, 21461-6.

112. Yang, X. L., Miura, N., Kawarada, Y., Terada, K., Petrukhin, K., Gilliam, T., and Sugiyama, T. (1997) Two forms of Wilson disease protein produced by alternative splicing are localized in distinct cellular compartments. *Biochem J 326 (Pt 3)*, 897-902.

113. Lutsenko, S., Efremov, R. G., Tsivkovskii, R., and Walker, J. M. (2002) Human copper-transporting ATPase ATP7B (the Wilson's disease protein): biochemical properties and regulation. *J Bioenerg Biomembr 34*, 351-62.

114. Vanderwerf, S. M., Cooper, M. J., Stetsenko, I. V., and Lutsenko, S. (2001) Copper specifically regulates intracellular phosphorylation of the Wilson's disease protein, a human copper-transporting ATPase. *J Biol Chem 276*, 36289-94.

115. Roelofsen, H., Wolters, H., Van Luyn, M. J., Miura, N., Kuipers, F., and Vonk, R. J. (2000) Copper-induced apical trafficking of ATP7B in polarized hepatoma cells provides a mechanism for biliary copper excretion. *Gastroenterology 119*, 782-93.

116. Barnes, N. (2002) Stucture/Function Studies of Mammalian Copper ATPases. In *School of Biological & Chemical Sciences* pp 260, Deakin University, Burwood, Australia.

117. Huster, D., and Lutsenko, S. (2003) The distinct roles of the N-terminal copper-binding sites in regulation of catalytic activity of the Wilson's disease protein. *J Biol Chem 278*, 32212-8.

118. Gitschier, J., Moffat, B., Reilly, D., Wood, W. I., and Fairbrother, W. J. (1998) Solution structure of the fourth metal-binding domain from the Menkes copper-transporting ATPase. *Nat Struct Biol 5*, 47-54.

119. Banci, L., Bertini, I., Ciofi-Baffoni, S., Huffman, D. L., and O'Halloran, T. V. (2001) Solution structure of the yeast copper transporter domain Ccc2a in the apo and Cu(I)-loaded states. *J Biol Chem 276*, 8415-26.

120. Jones, C. E., Daly, N. L., Cobine, P. A., Craik, D. J., and Dameron, C. T. (2003) Structure and metal binding studies of the second copper binding domain of the Menkes ATPase. *J Struct Biol 143*, 209-18.

121. Banci, L., Bertini, I., Del Conte, R., D'Onofrio, M., and Rosato, A. (2004) Solution structure and backbone dynamics of the Cu(I) and Apo forms of the second metal-binding domain of the Menkes protein ATP7A. *Biochemistry 43*, 3396-403.

122. Arnesano, F., Banci, L., Bertini, I., Cantini, F., Ciofi-Baffoni, S., Huffman, D. L., and O'Halloran, T. V. (2001) Characterization of the binding interface between the copper chaperone Atx1 and the first cytosolic domain of Ccc2 ATPase. *J Biol Chem 276*, 41365-76.

123. Arnesano, F., Banci, L., Bertini, I., and Bonvin, A. M. (2004) A docking approach to the study of copper trafficking proteins; interaction between metallochaperones and soluble domains of copper ATPases. *Structure (Camb) 12*, 669-76.

124. Wernimont, A. K., Huffman, D. L., Lamb, A. L., O'Halloran, T. V., and Rosenzweig, A. C. (2000) Structural basis for copper transfer by the metallochaperone for the Menkes/Wilson disease proteins. *Nat Struct Biol 7*, 766-71.

125. Walker, J. M., Tsivkovskii, R., and Lutsenko, S. (2002) Metallochaperone Atox1 transfers copper to the NH2-terminal domain of the Wilson's disease protein and regulates its catalytic activity. *J Biol Chem 277*, 27953-9.

126. Walker, J. M., Huster, D., Ralle, M., Morgan, C. T., Blackburn, N. J., and Lutsenko, S. (2004) The N-terminal metal-binding site 2 of the Wilson's disease protein plays a key role in the transfer of copper from Atox1. *J Biol Chem 279*, 15376-84.

127. O'Halloran, T. V., and Culotta, V. C. (2000) Metallochaperones, an intracellular shuttle service for metal ions. *J Biol Chem 275*, 25057-60.

128. Harrison, M. D., Jones, C. E., Solioz, M., and Dameron, C. T. (2000) Intracellular copper routing: the role of copper chaperones. *Trends Biochem Sci 25*, 29-32.

129. Culotta, V. C., Lin, S. J., Schmidt, P., Klomp, L. W., Casareno, R. L., and Gitlin, J. (1999) Intracellular pathways of copper trafficking in yeast and humans. *Adv Exp Med Biol 448*, 247-54.

130. Bradford, M. M. (1976) A rapid and sensitive method for the quantitation of microgram quantities of protein utilizing the principle of protein-dye binding. *Anal Biochem 72*, 248-54.

131. Laemmli, U. K. (1970) Cleavage of structural proteins during the assembly of the head of bacteriophage T4. *Nature 227*, 680-5.

132. Brenner, A. J., and Harris, E. D. (1995) A quantitative test for copper using bicinchoninic acid. *Anal Biochem 226*, 80-4.

133. Schagger, H., and von Jagow, G. (1987) Tricine-sodium dodecyl sulfate-polyacrylamide gel electrophoresis for the separation of proteins in the range from 1 to 100 kDa. *Anal Biochem 166*, 368-79.

134. Sarkadi, B., Enyedi, A., Foldes-Papp, Z., and Gardos, G. (1986) Molecular characterization of the in situ red cell membrane calcium pump by limited proteolysis. *J Biol Chem 261*, 9552-7.

135. Forbes, J. R., Hsi, G., and Cox, D. W. (1999) Role of the copper-binding domain in the copper transport function of ATP7B, the P-type ATPase defective in Wilson disease. *J Biol Chem 274*, 12408-13.

136. Loudianos, G., and Gitlin, J. D. (2000) Wilson's disease. *Semin Liver Dis 20*, 353-64.

137. DiDonato, M., Narindrasorasak, S., Forbes, J. R., Cox, D. W., and Sarkar, B. (1997) Expression, purification, and metal binding properties of the N-terminal

domain from the wilson disease putative copper-transporting ATPase (ATP7B). *J Biol Chem 272*, 33279-82.

138. Arnesano, F., Banci, L., Bertini, I., Ciofi-Baffoni, S., Molteni, E., Huffman, D. L., and O'Halloran, T. V. (2002) Metallochaperones and metal-transporting ATPases: a comparative analysis of sequences and structures. *Genome Res 12*, 255-71.

139. Ankudinov, A. L., Ravel, B., Rehr, J. J., and Conradson, S. D. (1998) Real Space Multiple Scattering Calculation of XANES. *Phys. Rev. B58*, 7565 - 7576.

140. George, G. N. (1995) EXAFSPAK. Stanford Synchrotron Radiation Laboratory, Menlo Park, CA.

141. Hu, Y. K., and Kaplan, J. H. (2000) Site-directed chemical labeling of extracellular loops in a membrane protein. The topology of the Na,K-ATPase alpha-subunit. *J Biol Chem 275*, 19185-91.

142. Lowry, O. J., Rosebrough, N. J., Farr, A. L., and Randall, R. J. (1951) Protein measurement with the Folin phenol reagent. *J.Biol.Chem. 193*, 265-275.

143. Chen, K., Yuldasheva, S., Penner-Hahn, J. E., and O'Halloran, T. V. (2003) An atypical linear CuI-S2 center constitutes the high-affinity metal-sensing site in the CueR metalloregulatory protein. *J Am Chem Soc 125*, 12088-9.

144. Tsivkovskii, R., MacArthur, B. C., and Lutsenko, S. (2001) The Lys1010-Lys1325 fragment of the Wilson's disease protein binds nucleotides and interacts with the N-terminal domain of this protein in a copper-dependent manner. *J Biol Chem 276*, 2234-42.

145. Koradi, R., Billeter, M., and Wuthrich, K. (1996) MOLMOL: a program for display and analysis of macromolecular structures. *J Mol Graph 14*, 51-5, 29-32.

146. van Dongen, E. M., Klomp, L. W., and Merkx, M. (2004) Copper-dependent protein-protein interactions studied by yeast two-hybrid analysis. *Biochem Biophys Res Commun 323*, 789-95.

147. Tanchou, V., Gas, F., Urvoas, A., Cougouluegne, F., Ruat, S., Averseng, O., and Quemeneur, E. (2004) Copper-mediated homo-dimerisation for the HAH1 metallochaperone. *Biochem Biophys Res Commun 325*, 388-94.

148. Sanokawa-Akakura, R., Dai, H., Akakura, S., Weinstein, D., Fajardo, J. E., Lang, S. E., Wadsworth, S., Siekierka, J., and Birge, R. B. (2004) A Novel Role for the Immunophilin FKBP52 in Copper Transport. *J Biol Chem 279*, 27845-8.